



# Durham E-Theses

---

## *Particle production at high energy*

Webber, David Morley

### How to cite:

---

Webber, David Morley (1974) *Particle production at high energy*, Durham theses, Durham University. Available at Durham E-Theses Online: <http://etheses.dur.ac.uk/8194/>

### Use policy

---

The full-text may be used and/or reproduced, and given to third parties in any format or medium, without prior permission or charge, for personal research or study, educational, or not-for-profit purposes provided that:

- a full bibliographic reference is made to the original source
- a [link](#) is made to the metadata record in Durham E-Theses
- the full-text is not changed in any way

The full-text must not be sold in any format or medium without the formal permission of the copyright holders.

Please consult the [full Durham E-Theses policy](#) for further details.

PARTICLE PRODUCTION  
AT HIGH ENERGY

by

David Morley Webber

A thesis presented for the degree of  
Doctor of Philosophy  
at the University of Durham

August 1974

Mathematics Department,  
University of Durham.



## P R E F A C E

The work presented in this thesis was carried out in the Department of Mathematics of the University of Durham between October 1971 and August 1974 under the supervision of Professor E.J.Squires.

The material herein has not been submitted previously for any degree in this or any other university. No claim of originality is made for the first part of chapter one. Much of the remainder has been published in three papers by the author in collaboration with Professor Squires. Relevant unpublished work by the author is also included.

The author wishes to express his gratitude to Professor Squires for his help, guidance, and continued encouragement throughout the course of this work. He should also like to extend his thanks to the members of the mathematics and theoretical physics departments of Durham for numerous invaluable discussions over the last three years. He also thanks the Science Research Council for a research studentship.

## A B S T R A C T

This thesis concerns the strong interactions of elementary particles and in particular the scattering of particles at the highest measured energies.

Chapter one is divided into two parts, of which the first is an introduction to those aspects of the strong interaction with which we are concerned. The ideas introduced are then discussed in the second part of the chapter in the context of antiproton production in high energy proton interactions. An approximate calculation of the production cross-section is presented which gives some insight into the unexpected features of this process.

Chapter two is a calculation of the multiplicity distribution produced in proton interactions in a two component model based on Regge pole exchange. With a view to reducing the number of free parameters, the multiplicity distribution arising from reggeon-particle collisions is assumed to be independent of which reggeon is involved (including, notably, the pomeron). Features of the model are discussed as they arise and finally a fit is performed to the observed multiplicity distribution.

In chapter three this model is discussed in the context of momentum dependent measurements. The observed correlation between two mesons is seen to be in agreement with the model, as is the multiplicity distribution in all but one of the particles produced when the momentum of one is measured. Particular attention is also paid to the correlation between a forward proton and a charged particle in the central region, which is well described without any free parameters.

In chapter four the proton inclusive distribution is discussed with regard to the triple pomeron coupling. Particle production from a model with a non-zero triple pomeron coupling is discussed in relation to the preceding chapters.

Finally a brief summary of the findings of these chapters is presented.





2.9	The pomeron as a projectile	89
2.10	Other two component models	90
	Figures for chapter 2	92
CHAPTER 3	<u>Inclusive distributions and correlations</u>	
	Introduction	104
3.1	The two component model	105
3.2	A simple semi-inclusive measurement	109
3.3	The reaction $pp \rightarrow p + \text{charged particle} + \text{any}$	111
3.4	Comparison with the data - global structure	117
3.5	Detailed comparison with the data as $x \rightarrow 1$	120
3.6	The correlation as $x \rightarrow 0$	122
3.7	Beyond two particle correlations	124
3.8	Semi-inclusive quantities	127
	Figures for chapter 3	132
CHAPTER 4	<u>The triple pomeron coupling</u>	
	Introduction	155
4.1	The reaction $pp \rightarrow pX$ in the triple Regge region	156
4.2	Particle production from a triple pomeron model	160
4.3	A three component model	165
4.4	Difficulties with the pomeron	168
	Figures for chapter 4	170
	CONCLUSIONS	177
	References	179

### 1.1 What does the strong interaction look like at high energy?

Before going on to perform calculations in an attempt to describe the strong interaction, it seems natural to present a description of the broader features found empirically.<sup>1</sup>

Picture, then, two particles colliding in their centre of momentum frame. As the strong interaction has a short range, then they behave like free particles until they achieve close proximity. What happens then is impossible for us to see. What we do see is that two or more particles emerge from the interaction, (again behaving like free particles by the time we see them) in such a way that their total charge, momentum, energy, and a number of other quantities are conserved.

Having taken these conservation laws into account one finds that this is a remarkably gentle process. To illustrate this let us consider a few of the possible interactions. If both the initial and final states consist of two protons, they have the freedom to come out at any angle (in opposite directions) relative to the initial direction. As shown in figure 1.1, they prefer overwhelmingly not to change their direction very much. The momentum of the final state particles transverse to the initial direction is limited. This phenomenon is not only observed in elastic interactions but is far more general. If we observe an interaction and don't bother to count the number of particles that are produced, but merely measure the momentum of one of them, we find that it too prefers to emerge without much momentum transverse to the initial direction. (e.g. figure 1.2).

Once we know that these interactions can produce more particles than went into them, it is natural to ask how many. Before we examine the experimental data here, we shall note how many the conservation laws allow. Conservation of energy-momentum requires at least two. If we take an interaction with a total centre of mass energy squared equal to  $s$ , then the maximum number of particles which could emerge is

$n_{\max} = \sqrt{s/m_{\pi}}$ , where  $m_{\pi}$  is the mass of the lightest known hadron, the pion. Even though an event where the whole energy is converted into a mass at rest is somewhat extreme and even at first glance may be a little improbable; the average number of particles produced is still a surprisingly small number compared to this, as shown in figure 1.3. Most of the initial energy, then, comes out in the form in which it went in, as kinetic energy. And energetic particles emerge in a direction not very different from the initial direction of the colliding particles. Furthermore, a large fraction of an initial particle's momentum is often carried by just one of the outgoing particles. This is thus often thought of as a 'fragment' of the initial particle. The frequent occurrence of a very fast outgoing particle is known as the 'leading particle effect', (see figure 1.4). These effects taken together provide a basic picture of the scattering of two particles into two or more.



## 1.2 Amplitudes and cross-sections

### (a) The total cross-section

For the scattering of particles from an initial state  $|i\rangle$  to an  $n$  particle final state  $|f\rangle$ , we have a scattering amplitude  $\langle f|A|i\rangle$  and we take the measured cross-section at a total squared energy of  $s$ , to be

$$\sigma_n = \frac{1}{2\lambda^2(s, m_a^2, m_b^2)} \int d\Phi_n |\langle f|A|i\rangle|^2 \quad (1.1)$$

and the total cross-section is

$$\sigma(s) = \sum_n \sigma_n(s) \quad (1.2)$$

We use here the conventional factors as in reference 2.

$d\Phi_n$  is the  $n$  particle Lorentz invariant phase space element.  $\lambda$  is the triangle function.

### (b) Unitarity and the optical theorem

The probability of producing any final state including the possibility that they remain in the initial state must be identically one. This provides us with a constraint on the amplitude.<sup>3</sup> This is expressed as the unitarity condition

$$SS^\dagger = S^\dagger S = 1 \quad (1.3)$$

on the operator

$$S = 1 + iA \quad (1.4)$$

It follows that

$$\text{Disc} \langle i|A|i\rangle = \sum_n \int d\Phi_n \langle n|A|i\rangle^* \langle n|A|i\rangle \quad (1.5)$$

where

$$\text{Disc } \langle i' | A | i \rangle = i \left( \langle i' | A | i' \rangle^* - \langle i' | A | i \rangle \right) \quad (1.6)$$

In particular for  $|i\rangle = |i'\rangle$  we have using (1.1) and (1.2)

$$\sigma_{\text{tot}}(i \rightarrow \text{anything}) = \frac{\text{Im } \langle i | A | i \rangle}{\lambda^2(s, m_a^2, m_b^2)} \quad (1.7)$$

This last is known as the optical theorem. Later we shall discuss a hypothesis due to Mueller<sup>4</sup>, which is analogous to this equation, and has formed the basis of one approach to the phenomenology of many-hadron problems.

(c) The Froissart bound

A bound on the total cross-section at high energy was deduced by Froissart, the prime ingredient of which is unitarity<sup>5</sup>.

The bound is

$$\sigma_{\text{tot}}(s) \leq c [\ln s]^2 \quad (1.8)$$

where  $c$  is a constant. It is valid for  $s$  larger than some constant  $s_0$ . As we shall see later, this bound is extremely useful in that it rules out a number of phenomenological ideas which might seem to be desirable with respect to some of the recent data on high energy proton-proton scattering.

(d) Inclusive and exclusive cross-sections

If one is performing an experiment to look at a specific interaction with a limited number of particles produced, then one can measure all their momenta and obtain more or less complete information on every event. However, this exclusive approach would clearly be a rather difficult task when one wants to look at a typical event at high energy. As seen from figure 1.3, the average number of particles pro-

duced at the highest accelerator energies is in excess of a dozen. Most of the experiments carried out at these energies are therefore inclusive in nature. In an inclusive experiment one only measures a certain number of the outgoing particles' momenta. Clearly complete information could be achieved by a knowledge of all exclusive experiments

$$a, b \rightarrow 1, 2, 3, \dots, n$$

for all  $n \geq 2$ . However it is also true that complete information can be obtained from a knowledge of all inclusive experiments

$$a, b \rightarrow 1, 2, 3, \dots, n + \text{anything unobserved}$$

for all  $n \geq 0$ . This is pointed out clearly in reference 6.

Whereas exclusive measurements have a complexity which rises directly with the number of produced particles, all inclusive measurements will reveal something of many particle production.

A class of experiments which do not perhaps fall neatly into either of these categories is that in which the number of particles are counted but momenta are not measured. Thus we can find  $\sigma_n / \sigma_{\text{tot}}$ ,  $\langle n \rangle$ ,  $\langle f(n) \rangle$  for some function  $f$ , at least for the case where  $n$  denotes the number of outgoing charged particles.

#### (e) Correlations

If we ask what the possibility is of a particle emerging from an interaction with a certain momentum  $p$ , then what we wish to measure is the inclusive cross-section

$$N_1(p) = \frac{1}{\sigma} \frac{d\sigma}{dp} \quad (1.9)$$

We use the notation  $dp$  for the Lorentz invariant phase space element  $d^3p/2E$  and have normalised to the total cross-section so that

$$\int N_1(p) dp = \langle n \rangle \quad (1.10)$$

For the probability of producing  $k$  particles with specified momenta, and

any others, we wish to know the inclusive cross-section

$$N_k(p_1, \dots, p_k) = \frac{1}{\sigma} \frac{d\sigma}{dp_1 \dots dp_k} \quad (1.11)$$

For identical particles

$$\int N_k(p_1, \dots, p_k) dp_1 \dots dp_k = \langle n(n-1) \dots (n-k+1) \rangle \quad (1.12)$$

It is perhaps more interesting to ask how much more or less probable it is to find particles with momenta  $p_1, p_2, \dots, p_k$  than it would be to find them individually from different events. We construct the quantity

$$C_2(p_1, p_2) = N_2(p_1, p_2) - N_1(p_1)N_1(p_2) \quad (1.13)$$

which is called the two particle correlation. We then successively construct the  $k$  particle correlation by writing

$$\begin{aligned} N_3(1, 2, 3) = & N_1(1)N_1(2)N_1(3) + N_1(1)N_2(2, 3) \\ & + N_1(3)N_2(2, 1) + N_1(2)N_2(3, 1) + C_3(1, 2, 3) \end{aligned} \quad (1.14)$$

and so on. The possibility  $C_n=0$  is referred to as uncorrelated production. (This is technically ruled out by momentum conservation<sup>7</sup> but may be approximately true in that  $C_n$  can be much smaller than  $N_1$ .) A measure of the overall size of the correlation is provided by the integrated correlation

$$f_k(s) = \int dp_1 \dots dp_k C_k(p_1, \dots, p_k) \quad (1.15)$$

$$f_1(s) = \int dp_1 N_1(p_1) = \langle n \rangle \quad (1.16)$$

(f) The multiplicity distribution

Perhaps the most basic measurement that can be made of a particle interaction is just to count the multiplicity of particles emerging from it. By doing this experiment one can find the fraction  $\sigma_n/\sigma$ , of the total interaction cross-section which goes into the production of  $n$  particles. We define the generating function for the multiplicity distribution (first introduced to particle physics in reference 8) by

$$\Phi(s, z) = \sum_n z^n \frac{\sigma_n}{\sigma} \quad (1.17)$$

We have that

$$\sigma = \sum_n \sigma_n \quad (1.18)$$

and so

$$\Phi(s, 1) = 1 \quad (1.19)$$

It will also be convenient later if we define

$$I(s, z) = \sum_n z^n \sigma_n = \sigma \cdot \Phi(s, z) \quad (1.20)$$

Clearly

$$\frac{\sigma_n}{\sigma} = \frac{1}{n!} \left( \frac{\partial}{\partial z} \right)^n \Phi(s, z) \Big|_{z=0} \quad (1.21)$$

and

$$\langle n(n-1)\dots(n-k+1) \rangle = \left( \frac{\partial}{\partial z} \right)^k \Phi(s, z) \Big|_{z=1} \quad (1.22)$$

The generating function can also be expressed in the form

$$\Phi(s, z) = \exp \left\{ \sum_{n=1}^{\infty} \frac{(z-1)^n}{n!} f_n(s) \right\} \quad (1.23)$$

where it turns out<sup>9</sup> that the  $f_n$  are just the integrated correlations that we have already introduced. Considering, for now, identical particles we have

$$f_1 = \langle n \rangle \quad (1.24)$$

$$f_2 = \langle n(n-1) \rangle - \langle n \rangle^2 \quad (1.25)$$

The standard deviation  $D$  of the distribution is defined by

$$D^2 = \langle n^2 \rangle - \langle n \rangle^2 \quad (1.26)$$

and so

$$f_2 = D^2 - \langle n \rangle \quad (1.27)$$

If the multiplicity distribution is a singly peaked distribution, then one may expect that the sum in (1.23) is the most rapidly convergent description of the generating function, as  $f_1$  gives the mean,  $f_2$  the width, and then  $f_3 \dots f_\infty$  are more subtle quantities to do with the shape of the distribution.

From this generating function approach Le Bellac<sup>9</sup> has derived an interesting theorem. It says essentially that if the correlations  $f_n$  are asymptotically like  $\ln(s)$  then the quantities  $\sigma_n / \sigma$  fall asymptotically like a power of  $s$ . This is interesting primarily because many models suggest that  $f_n \sim \ln(s)$ .

(g) The generalised optical theorem

The simplest inclusive reaction is the one which may be described as



which is the measurement of the total cross-section.

This is related by the optical theorem to the forward elastic process  $a, b \rightarrow a', b'$ , where  $p_{a'} = p_a$ ,  $p_{b'} = p_b$ . This is illustrated in

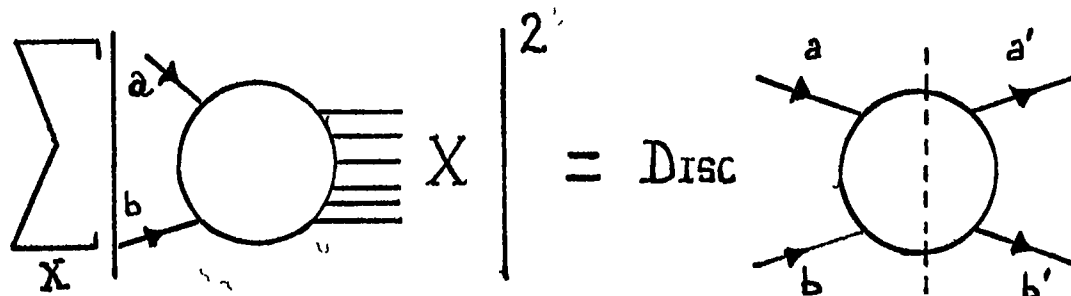


DIAGRAM 1.1 : The optical theorem

diagram 1.1. The discontinuity referred to is

$$\lim_{\epsilon \rightarrow 0^+} \left[ A_{2 \rightarrow 2}(s+i\epsilon) - A_{2 \rightarrow 2}(s-i\epsilon) \right] \quad (1.29)$$

Mueller<sup>4,6</sup> hypothesised that the inclusive cross-sections might be treatable in a similar way. For the reaction

$$a, b \rightarrow c, X \quad (1.30)$$

we observe c and sum over all possible X. The corresponding diagram is diagram 1.2. The discontinuity here is

$$\lim_{\epsilon_{1,2,3} \rightarrow 0^+} \left[ A_{3 \rightarrow 3}(s_{ab}=s+i\epsilon_1, s_{abc}=M^2+i\epsilon_2, s_{a'b'}=s-i\epsilon_3) - A_{3 \rightarrow 3}(s_{ab}=s+i\epsilon_1, s_{abc}=M^2-i\epsilon_2, s_{a'b'}=s-i\epsilon_3) \right] \quad (1.31)$$

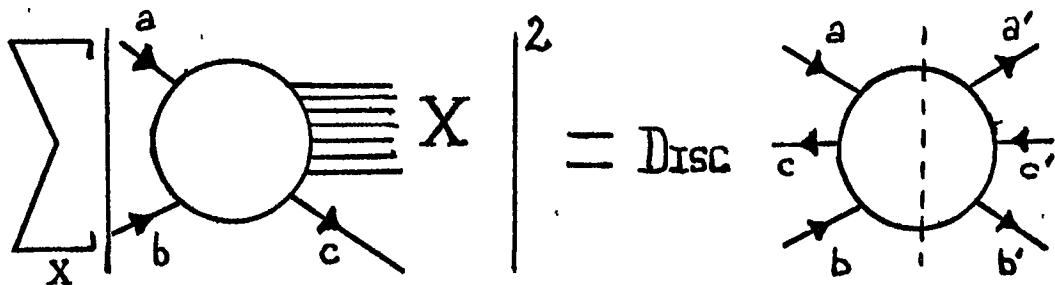


DIAGRAM 1.2 : The generalised optical theorem

The discontinuity is only across the cut in one of the variables (the squared missing mass), but the hypothesis rests on the possibility of the analytic continuation in the variables shown. The higher order inclusive cross-sections can then be hoped to satisfy a similar relation shown in diagram 1.3. In each case the discontinuity is taken

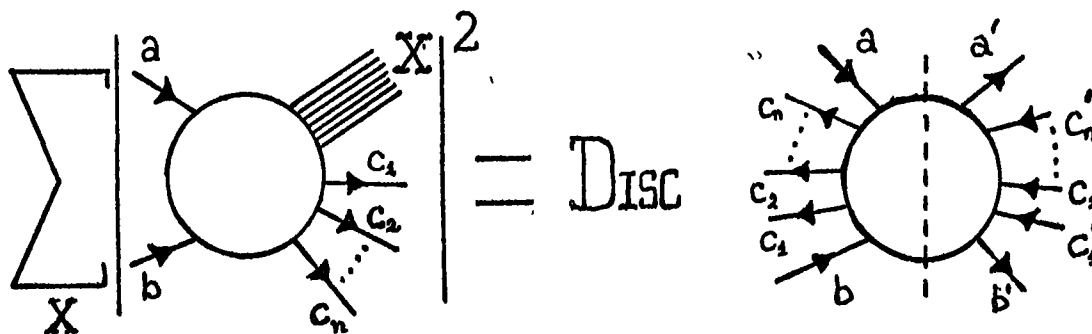


DIAGRAM 1.3

The optical theorem for  $a, b \rightarrow c_1, c_2, \dots, c_n, X$

---

in the forward direction,  $p_a = p_{a'}$ ,  $p_b = p_{b'}$ ,  $p_{c_1} = p_{c_1'}$ , etc. This hypothesis has been used extensively in conjunction with Regge phenomenology, (See for example references 6,10).



1.3 Regge theory(a) Regge trajectories

So far we have merely defined the quantities which one might wish to discuss to gain some understanding of physics at very high energies. No mention has been made of how one might go about working out what these quantities might look like. Regge analysis<sup>11</sup> provides a framework in which to discuss such calculations, at least for the high energy behaviour of amplitudes. For two body reactions, briefly, Regge theory involves expanding the scattering amplitude for large  $s$  and small  $t$  in a  $t$  channel partial wave series and continuing to complex values of  $t$  channel angular momentum,  $j$ . The analytic structure of the amplitude in the complex  $j$  plane determines the high energy (large  $s$ ) behaviour of the amplitude. A (Regge) pole at  $j=\alpha(t)$  implies a high energy behaviour like  $s^{\alpha(t)}$ .  $\alpha(t)$  is known as a Regge trajectory and in the positive  $t$  region when  $\alpha$  takes on physical values (integral or half integral), it will correspond to the existence of a particle of mass  $m$  and spin  $\sigma$  such that  $\alpha(m^2)=\sigma$ . (For reasons that we shall not go into here, these particles are expected to be spaced at intervals of 2 units in angular momentum - e.g. the proton may have recurrences of spins  $\frac{5}{2}, \frac{3}{2}$ , etc.). The high energy  $s$  channel scattering is of course determined by the trajectory when  $t$  is negative. These Regge trajectories have the advantage that the same trajectories should appear in different processes with the same  $t$  channel quantum numbers. Diagram 1.4 gives a pictorial representation of the Regge

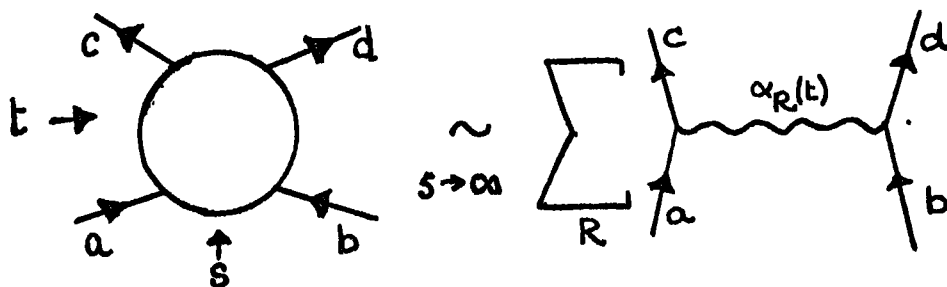


DIAGRAM 1.4 : Regge behaviour of amplitudes

---

trajectory in two body scattering. Although more complicated singularities in the  $j$  plane are now generally thought necessary to explain the detailed features (e.g. polarisation) found in two body interactions, the data for many body interactions are generally less precise in the information given about amplitudes, and so one may seek to use a phenomenological extension of the simple Regge pole ideas to describe particle production processes. This of course will be based upon the knowledge of trajectories gained from two body scattering.

(b) The pomeron

It has long been clear from the data that total cross-sections do not fall with energy. The optical theorem implies that if the elastic two particle cross-section is dominated by a simple pole trajectory  $\alpha(t)$  then

$$\sigma \underset{s \rightarrow \infty}{\sim} S^{\alpha(0) - 1} \quad (1.32)$$

The Froissart bound then implies that

$$\alpha(0) \leq 1 \quad (1.33)$$

The approximate constancy of the total cross-section indicated a trajectory having  $\alpha(0)=1$ . As all the known mesons with vacuum quantum numbers seem to lie on lower trajectories (which appear roughly linear in  $t$  with a slope of approximately  $1 \text{ GeV}^{-2}$ , see figure 1.5), this trajectory was something new. It was named after Pomeranchuk and is now generally referred to as the pomeron. The recent observation of rising total cross-sections indicate that the pomeron is perhaps something more complicated than a simple pole. The cross-sections may reach a constant from below or may not. The Froissart bound may or may not be saturated asymptotically. If cross-sections do rise asymptotically, then complete  $s$  channel unitarity which provides the Froissart bound

will presumably be crucial to any model for particle production. In any event the existence of a trajectory having  $\alpha(0)=1$  gives rise to certain difficulties when one tries to use it in a simple way in particle production processes.<sup>9,12,16</sup>

(c) Duality

The statement of duality<sup>13</sup> is that a sum of  $s$  channel resonances or a sum of  $t$  channel Regge exchanges form alternative descriptions of an amplitude, rather than the amplitude being a sum of both. A further conjecture<sup>14</sup> would have the resonances 'dual' in this way to Regge exchanges other than the pomeron, whereas the pomeron should be 'dual' to the background. This is extremely attractive in two body scattering as reactions in which the total  $s$  channel quantum numbers are exotic should have no resonances and therefore only the pomeron in the  $t$  channel of the imaginary part of the elastic amplitude. The cross-section should thus display a more rapid approach to the asymptotic pomeron behaviour, whether it be constant or otherwise. This is clearly displayed for  $pp$  and  $K^+p$  interactions. (See figure 1.6)

#### 1.4 Regge ideas in particle production

##### (a) The single Regge limit

Just as Regge behaviour in an elastic amplitude gives, via the optical theorem, information about the total cross-section, we can gain information about inclusive reactions if we assume that the discontinuity (unphysical though it is) of the three to three elastic amplitude also has Regge behaviour.

Consider the reaction  $a, b \rightarrow c, X$  with  $c$  in the fragmentation region of  $b$ , (that is  $c$  is slow in the rest frame of  $b$ ). In the optical theorem diagram we can think of a 'pseudoparticle' with the quantum numbers of  $b\bar{c}$ , and assume Regge behaviour for  $M^2$  large. ( $M$  is the total mass of the unobserved  $X$ . See diagram 1.5)

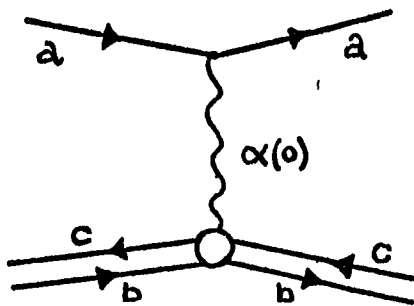


DIAGRAM 1.5 : Fragmentation region of  $a, b \rightarrow c, X$ .

If we define  $t = (p_b - p_c)^2$ , then a pole contribution will lead to an expression

$$\sum_i B_i(t, \frac{M^2}{s}) \cdot (M^2)^{\alpha_i(0) - 1} \quad (1.34)$$

for the inclusive distribution in this region, or equivalently

$$\sum_i \tilde{B}_i(t, \frac{M^2}{s}) \cdot s^{\alpha_i(0) - 1} \quad (1.35)$$

Pomeron dominance of this process at high energy immediately gives the scaling criterion suggested by Feynman that

$$\frac{d\sigma^{inc}}{dp_c} (s, \frac{s}{M^2}, t) \xrightarrow{s \rightarrow \infty} \frac{d\sigma^{inc}}{dp_c} (\frac{s}{M^2}, t) \quad (1.36)$$

This is also equivalent to Yang's statement of limiting fragmentation.

Ideas concerning the exoticity of quantum numbers may again lead via duality to some expectation of how rapidly scaling should occur. After a long discussion by various authors<sup>15</sup>, no absolute agreement upon any exact criterion was reached. Reference 6 does however draw the tentative conclusion that if  $b\bar{c}$  is not exotic, thus allowing small  $t$  dominance, and  $ab\bar{c}$  is exotic, then the pomeron should dominate the amplitude depicted in diagram 1.5, leading to rapid scaling. It is also pointed out there, that in the fragmentation region, the singularities (especially the pomeron) seem to factorise extremely well. (It is easier to test factorisation here than in elastic two to two scattering as the quantum numbers of the 'pseudotarget'  $b\bar{c}$  can be varied easily at will.)

(b) The double Regge limit

In the case where the particle  $c$  is slow in neither of the rest frames of the colliding particles, diagram 1.6 may be thought more

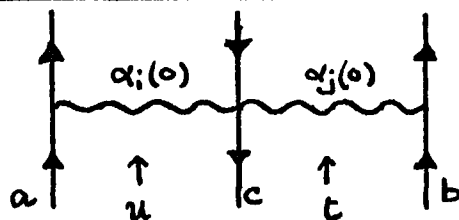


DIAGRAM 1.6 : The double Regge limit

appropriate. The inclusive cross-section in this case will have the form

$$\frac{d\sigma}{dp_c} = \sum_{ij} \beta_{ij}(k) |t|^{\alpha_j(0)-1} \cdot |u|^{\alpha_i(0)-1} \quad (1.37)$$

where

$$K = \frac{ut}{s} \approx p_{c\perp}^2 + m_0^2 \quad (1.38)$$

and

$$s+t+u \approx M^2 \quad (1.39)$$

Asymptotically as  $s \rightarrow \infty$  with  $p_{c\perp}$  fixed we now have the prediction that out of the possible three variables this quantity only depends upon one, the transverse momentum of the observed particle. The approach to scaling is slower here however than in the fragmentation region. If  $p_{c\parallel} \approx 0$  in the centre of mass frame, then  $u, t \sim s^{\frac{1}{2}}$  and so the first non leading terms are like  $s^{\frac{1}{2}(\alpha_m(0)-1)}$ , rather than  $s^{\alpha_m(0)-1}$  as in the fragmentation region.

(c) The triple Regge limit

The triple Regge limit is a special case in which we can say a little more about the single Regge limit. It is appropriate in the region of phase space where  $M^2$  is large ( $M^2 > m_0^2$  say), and  $s/M^2$  is also large, ( $s/M^2 > (1-x_0)^{-1}$  say). We define as usual the variable  $x$  to be the longitudinal momentum of the observed particle in the centre of mass frame, normalised so that  $-1 \leq x \leq 1$ , i.e.  $x = 2p_{c\parallel}^{c.m.} / \sqrt{s}$ . For  $s$  large then

$$x = 1 - \frac{M^2}{s} \quad (1.40)$$

In terms of this variable we are now discussing the region

$$x_0 \leq x \leq 1 - \frac{m_0^2}{s} \quad (1.41)$$

(The central (double Regge) region is confined in this variable to a very small area  $|x| < O(1/\sqrt{s})$  and so it is not very suitable for discussing the details of the central region.)

For  $s/M^2$  large the amplitude for  $a, b \rightarrow c, X$  is expanded as

in diagram 1.7 before taking the square modulus. Then doing this and summing over the missing X one finds

$$\frac{ds}{dp} \propto \frac{d\omega}{dx dt} \propto \sum_{ijk} G_{ijk}(t, t, 0) g_i(t) g_j(t) g_k(0) S_i(t) S_j^*(t) \left(\frac{s}{M^2}\right)^{\alpha_i(t) + \alpha_j(t) - 1} (M^2)^{\alpha_k(0) - 1} \quad (1.42)$$

where  $S_i(t)$  is the unit modulus phase (signature) factor predicted by

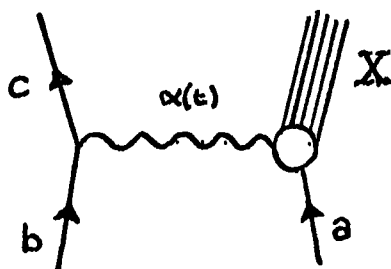


DIAGRAM 1.7

Regge theory. The diagram corresponding to this limit is diagram 1.8. In this region we have the dependence on the  $s$  and  $M^2$  variables and the only arbitrary dependence is that on  $t$ , in each of the terms in equation (1.42). The advent of the CERN Intersecting Storage Rings and the NAL accelerator which allow us to study the otherwise inaccessible region where  $s \gg M^2 \gg 1 \text{ GeV}^2$ , has made this triple Regge expansion very popular amongst phenomenologists. We shall discuss it in greater detail in the following chapters.

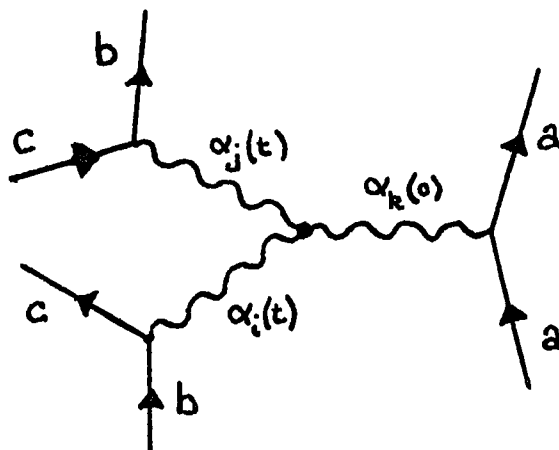


DIAGRAM 1.8 : The triple Regge limit

(d) The multi-Regge limit

We have so far considered the single particle inclusive distribution in a number of different limits. The many particle inclusive distribution can be treated in a similar way. In chapter three we shall look in detail at the two particle correlation, so here we shall point out the broad features indicated by Regge phenomenology. Consider diagram 1.9. We shall take the limit where all the sub-energies are at least large enough for the amplitude to be

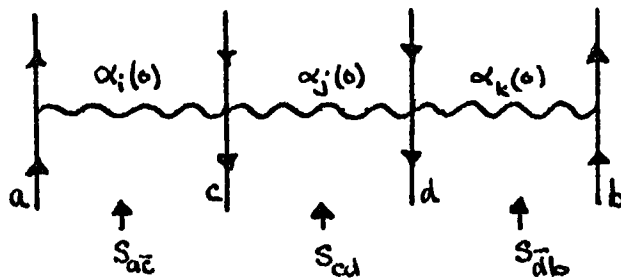


DIAGRAM 1.9 : The multi-Regge limit of the two particle inclusive distribution

approximated by a sum of Regge terms. If we assume factorisation (which seems to be good in the fragmentation region), then the leading Regge term ( $\alpha_i = \alpha_j = \alpha_k = \alpha_P$ ) in the sum

$$\sigma N_2(p_c, p_d) = \sum_{ijk} \beta_{ijk}(k_c, k_d) S_{a\bar{c}}^{\alpha_i-1} S_{cd}^{\alpha_j-1} S_{\bar{d}b}^{\alpha_k-1} \quad (1.43)$$

becomes

$$\sigma N_2 \sim \gamma_{aP} \gamma_{PcP}(k_c) \gamma_{PdP}(k_d) \cdot \gamma_{bP} \quad (1.44)$$

where

$$K_c = \frac{S_{a\bar{c}} S_{cd}}{S_{a\bar{d}}}, \quad K_d = \frac{S_{cd} S_{\bar{d}b}}{S_{\bar{c}b}}$$

The  $\gamma$  are the vertex factors relating to diagram 1.9. From the optical



theorem for a pomeron dominated cross-section  $\sigma \sim \gamma_{aP} \gamma_{Pb}$  where factorisation gives the same  $\gamma$  factors.

Therefore

$$N_2 \sim \gamma_{PcP} \gamma_{PdP}$$

Similarly (see diagram 1.6)

$$N_1 \sim \gamma_{PcP}$$

Hence

$$C_2(p_c, p_d) \sim 0$$

Thus when  $s_{a\bar{c}}$ ,  $s_{cd}$ , and  $s_{\bar{d}b}$  are large we expect no correlation. This is the statement of no long range correlation. (Long range implying very different momenta and hence large sub-energies.) Putting lower singularities  $\alpha$  into the cd channel will result in a behaviour like  $s_{cd}^{\alpha-1}$ . In terms of the longitudinal rapidities of the particles, defined from their momenta by

$$p = (m_1 \cosh y, \vec{p}_1, m_1 \sinh y) \quad (1.45)$$

with

$$m_1 = (m^2 + p_1^2)^{1/2} \quad (1.46)$$

this gives

$$C_2 \propto [\cosh(y_c - y_d)]^{\alpha-1} \quad (1.47)$$

which is clearly a typical short range correlation vanishing rapidly for  $|y_c - y_d|$  large. The correlation length may be thought of as  $L = (1-\alpha)^{-1}$  units of rapidity.

### 1.5 An idealised picture of inclusive reactions

The previous sections give us a very nice picture of what inclusive distributions should look like, and show the Mueller hypothesis combined with Regge phenomenology to be a very powerful pair of ideas. The world viewed this way should provide us with inclusive distributions which scale in the fragmentation region, and which in the fragmentation region of one of the colliding particles should be independent of the nature of the other. In the central region the inclusive distribution should also scale (albeit more slowly) and depend only upon the transverse momentum of the observed particle. This should result in a plateau when plotted against the rapidity variable which has a range of  $\ln(s)$ . The fragmentation region, we picture as being where observed particles are within a correlation length of the end of the rapidity distribution. The central region, we thus expect, should be clearly visible when  $\ln(s) \gg 4$ . (The scale of  $s$  is set by the transverse masses involved.) Correlations should fall rapidly as the particles' momenta become separated on the rapidity plot, and should not depend on absolute rapidities but only on differences of rapidities. These ideas are depicted in figure 1.7. The integrated correlations should thus be linear in  $\ln(s)$ , as should the mean multiplicity.

Empirical observation provides a tantalising combination of confirmation and denial of our efforts. The mean multiplicity is excellently consistent with  $\ln(s)$ , however the integrated correlations would prefer a more rapid  $s$  dependence. (See figures 1.8-1.11). Factorisation in the fragmentation region, as discussed, seems good. There is also evidence for a rapidity plateau. (See figure 1.12). Short range correlations are not necessarily the only ones present as indicated by the integrated correlation data. One of the more interesting problems is the difficulty of incorporating the pomeron into many-particle problems in a consistent way. (For instance the triple Regge region produces rather strange results for the three pomeron case<sup>16</sup>)

We shall discuss these problems further. The objects of the following chapters are to try to realise why this short range correlation approach is not sufficient in certain respects, and to test certain models which might, in these respects, improve on the basic short range correlation idea.

## PART II

The reaction  $pp \rightarrow \bar{p}X$ 

## INTRODUCTION

The reaction  $pp \rightarrow \bar{p}X$  is discussed. Its interest lies in that it satisfies a number of exoticity criteria. The data do not scale as expected. A calculation is presented which, whilst being somewhat simplistic, takes more carefully into account what we believe to be the more important of the kinematic features of this process when the antiproton is observed to be slow in the centre of momentum frame.

### 1.6 Antiproton production : the Mueller-Regge approach

Whilst the Mueller-Regge phenomenology works very well in the fragmentation region, certain difficulties appear when specific applications are made in the central (double Regge) region. As pointed out by Chan et al.<sup>17</sup>, the process  $pp \rightarrow \bar{p}X$  ought, at first glance, to provide an excellent testing ground for phenomenology in the double Regge region. In the notation of the previous sections the channels  $ab\bar{c}$ ,  $a\bar{c}$ ,  $b\bar{c}$  are all exotic and so one might justifiably expect that the inclusive cross-section should rapidly become independent of energy.

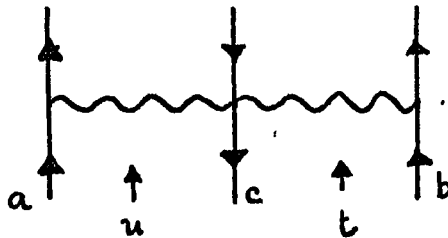


DIAGRAM 1.10 : The double Regge limit

Furthermore for the amplitude shown in diagram 1.10, the kinematic relation

$$K = \frac{ut}{s} = m_c^2 \quad (1.48)$$

holds when  $u, t, s \rightarrow \infty$ . In the central region then

$$u \sim m_c \sqrt{s} \quad ; \quad t \sim m_c \sqrt{s} \quad (1.49)$$

and so it might be considered better to have a heavy particle  $c$  so that at smaller  $s$  we have large  $u, t$ . Antiproton production, then, is ideal in this respect. However the inclusive distribution for  $pp \rightarrow \bar{p}X$  in the central region continues to rise, even at I.S.R. energies. (The rise is even more difficult<sup>17</sup> for dual ideas in the Mueller-Regge approach than would be a fall.) In reference there is introduced a

singularity with vacuum quantum numbers, in addition to the pomeron and usual meson terms. It has to couple negatively to give the rising distribution and its intercept is tentatively set at around zero.

### 1.7 Antiproton production : a direct approach

In this section we shall perform a simple calculation which illustrates that the rise in antiproton production is a kinematical effect.<sup>I</sup> This conclusion stems essentially from the fact that the lowest multiplicity event which contributes to this process is  $p, p \rightarrow p, p, p, \bar{p}$ . If one takes this to be definitive of the energy scale, then one should expect that the features of the  $s$  dependence will be present when  $s$  is a factor of four or so, higher than in the total cross-section (which depends upon  $\text{Im} A(pp \rightarrow pp)$ ). Whilst this is undoubtedly a contributing factor, far more important is the size of any of the momentum transfers involved. Owing to the massive particles in the final state, the invariant momentum transfer from an initial proton to a final one can only become small at large  $s$ . This problem is aggravated by demanding that, if the antiproton is observed with small momentum in the centre of mass frame, there should be two small momentum transfers as suggested by diagram 1.11. We take this to be our model for antiproton production.

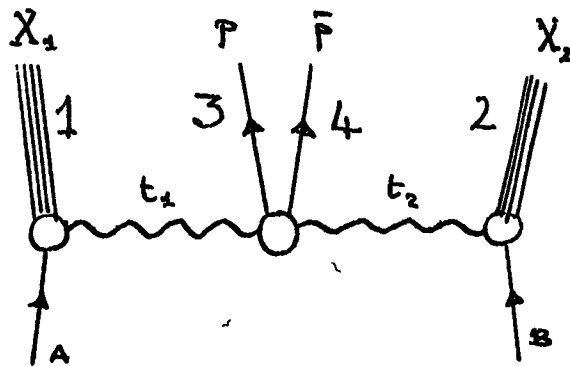


DIAGRAM 1.11 : A model for  $p, p \rightarrow \bar{p}, X$

It is suitable for production in the central region, as for  $x_{\bar{p}} \approx 0$  with fixed momentum transfers and transverse masses and with small  $s_{34}$

$$s_{134} \propto \sqrt{s} \quad ; \quad s_{234} \propto \sqrt{s} \quad (1.50)$$

$$s \rightarrow \infty \quad ; \quad s \rightarrow \infty$$

The central vertex is taken with a proton-antiproton pair so that the asymptotically non-vanishing pomeron contribution can be calculated. To illustrate the kinematic effect we set  $m_1 = m_2 = m_3 = m_4 = m$ , and take the two reggeons to be zero slope pomerons. Thus we write the amplitude for the process as

$$A = N \cdot \frac{s_{134}}{s_{34}} \cdot \frac{s_{234}}{s_{34}} \cdot e^{\beta t_1} \cdot e^{\beta t_2} \quad (1.51)$$

This is the simplest phenomenological prescription where we take all the 'pomeron mass' dependence of the  $PP \rightarrow p\bar{p}$  amplitude into  $\beta$  and assume no dependence on the variable  $\eta = (s_{134} \cdot s_{234} / s)$ . We expect the dominant contribution to be that where  $s_{34}$  is small as this not only allows  $s_{134}/s_{34}$  to become large more rapidly, but also allows smaller  $|t|$ . Also the amplitude for  $PP \rightarrow p\bar{p}$  as  $s_{34}$  becomes large might be expected to involve baryon exchange and thus become small. We therefore regard it as a reasonable approximation to set  $s_{34} = 4m^2$ , and calculate the contribution to the amplitude here. Thus

$$E_u \frac{d\sigma}{d^3p_u} = N^2 \int \frac{d^3p_1}{E_1} \frac{d^3p_2}{E_2} \cdot s_{134}^2 s_{234}^2 e^{2\beta(t_1+t_2)} \delta(\sqrt{s}-E_1-E_2-2E_u) \delta^2(\mathbf{p}_1+\mathbf{p}_2+2\mathbf{p}_u) \quad (1.52)$$

where we have set  $p_3 = p_4$  ( $s_{34} = 4m^2$ ) and absorbed all constant factors into  $N^2$ .

$$\left. \begin{aligned} s_{134} &= s + m^2 - 2\sqrt{s} E_2 \\ s_{234} &= s + m^2 - 2\sqrt{s} E_1 \end{aligned} \right\} \quad (1.53)$$

$$\left. \begin{aligned} t_1 &= 2m^2 - 2p_A^\mu p_A^\mu \\ t_2 &= 2m^2 - 2p_B^\mu p_B^\mu \end{aligned} \right\} \quad (1.54)$$

We now integrate over the phase space in (1.52) keeping the exact



kinematical limits on the momenta. The assumptions that we have made simplify the remaining integrals a great deal. We write

$$\frac{d^3 p_1}{E_1} \cdot \frac{d^3 p_2}{E_2} = |p_1| dE_1 d\chi d\phi \frac{d^3 p_2}{E_2} \quad (1.55)$$

$\chi$  is the cosine of the angle made by  $\underline{p}_1$  with the as yet unspecified  $z$  axis.

The integration  $d^3 p_2 dE_1$  now serves to remove the  $\delta$ -functions. Integrating  $d^3 p_2$

$$\left. \begin{aligned} p_2 &\rightarrow -p_1 - 2p_4 \\ E_2 &\rightarrow [E_1^2 + 4|p_4|^2 + 4p_4 \sqrt{E_1^2 - m^2} \cos \theta_{14}]^{1/2} \end{aligned} \right\} \quad (1.56)$$

and the remaining delta function (after some algebra) becomes

$$\begin{aligned} &\delta \left( [E_1^2 + 4p_4^2 + 4p_4 \sqrt{E_1^2 - m^2} \cos \theta_{14}]^{1/2} + E_1 + 2E_4 - \sqrt{s} \right) \frac{p_1 dE_1}{E_2} \\ &= \frac{\delta(E_1 - \Omega) (E_1^2 - m^2) dE_1}{(\sqrt{s} - 2E_4) \sqrt{E_1^2 - m^2} + 2E_1 p_4 \cos \theta_{14}} \end{aligned} \quad (1.57)$$

where  $\Omega$ , the root of the argument of the delta function on the left of equation (1.57) is given by

$$\Omega = \frac{(\sqrt{s} - 2E_4)(s + 4m^2 - 4E_4\sqrt{s}) - 2p_4 \cos \theta_{14} \sqrt{(s + 4m^2 - 4E_4\sqrt{s})^2 - 4m^2((\sqrt{s} - 2E_4)^2 - 4p_4^2 \cos^2 \theta_{14})}}{2((\sqrt{s} - 2E_4)^2 - 4p_4^2 \cos^2 \theta_{14})} \quad (1.58)$$

The remaining integration is now

$$E_4 \frac{d^3 \sigma}{d^3 p_4} = N^2 \int d\chi d\phi \frac{s_{13u}^2 s_{23u}^2}{\sqrt{s(s - 4m^2)}} e^{2\beta(t_1 + t_2)} \frac{(\Omega^2 - m^2)}{(\sqrt{s} - 2E_4) \sqrt{\Omega^2 - m^2} + 2\Omega p_4 \cos \theta_{14}} \quad (1.59)$$

where now

$$\left. \begin{aligned} S_{234} &= [s + m^2 - 2\sqrt{s} \cdot \Omega] \\ S_{134} &= [s + m^2 - 2\sqrt{s} (\sqrt{s} - 2E_4 - \Omega)] \end{aligned} \right\} (1.60)$$

and

$$\left. \begin{aligned} t_1 &= 2m^2 - \Omega\sqrt{s} + \sqrt{(s-4m^2)(\Omega^2-m^2)} \cos \theta_{A1} \\ t_2 &= 2m^2 - \sqrt{s}(\sqrt{s} - 2E_4 - \Omega) + \sqrt{(s-4m^2)(\Omega^2-m^2)} \cos \theta_{A1} + 2\sqrt{s-4m^2} p_4 \cos \theta_{A4} \end{aligned} \right\} (1.61)$$

We also have

$$\cos \theta_{A1} = \cos \theta_{A4} \cos \theta_{14} - \sin \theta_{A4} \sin \theta_{14} \cos(\phi_1 - \phi_4) \quad (1.62)$$

$\theta_{A4}$  is of course known. For  $p_{\perp 4} \neq 0$  we choose the z axis along  $p_{\perp 4}$  and so  $x = \cos \theta_{14}$ , and the x axis such that  $\phi = \phi_1 - \phi_4$ . The remaining expression is integrated numerically\* for various values of s and  $p_{\perp 4}$ . The constant N was chosen to normalise the model to the data at the point  $s = 1100 \text{ GeV}^2$ ,  $p_{\perp 4} = .95 \text{ GeV}/c$ ,  $x = 0$ , and  $\beta = 0.7 \text{ GeV}^{-2}$  was found to give the observed  $p_{\perp 4}$  dependence for  $x=0$  at I.S.R. energies. (See figure 1.13). Away from  $x=0$  the cross-section falls rather too rapidly with x. This perhaps is not too surprising in view of the fact that the whole central region is concentrated into a very small region of x and outside this region we do not expect the Regge amplitude in diagram 1.11 to be so good. The s dependence is now completely determined and is shown in figure 1.14. Although this is a little too rapid over I.S.R. energies, it extrapolates very well down to con-

---

\* Computer calculations here and later were done on the Northern Universities Multiple Access Computer and also the Rutherford High Energy Laboratory Computer.

ventional accelerator energies. The transverse momentum dependence at the lower energy is also remarkably good (see figure 1.15). Notice here that the data are over a somewhat different range from the I.S.R. data. The small value of  $\beta$  (as compared with the  $t$  dependence in proton-proton elastic scattering for example) must presumably be ascribed to a rising  $PP \rightarrow p\bar{p}$  amplitude as the 'masses' of the pomerons go away from zero. Although the model is clearly oversimplified, it does provide an illustration of the points made in the first paragraph of this section.

We should like to refer to two other calculations relevant to this process. Humble<sup>18</sup> uses a model similar in spirit to ours but instead of producing a proton-antiproton pair, couples the antiproton directly to meson and baryon Regge poles.

Jengo et al.<sup>19</sup> have related the  $pp \rightarrow p\bar{X}$  process to pion production by assuming that the production of a  $\pi^+\pi^-$  pair and that of  $p\bar{p}$  pair are the same if the two pairs have the same total 4-momentum. Our model demonstrates this feature as it is not important what we call the particle antiparticle pair at the central vertex.

We conclude, then, that we are not yet observing high enough energies to apply the Mueller-Regge phenomenology successfully in the central region for antiproton production. The lower singularity needed in reference 17 is thus not too surprising.

FIGURES FOR CHAPTER ONE

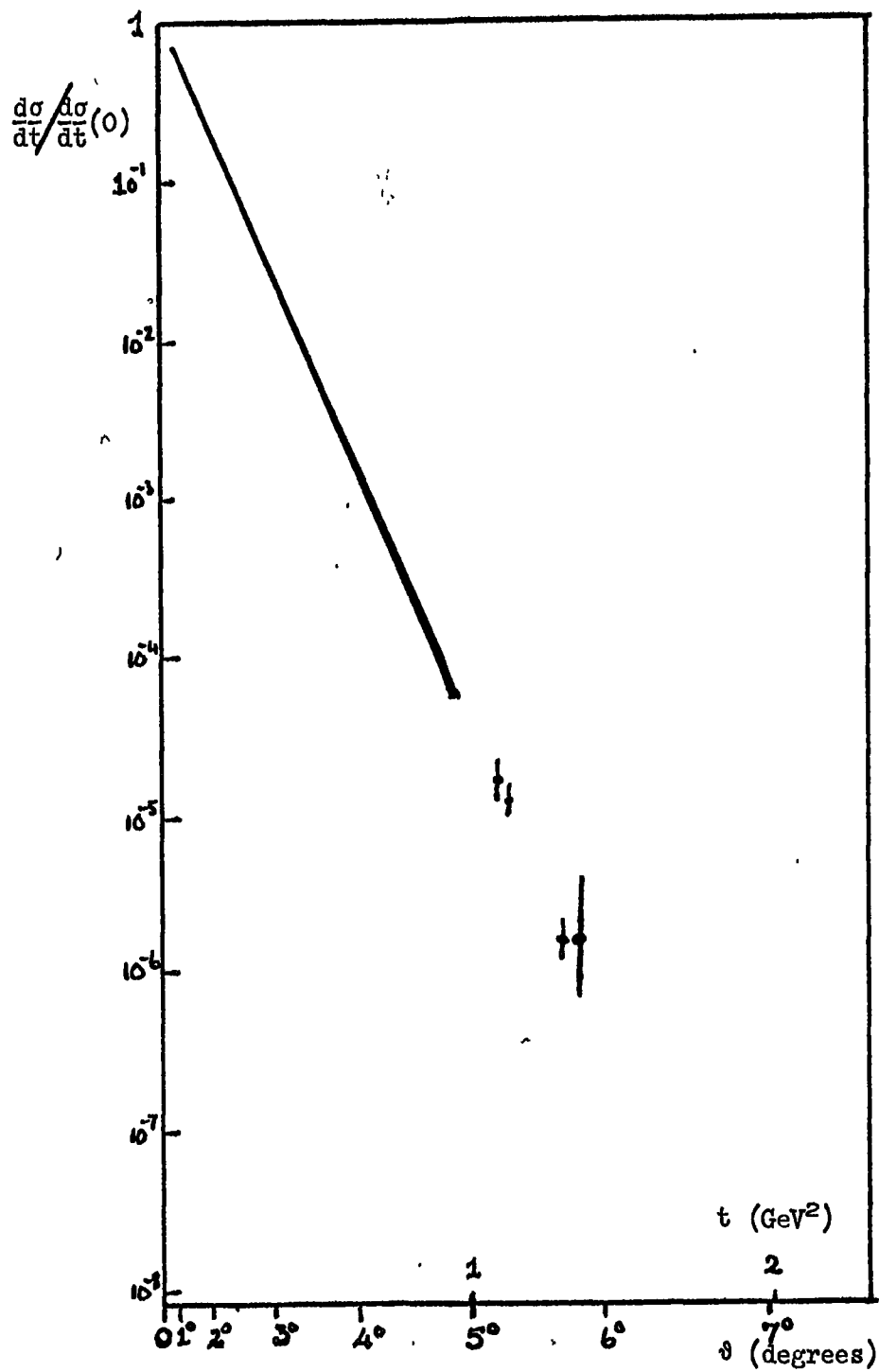


FIGURE 1.1a : The elastic differential cross-section for proton-proton scattering.  $\sqrt{s}=23$  GeV. (Data are shown in reference 1c)

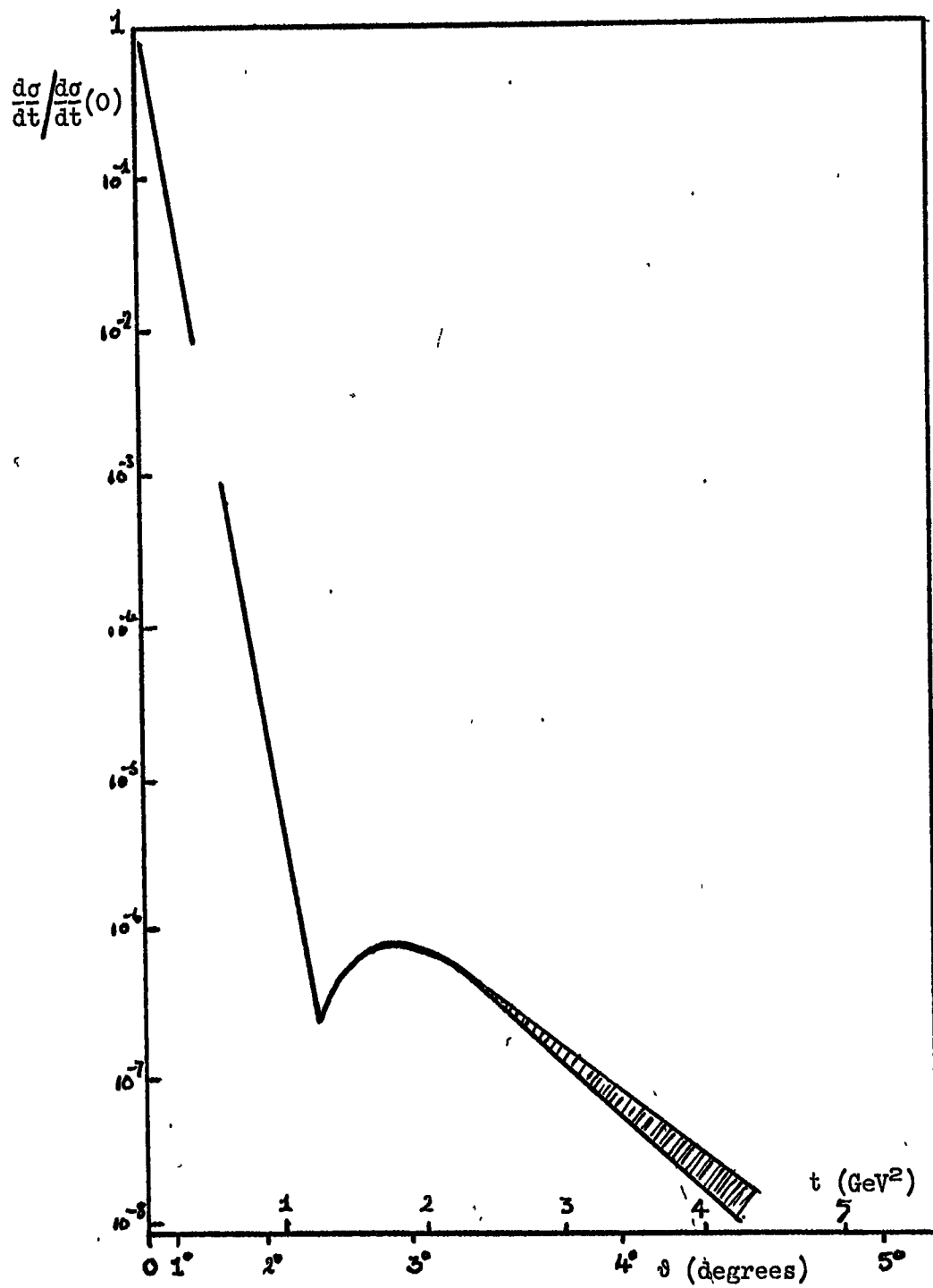


FIGURE 1.1b : The elastic differential cross-section for proton-proton scattering.  $\sqrt{s} = 53$  GeV .

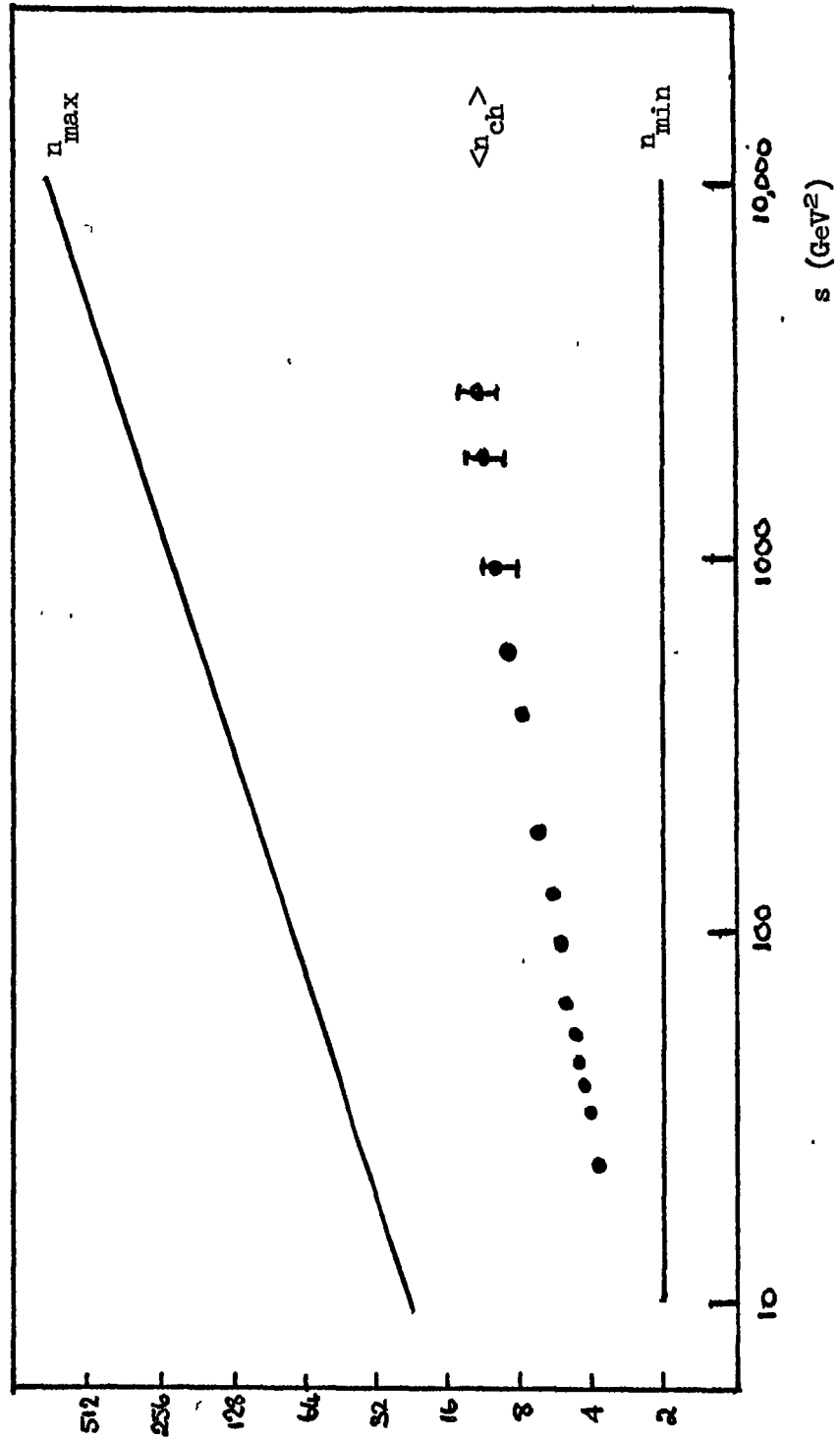


FIGURE 1.3 : The mean multiplicity of charged particles from proton-proton interactions. Also shown for comparison are the minimum and maximum kinematically allowed.

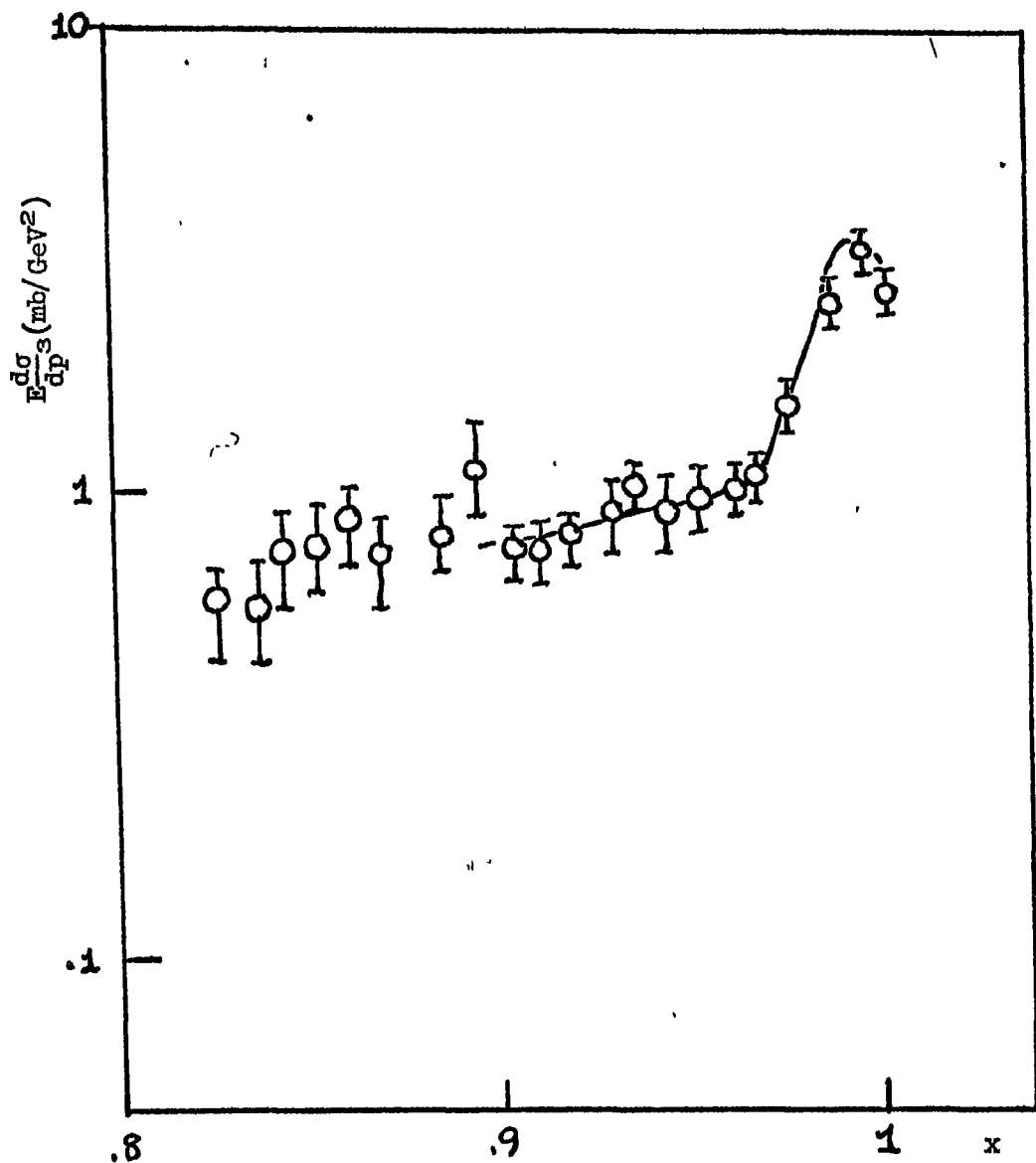


FIGURE 1.4 : The inclusive cross-section for  $pp \rightarrow pX$  near the forward direction showing the leading particle effect.  $p_t = 0.8 \text{ GeV}/c$ ,  $\sqrt{s} = 23 \text{ GeV}$ . Data from reference 43. The line is solely to guide the eye.



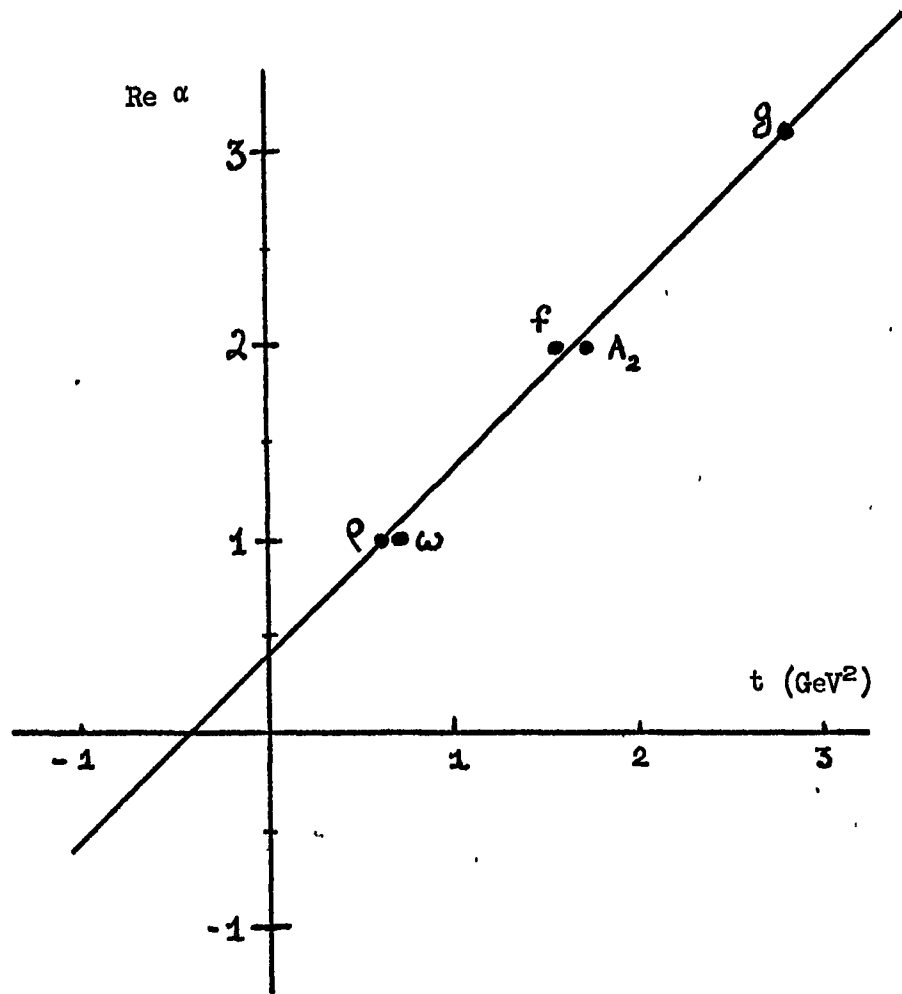


FIGURE 1.5 : A Chew-Frautschi plot showing the leading meson resonances. (For further evidence regarding linearity of trajectories see references 11 )

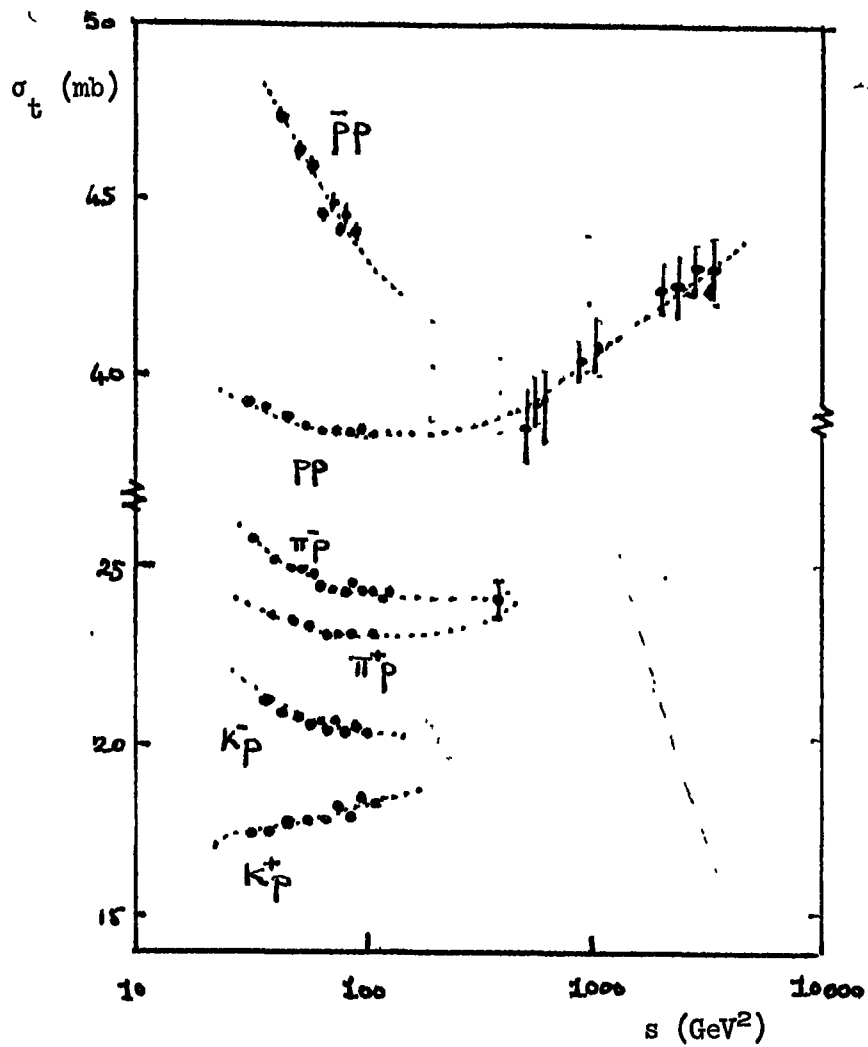


FIGURE 1.6 : Total cross-sections for various processes illustrating that non-exotic processes have a more significant falling contribution at small  $s$ . Data are summarised in reference 44 .

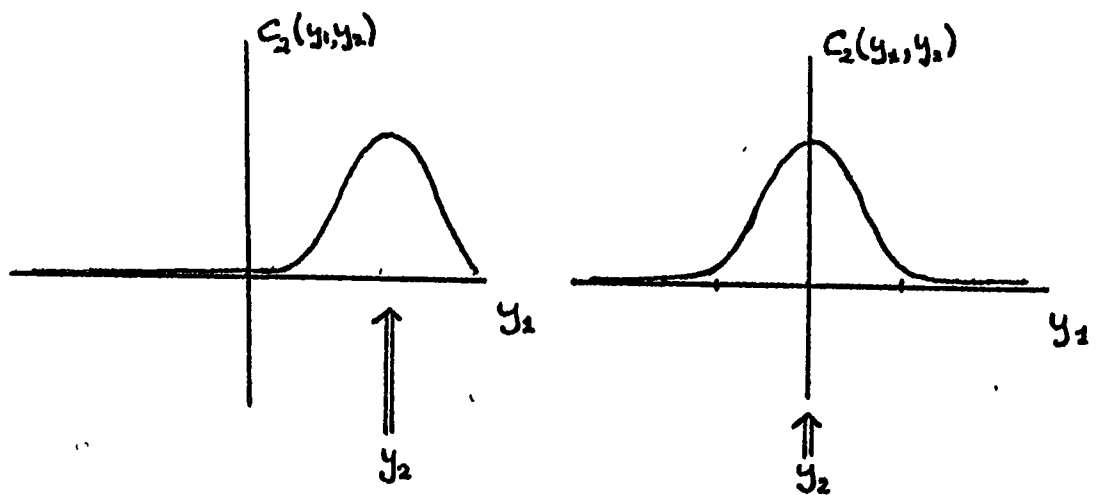
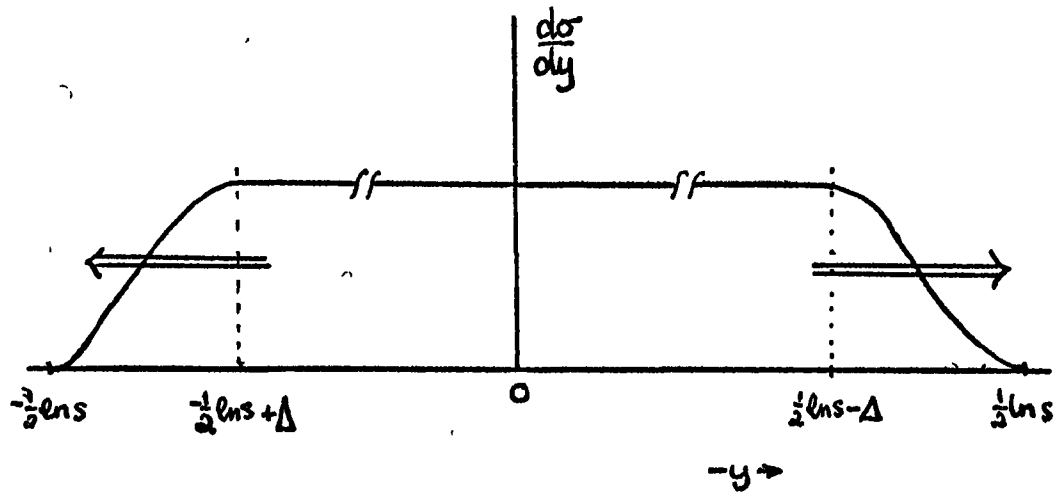


FIGURE 1.7 : The inclusive distribution and short range correlations predicted by the Mueller-Regge model. The arrows in the upper figure indicate the behaviour as  $s$  increases.

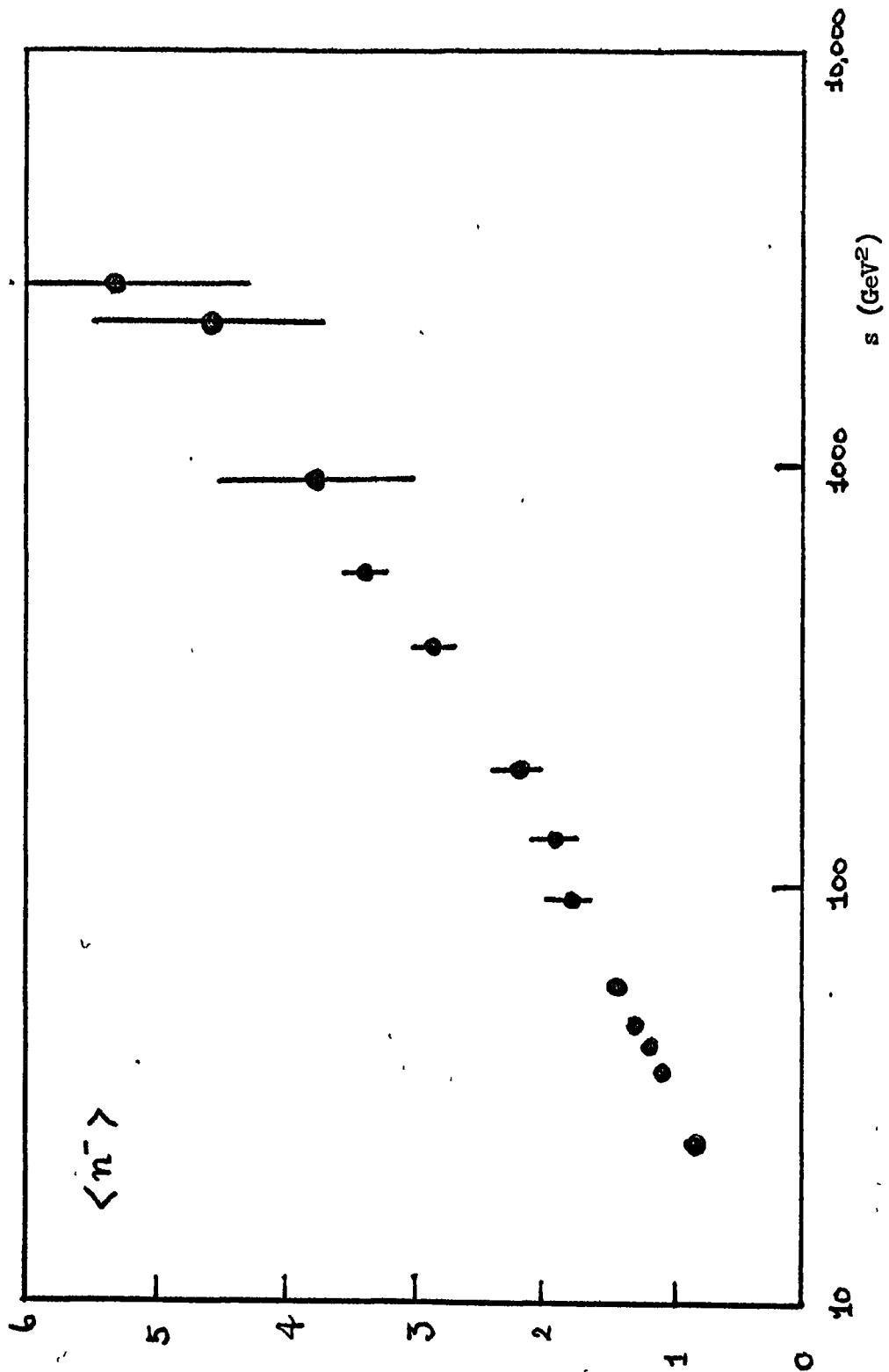


FIGURE 1.8 : The mean multiplicity from proton-proton collisions. The data in this and the following two figures is summarised in reference 1b, where references to the original papers may be found.

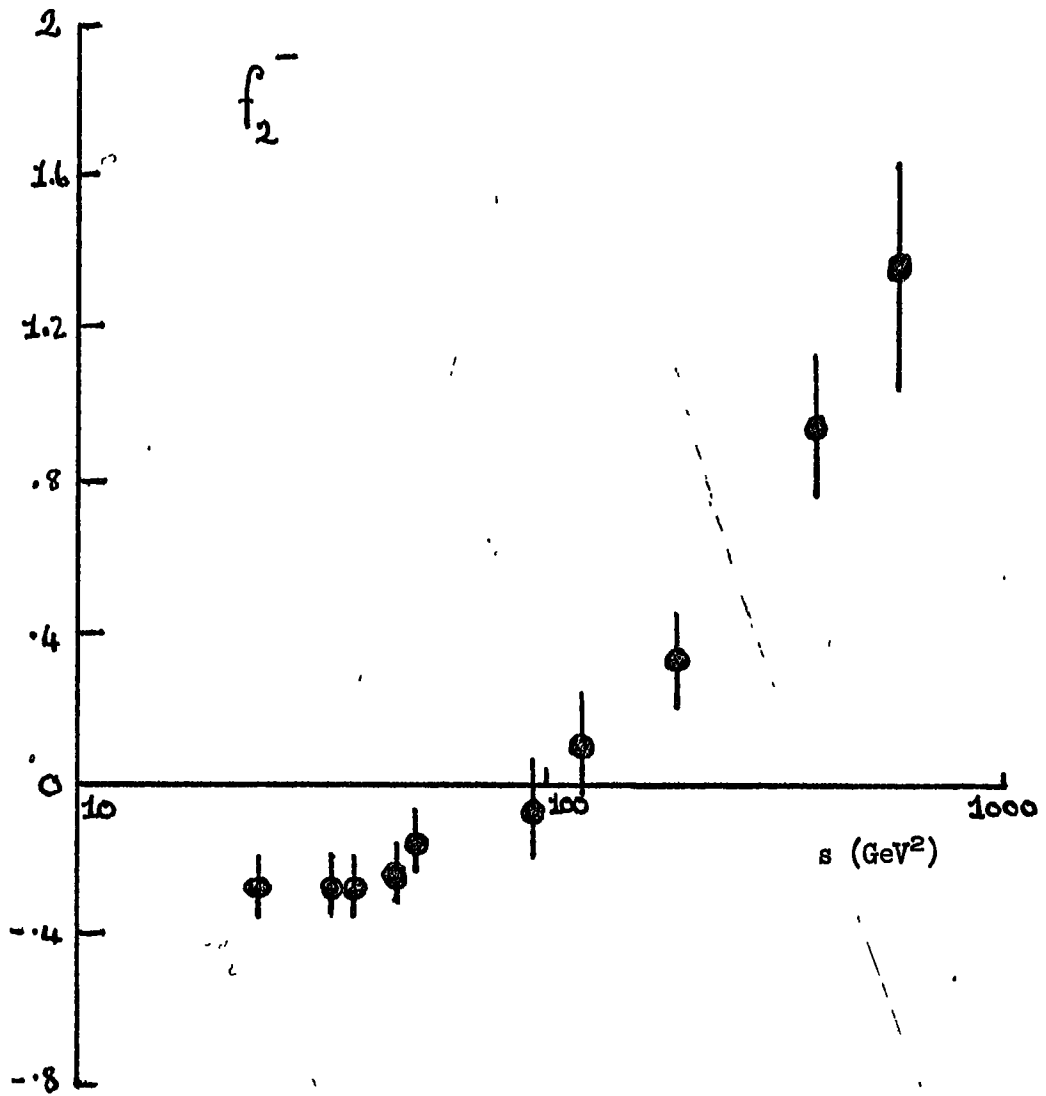


FIGURE 1.9 : The integrated two particle correlation  
in proton-proton interactions.

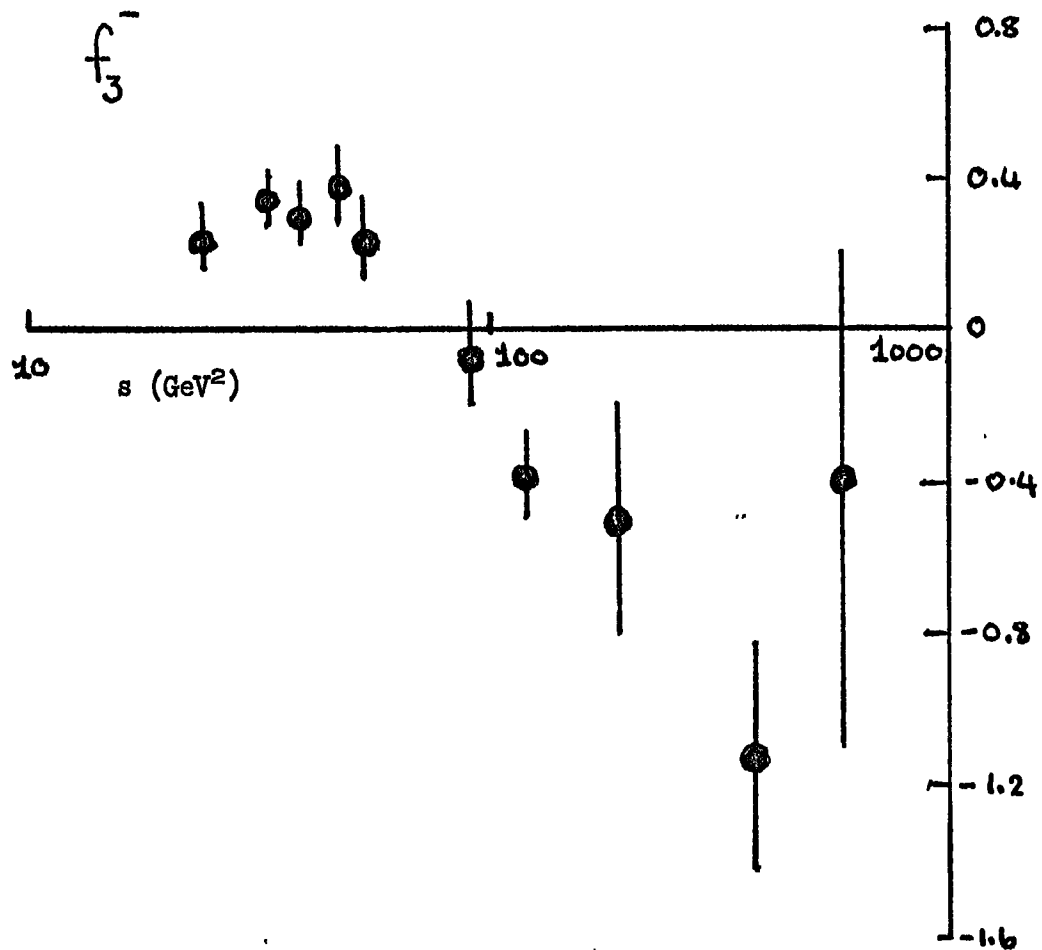


FIGURE 1.10 : The integrated three particle correlation in proton-proton interactions.

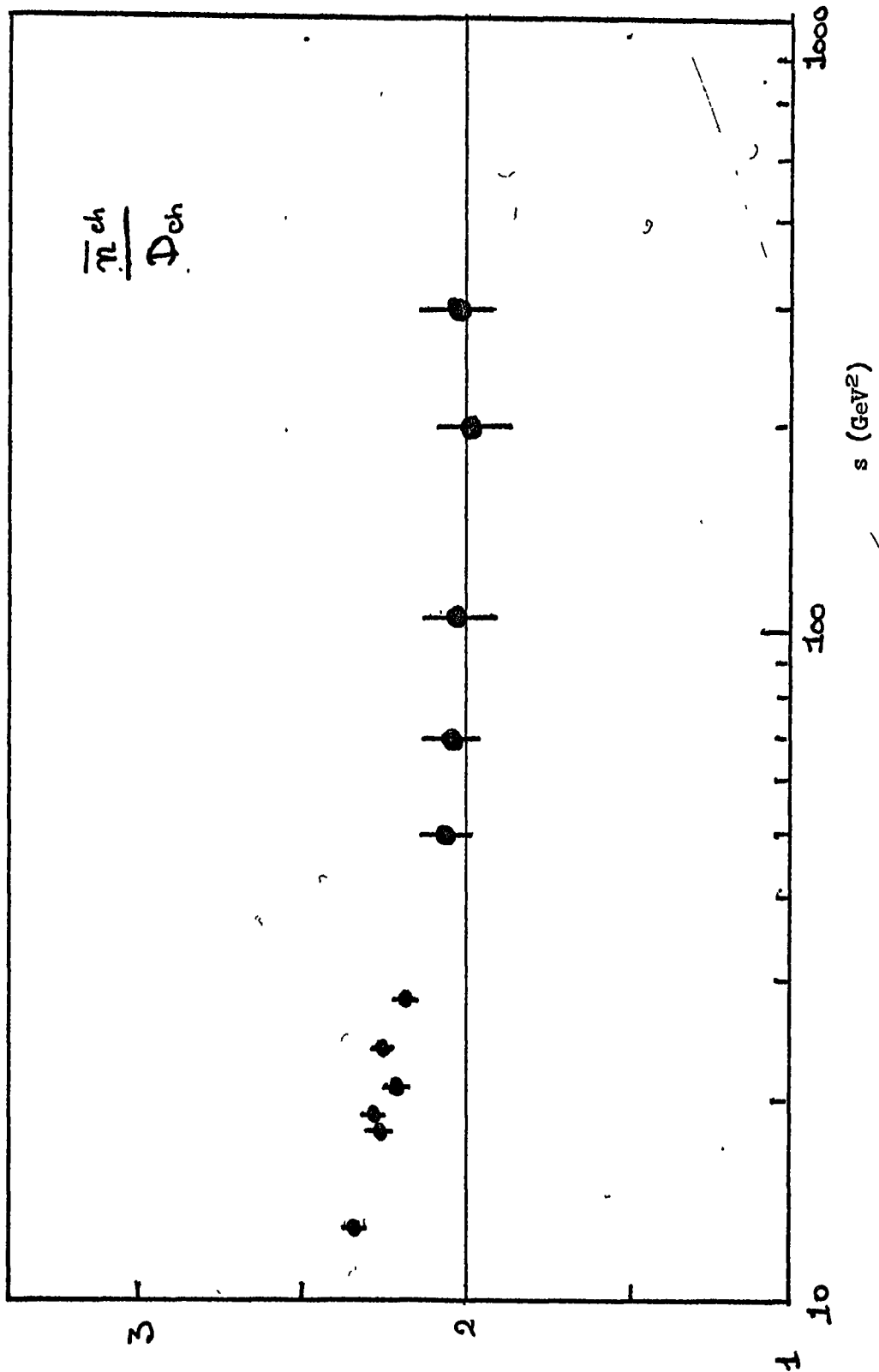


FIGURE 1.11 : The mean to width ratio for the multiplicity distribution in proton-proton interactions.

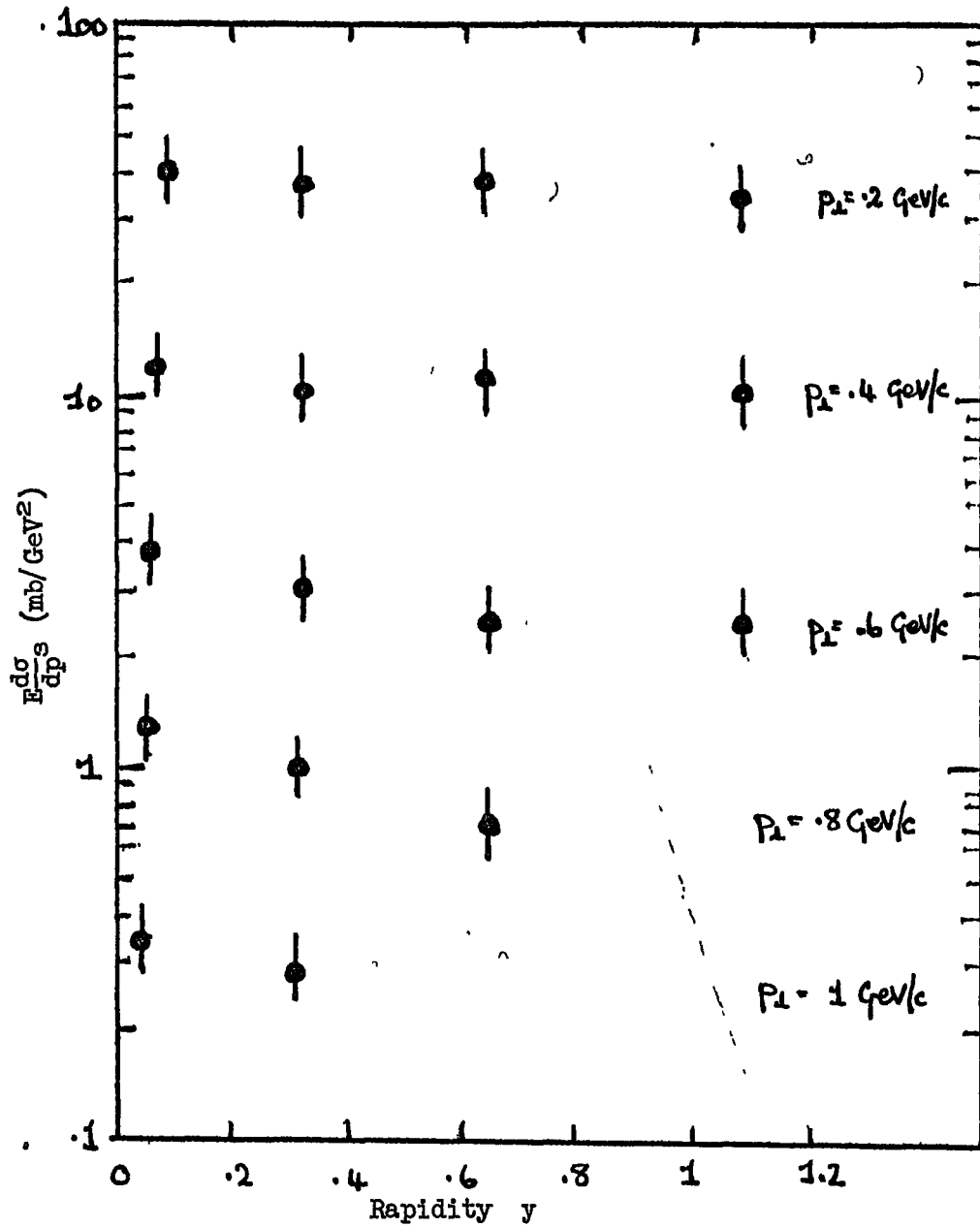


FIGURE 1.12 : The inclusive distribution for  $pp \rightarrow \pi$  in the central region with  $\sqrt{s} = 30.4$  GeV, for various values of  $p_t$ . Data are shown in reference 1b.



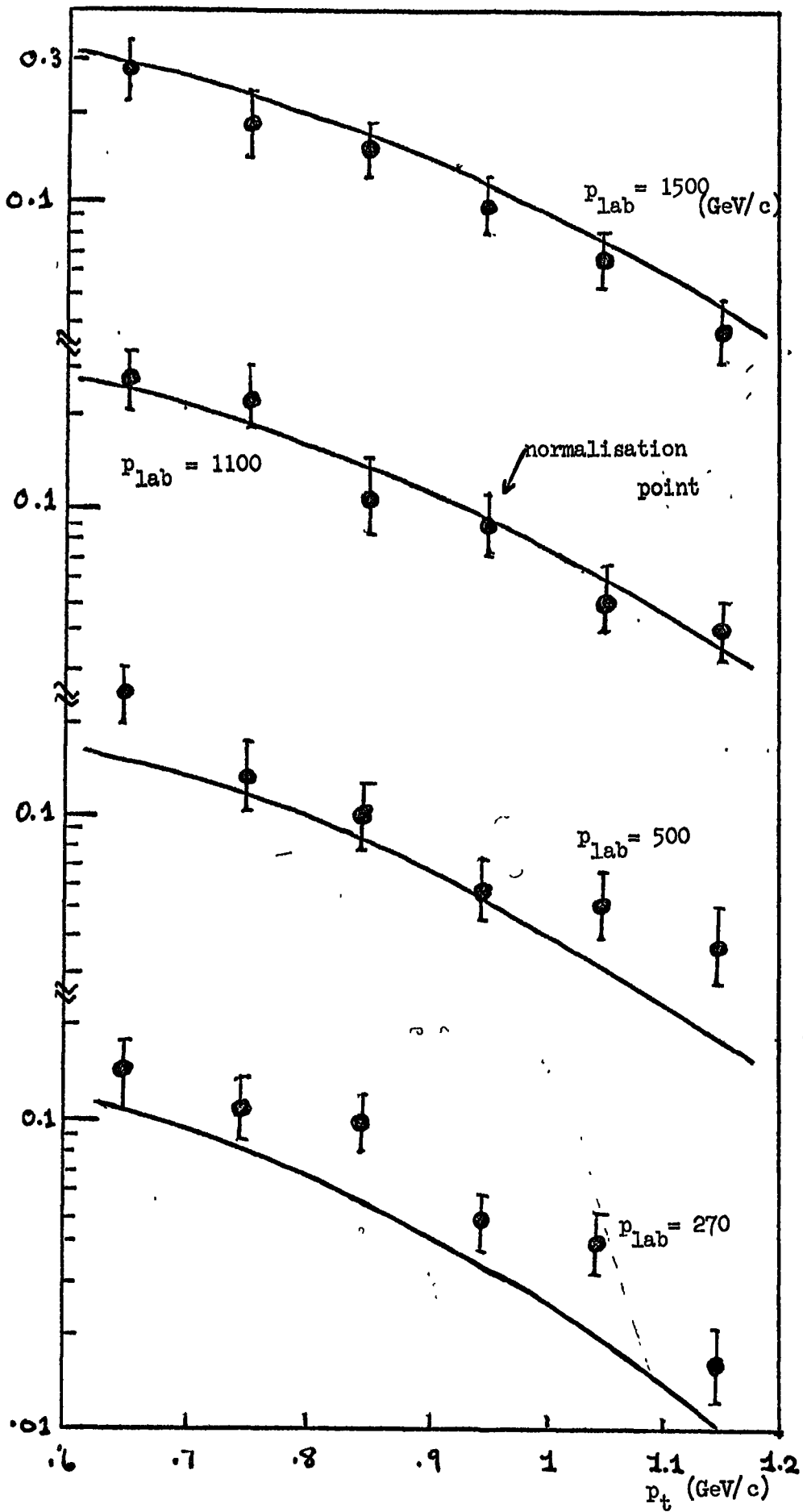


FIGURE 1.13 : Our fit to the antiproton production inclusive cross-section at  $x = 0$  over the I.S.R. energies. Data are from reference 45.

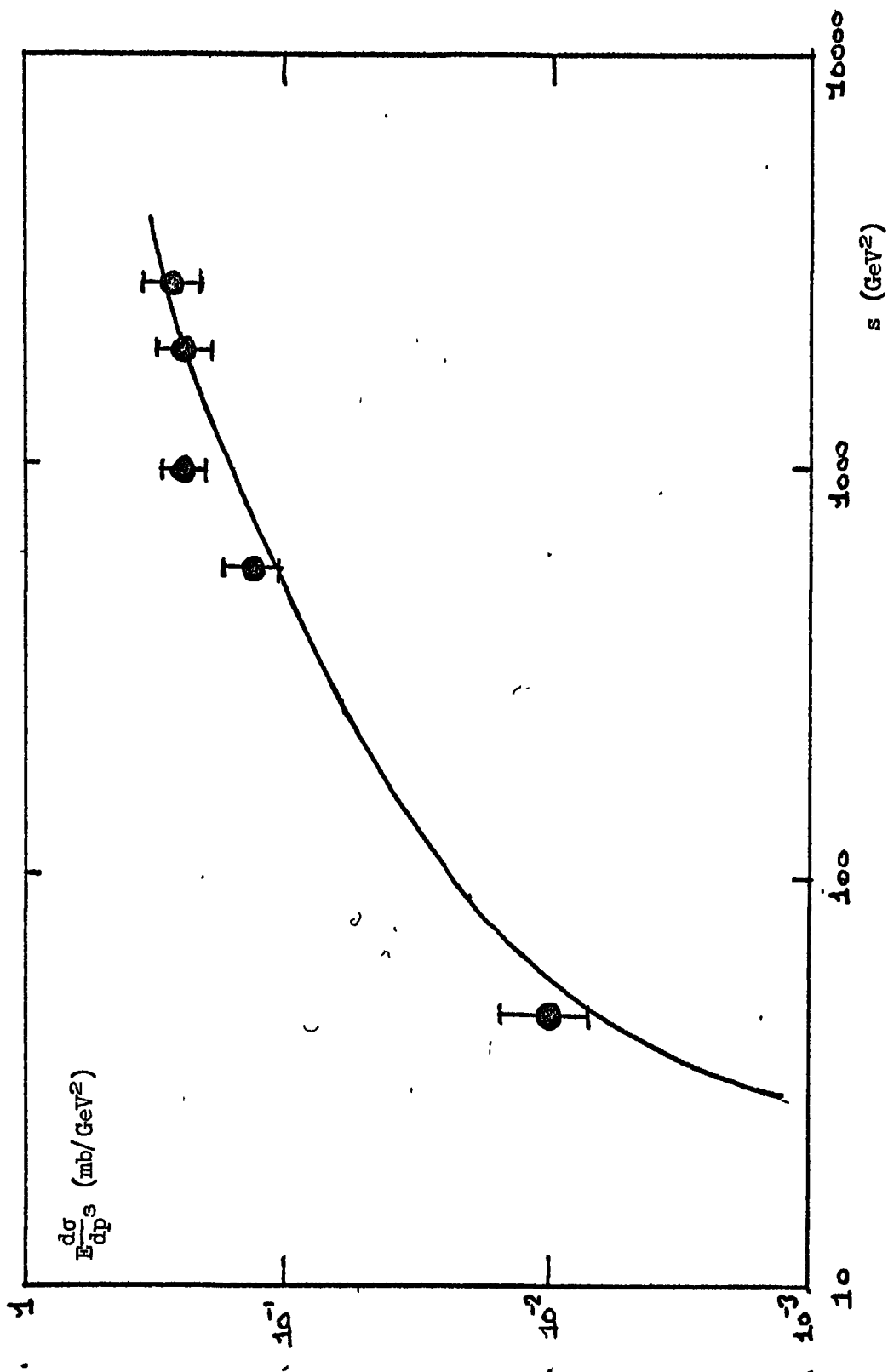


FIGURE 1.14 : The  $s$  dependence of the antiproton production cross-section at  $x=0$  and  $p_t=0.65$   $\text{GeV}/c$ , showing the extrapolation down to lower energy. The low energy datum is from reference 46.

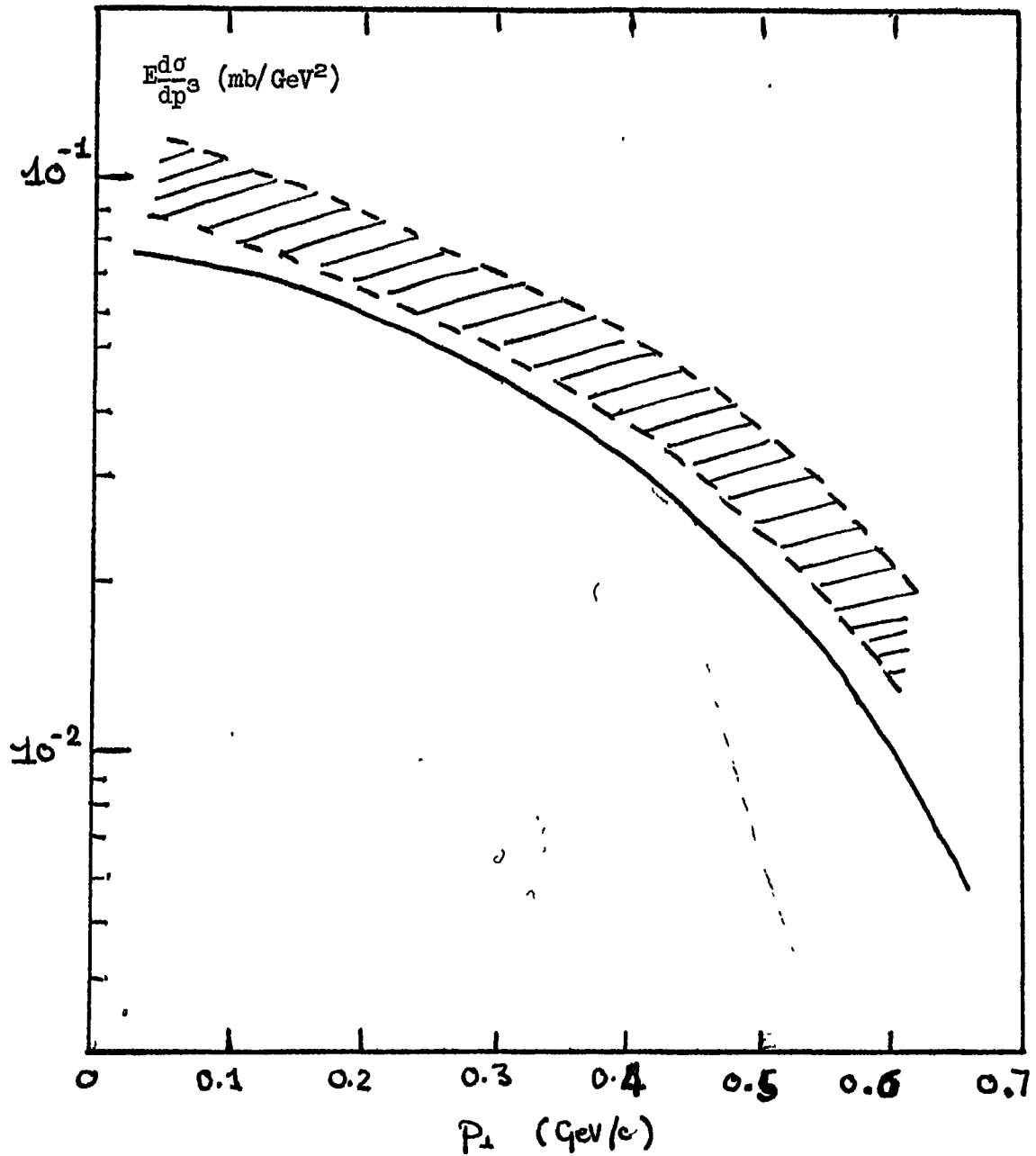


FIGURE 1.15 : The antiproton production cross-section. at  $p_{\text{lab}} = 24 \text{ GeV}/c$ , and  $x = 0$ . The line is the prediction of our model and the data<sup>46</sup> are represented by the shaded region.

## CHAPTER TWO

### A two component model

#### INTRODUCTION

This chapter concerns general features of the multiplicity distribution of particles produced in high energy collisions of protons, in particular with regard to a two component model. The model in its most general form is defined and discussed in the first section. The rest of the chapter is devoted to the formulation of a specific model<sup>II</sup> based on factorisable Regge pole exchange. The basis for the model is introduced in section two. In section three one possible mechanism (essentially multiperipheral) is introduced and an integral equation for the generating function of the multiplicity distribution is derived. Its solution is presented and discussed in sections four and five. The second, diffractive, mechanism is introduced in section six and the two mechanisms are compared in section seven. In section eight we discuss the features of the model arising from a fit to the proton-proton multiplicity distribution. In section nine we show that our fundamental assumption, that the multiplicity distribution is independent of the nature of the projectile, is in fact very restrictive. The final section discusses our model in the context of contemporary literature.

## 2.1 Features of the two component model

Before going on to describe our model, we shall in this section discuss the definitive features of the two component model and why such a model seems desirable.

The essence of the two component model lies in the supposition that particles may interact through two mechanisms which must be mutually distinct and must both (in any energy range one wishes to consider - usually asymptotically) give a non zero contribution to the total cross section. (Clearly if one of these conditions fails to hold, then one is back to having only one component.) The two mechanisms are usually supposed not to interfere, either on the grounds that their contributions are to different regions of phase space, or that their amplitudes are ninety degrees out of phase, one mechanism arising due to the pomeron which in the forward direction is purely imaginary, and the other to a purely real sum of exchange degenerate meson exchanges. We can now, even without further definition of the components, make some observations concerning some of the features of particle interactions according to this model.

To do this we write down the generating function for the multiplicity distribution of particles produced by each mechanism. (We shall denote the mechanisms a and b.)

$$\Phi_a(s, z) = \sum_n z^n \frac{\sigma_n^{(a)}(s)}{\sigma^{(a)}(s)} = \exp \left\{ \sum_{n=1}^{\infty} \frac{(z-1)^n}{n!} f_n^{(a)}(s) \right\} \quad (2.1)$$

$$\Phi_b(s, z) = \sum_n z^n \frac{\sigma_n^{(b)}(s)}{\sigma^{(b)}(s)} = \exp \left\{ \sum_{n=1}^{\infty} \frac{(z-1)^n}{n!} f_n^{(b)}(s) \right\}$$

And the generating function for the resultant multiplicity distribution :

$$\Phi(s, z) = \sum_n z^n \frac{\sigma_n(s)}{\sigma(s)} = \exp \left\{ \sum_{n=1}^{\infty} \frac{(z-1)^n}{n!} f_n(s) \right\} \quad (2.2)$$

$\sigma_n^{(a)}$ ,  $\sigma_n^{(b)}$ ;  $\sigma_n$  are the cross-sections for producing  $n$  particles from each mechanism and the resultant;  $\sigma^{(a)}$ ,  $\sigma^{(b)}$  are the total contributions of each mechanism, and  $\sigma$  is the total contribution of both. The  $f_n$  are the correlations defined in chapter one.

If there is no interference between the mechanisms we have

$$\sigma_n = \sigma_n^{(a)} + \sigma_n^{(b)} \quad (2.3)$$

and

$$\sigma = \sigma^{(a)} + \sigma^{(b)} \quad (2.4)$$

and hence

$$\Phi(s, z) = \alpha_a \Phi_a(s, z) + \alpha_b \Phi_b(s, z) \quad (2.5)$$

where

$$\alpha_a = \frac{\sigma^{(a)}}{\sigma} \quad ; \quad \alpha_b = \frac{\sigma^{(b)}}{\sigma} \quad (2.6)$$

and so

$$\alpha_a + \alpha_b = 1 \quad (2.7)$$

For quantities which are solely dependent on the total available energy  $\sqrt{s}$  and the multiplicity of the final state, equations (2.5) and (2.7) form the basic statement of the two component model. From (2.5) we can see how to sum the distributions in terms of their means and integrated correlations. Recovering these with

$$f_m = \left( \frac{\partial}{\partial z} \right)^m \ln \Phi \Big|_{z=1} \quad (2.8)$$

one finds (with some algebra in the case of the higher moments)

$$f_1 = \alpha_a f_1^{(a)} + \alpha_b f_1^{(b)} \quad (2.9)$$

$$f_2 = \alpha_a f_2^{(a)} + \alpha_b f_2^{(b)} + \alpha_a \alpha_b (f_1^{(a)} - f_1^{(b)})^2 \quad (2.10)$$

$$f_3 = \alpha_a f_3^{(a)} + \alpha_b f_3^{(b)} + 3\alpha_a \alpha_b (f_1^{(a)} - f_1^{(b)}) (f_2^{(a)} - f_2^{(b)}) - \alpha_a \alpha_b (\alpha_a - \alpha_b) (f_1^{(a)} - f_1^{(b)})^3 \quad (2.11)$$

$$f_4 = \alpha_a f_4^{(a)} + \alpha_b f_4^{(b)} + 4\alpha_a \alpha_b (f_3^{(a)} - f_3^{(b)}) (f_1^{(a)} - f_1^{(b)}) + 3\alpha_a \alpha_b (f_2^{(a)} - f_2^{(b)})^2 - 6\alpha_a \alpha_b (\alpha_a - \alpha_b) (f_2^{(a)} - f_2^{(b)}) (f_1^{(a)} - f_1^{(b)})^2 + \alpha_a \alpha_b (1 - 6\alpha_a \alpha_b) (f_1^{(a)} - f_1^{(b)})^4 \quad (2.12)$$

Inspecting these equations we see that the mean multiplicity  $f_1$  is, as one would perhaps have guessed, just the weighted sum of the mean multiplicities of each component mechanism. The correlations  $f_n$  ( $n > 1$ ) are, however, not quite so simple. There are in addition to the expected weighted sum of  $f_n^{(a)}$  and  $f_n^{(b)}$ , extra terms. To illustrate the importance of these terms it is interesting to see what happens if a and b are Poisson distributions. In this case

$$f_n^{(a)} = f_n^{(b)} = 0 \quad n \geq 2 \quad (2.13)$$

and hence

$$\bar{n} = \alpha_a \bar{n}_a + \alpha_b \bar{n}_b \quad (2.14)$$

$$f_2 = \alpha_a \alpha_b (\bar{n}_a - \bar{n}_b)^2 \quad (2.15)$$

$$f_3 = -\alpha_a \alpha_b (\alpha_a - \alpha_b) (\bar{n}_a - \bar{n}_b)^3 \quad (2.16)$$

$$f_4 = \alpha_a \alpha_b (1 - 6\alpha_a \alpha_b) (\bar{n}_a - \bar{n}_b)^4 \quad (2.17)$$

Thus in the case where we add uncorrelated distributions  $f_2$  is positive ;

$f_3$  is negative if the stronger component (the one with the larger  $\alpha$ ) has the higher mean and positive if otherwise ;  $f_4$  is positive unless  $\alpha_a$  and  $\alpha_b$  are sufficiently near to  $\frac{1}{2}$ . This illustrates clearly how the two component model can generate significant correlations from weakly correlated interaction mechanisms. But more than that, it predicts a particular form for the energy dependence of the correlations. To see what this is let us look again at the simple case where the individual mechanisms have weak correlations. From equations (2.9) - (2.17) we see that the two component effect will be most clearly dominant when the mean multiplicities of the components are very different. Let us examine how the width  $D$  of the multiplicity distribution varies, under the assumption that at high energies  $\bar{n}_a \gg \bar{n}_b$ . Recalling that

$$D^2 = f_2 + \bar{n} \quad (2.18)$$

we expand  $\bar{n}/D$  in inverse powers of  $(\bar{n}_a - \bar{n}_b)$  and find that

$$\frac{\bar{n}}{D} = \sqrt{\frac{\alpha_b}{\alpha_a}} + \frac{1}{(\bar{n}_a - \bar{n}_b)} \left\{ \frac{\bar{n}_b}{\sqrt{\alpha_a \alpha_b}} - \frac{\sqrt{\alpha_a}}{2\alpha_b \sqrt{\alpha_b}} \right\} + O\left(\frac{1}{(\bar{n}_a - \bar{n}_b)^2}\right) \quad (2.19)$$

This equation is true even if  $f_2^{(a)}$  and  $f_2^{(b)}$  are non-zero, provided that they are small compared to  $(\bar{n}_a - \bar{n}_b)^2$ . We can compare this expression directly with the data. This is shown in figure 2.1\*. The comparison is remarkably encouraging as  $\bar{n}/D$  may well have reached a constant at as low an energy as  $p_{\text{LAB}} = 50 \text{ GeV}/c$ . The immediate suggestion is that  $\alpha_a/\alpha_b \sim 4$ , or  $\alpha_a \sim 80\%$ ,  $\alpha_b \sim 20\%$ . Putting these values into equation (2.19) we have

$$\frac{\bar{n}}{D} = 2 + \frac{1}{(\bar{n}_a - \bar{n}_b)_{\text{ch}}} \left[ \frac{(\bar{n}_b^{\text{ch}} - 2)}{0.4} \right] + O\left(\frac{1}{(\bar{n}_a - \bar{n}_b)^2}\right) \quad (2.20)$$

---

\* This plot is often named after Wroblewski.



We note that we are comparing the model with the multiplicity distribution for charged particles arising from proton-proton collisions and so  $\bar{n}_b^{\text{ch}} \geq 2$ . Hence we are again encouraged in that the second order term in (2.19) and (2.20) has a positive sign in agreement with the data. We may also speculate from the rapid scaling behaviour of  $\bar{n}^{\text{ch}}/D^{\text{ch}}$  that the second order term is small.\* This is clearly ensured if  $\bar{n}_b^{\text{ch}}$  remains small (near to 2) whilst  $\bar{n}_a$  rises with energy. This is indeed a feature that will be necessary to our model, as will be seen in the following sections of this chapter. This feature also occurs in references 20-22.

At this point we could go on to discuss the momentum dependence of correlation functions in the two component model, but we postpone this until the next chapter, which is concerned specifically with this. We shall now proceed to formulate our model which gives us most naturally the integrated correlations discussed above. To summarise this section, then, we have seen that the two component model can generate significant correlations from weakly correlated mechanisms. If the two mechanisms have different mean multiplicities, the model has a very characteristic prediction for the correlations and in particular, with no further assumptions, it predicts very well the qualitative form of the mean to width ratio of the multiplicity distribution. We should like to note in passing that if the mean multiplicities of the two mechanisms are the same, then irrespective of any differences in their distributions, the two component effect would not occur in correlations lower than  $f_4$ , and so we stress that the two component effect is in essence due to a difference in the mean multiplicities of the mechanisms.

---

\* When we say here 'rapid' scaling we have in mind the slow energy dependence of the mean multiplicity discussed in chapter one.

Although the model has the characteristic features discussed above, it still has of course an enormous amount of freedom remaining in all that we have not said about the nature of the components. One of the objectives of the following sections is to reduce this freedom by constructing a model for the components, and by comparison with the measured multiplicity distribution from proton interactions to find what properties are required of our model.

## 2.2 A factorising model.

We shall now discuss the form of the multiplicity distribution generating function for a model in which interactions proceed through the exchange of a factorising Regge pole trajectory  $\alpha(t)$ . Factorisability allows us to talk of reggeon-particle scattering amplitudes and cross-sections etc., and we shall do so freely as it considerably simplifies discussion of the model. We factorise the scattering amplitude for particle-particle scattering as shown in diagram 2.1.

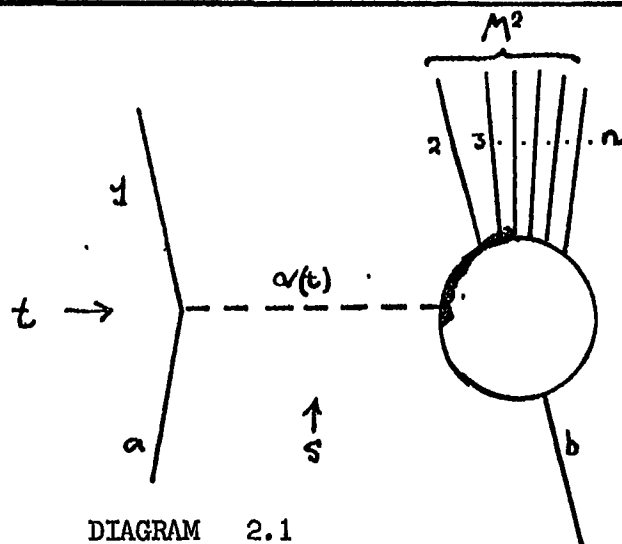


DIAGRAM 2.1

We write, therefore,

$$A_n(s; p_1 \dots p_n) = V(t) \left( \frac{s}{M^2} \right)^{\alpha(t)} \tilde{A}_{n-1}(M^2, t; p_2, \dots, p_n) S(t) \quad (2.21)$$

The notation here is as in chapter one.  $V(t)$  is the vertex function on the left of diagram 2.1.  $A_n$  is the particle scattering amplitude for  $a, b \rightarrow n$  particles;  $\tilde{A}_{n-1}$  is the reggeon-particle scattering amplitude for the production of  $n-1$  particles;  $(s/M^2)^{\alpha(t)}$  is the reggeon propagator factor in the large  $s$  limit when  $M^2$  may also be large.  $S(t)$  is the signature factor defined such that  $|S| = 1$ . We now factorise the phase space<sup>2</sup> in accord with 2.21.

$$d\Phi_n(s; p_1 \dots p_n) = \frac{dt dM^2 d\Phi_{n-1}(M^2; p_2 \dots p_n)}{16\pi^2 \lambda^2(s, m_a^2, m_b^2) \mu^2} \quad (2.22)$$

where

$$d\tilde{\Phi}_n(s; p_1, \dots, p_n) = \mu^{2-2n} (2\pi)^{4+3n} \delta^4(p - \sum_{i=1}^n p_i) \prod_{i=1}^n \frac{d^3 p_i}{2E_i} \quad (2.23)$$

$\mu$  is a unit mass solely to keep  $d\tilde{\Phi}_n$  dimensionless, and  $P_{\mu}^{\mu} = s$ .  $m_a$  and  $m_b$  are the masses of the incoming particles a and b.  $\lambda(a, b, c)$  is the usual triangle function. The cross-section  $\sigma_n(s)$  for  $a, b \rightarrow n$  is just

$$\sigma_n(s) = \frac{1}{2s} \int |A_n(s; p_1, \dots, p_n)|^2 d\tilde{\Phi}_n(s; p_1, \dots, p_n) \quad (2.25)$$

Inserting (2.21) and (2.22) into here we have

$$\sigma_n(s) = \frac{1}{16\pi^2 s} \int \frac{dt dM^2}{\mu^2} \left(\frac{s}{M^2}\right)^{2\alpha(t)-1} |V(t)|^2 \tilde{\sigma}_{n-1}(M^2; t) \quad (2.26)$$

where we have again assumed  $s \gg m_a^2, m_b^2$ , and have done the integration over the  $n-1$  particle phase space to get the cross-section for the scattering of a particle and a reggeon of mass  $t$  at total energy  $M$  into  $n-1$  particles. The tilde in this chapter and the following ones will always distinguish quantities which refer to reggeon-particle (including pomeron-particle) scattering.  $\tilde{\sigma}_1(M^2, t)$  must clearly be defined as

$$\tilde{\sigma}_2(M^2; t) = \pi \frac{s_0}{\mu^2} |V(t)|^2 \delta(M^2 - s_0) \quad (2.27)$$

with the normalisation so as to give

$$\frac{1}{\pi} \frac{d\sigma_2}{dt} = \frac{|V(t)|^4}{16\pi^2 \mu^4} \left(\frac{s}{s_0}\right)^{2\alpha(t)-2} \quad (2.28)$$

This is just the usual form for the differential cross-section for two particle scattering with Regge pole exchange. Equation (2.27) implies

that  $s_0$  should be interpreted as the average mass squared of one of the final state particles.

We next define the generating function discussed in the previous section. It is convenient here to have it normalised to the cross-section and so we write

$$\bar{I}(s, z) = \sum_{n=2}^{\infty} z^n \sigma_n(s) = \sigma_{\text{tot}}(s) \cdot \phi(s, z) \quad (2.29a)$$

and so

$$\bar{I}(s, 1) = \sigma_{\text{tot}}(s) \quad (2.29b)$$

We also define

$$\tilde{I}_+(s, t; z) = \sum_{n=1}^{\infty} z^n \tilde{\sigma}_n(s; t) \quad (2.30)$$

(The subscript + will later be useful to indicate that the  $n=1$  term is included) Thus from (2.26) we readily obtain

$$I(s, z) = \frac{z}{16\pi^2 \mu^2} \int dt \frac{dM^2}{M^2} \left(\frac{s}{M^2}\right)^{2\alpha(t)-2} |V(t)|^2 \tilde{I}_+(s, t; z) \quad (2.31)$$

This equation just takes us from the generating function for the multiplicity distribution in reggeon-particle scattering to that in particle-particle scattering. We have written it down in this section as we shall refer back to it to use it more than once in the following sections. We note here that because of the integral over the  $M^2$  variable, we must assume that the factorised Regge form is a reasonable average of what is happening when the  $t$  channel scattering angle is small ( $M^2$  large). This is an assumption of some form of global duality. (Note that we are not discussing the resonance region, but have  $s$  large throughout and are discussing the large  $M^2$  region). Our results should not in any event be very sensitive to this as we expect  $V(t)$  to contain a cut-off at large  $|t|$ , thus stressing the small  $M^2$  region strongly.

### 2.3 The multiperipheral integral equation

The last section made the statement that if we assume that interactions at high energy proceed through the exchange of a factorisable Regge pole and we know the reggeon-particle multiplicity distribution, then we can calculate the particle-particle multiplicity distribution. In this section we calculate the reggeon-particle generating function by assuming that reggeon-particle interactions proceed by Regge pole exchange. If, at sufficiently high energy we continue to apply this hypothesis we generate the multiperipheral model. This is shown diagrammatically in figure 2.2. We factorise the reggeon-particle amplitude exactly as in the last section.

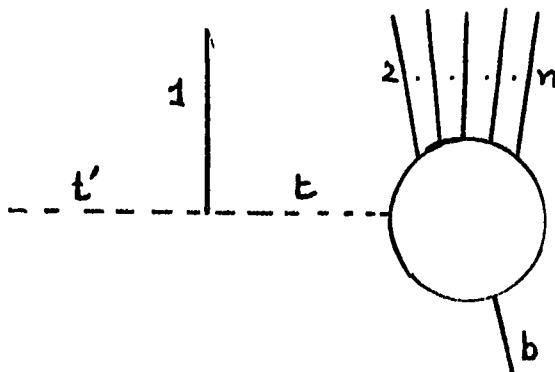


DIAGRAM 2.2 :  $t$  and  $t'$  are the 'masses' of the reggeons.

Instead of 2.26 we have now

$$\tilde{\sigma}_n(s; t') = \frac{1}{16\pi^2 \mu^2} \int dt \frac{dM^2}{M^2} \left(\frac{s}{M^2}\right)^{2\nu(t)-2} |\tilde{V}(t', t)|^2 \tilde{\sigma}_{n-1}(M^2; t) \quad (2.32)$$

$\tilde{V}(t', t)$  is the vertex on the left of diagram 2.2. If we assume that  $|\tilde{V}(t', t)|^2$  takes the form

$$|\tilde{V}(t', t)|^2 = g(t') g(t) \quad (2.33)$$

it follows that  $\tilde{\sigma}_n$  has the form

$$\tilde{\sigma}_n(s; t') = g(t') \tilde{\sigma}_n(s) \quad (2.34)$$

leaving

$$\tilde{\sigma}_n(s) = \frac{1}{16\pi^2 u^2} \int \frac{dM^2}{M^2} dt \left(\frac{s}{M^2}\right)^{2\alpha(t)-2} g^2(t) \tilde{\sigma}_{n-1}(M^2) \quad (2.35)$$

and thus the  $t'$  dependence is removed.

It will be convenient to define the variable

$$e = \frac{M^2}{s} \quad (2.36)$$

We also define

$$K(\rho) = \int_{-\infty}^{t_{\min}(\rho, s)} \frac{dt}{16\pi^2 u^2} g^2(t) e^{2-2\alpha(t)} \quad (2.37)$$

(We have not, here, made explicit any  $s$  dependence of  $K$  other than through  $\rho$  but we shall return to this point later.) Equation (2.35) now becomes

$$\tilde{\sigma}_n(s) = \int \frac{de}{e} K(\rho) \tilde{\sigma}_{n-1}(\rho s) \quad (2.38)$$

We now multiply by  $z^n$  and sum, obtaining in exactly the same way as in the previous section

$$\tilde{I}(s, z) = z \int \frac{de}{e} K(\rho) \tilde{I}_+( \rho s, z) \quad (2.39)$$

where

$$\tilde{I}_+(s, z) = \sum_{n=1}^{\infty} z^n \tilde{\sigma}_n(s) \quad (2.40)$$

and

$$\tilde{I}(s, z) = \tilde{I}_+(s, z) - z \tilde{\sigma}_1(s) \quad (2.41)$$

Equation (2.39) thus forms an integral equation which will determine the generating function for the reggeon-particle multiplicity distribution. The multiplicity distribution for particle scattering can then be obtained using (2.31).<sup>\*</sup> This integral is a generalisation of that obtained for the cross-section in multiperipheral models by Chew et al.<sup>24</sup>

---

\* This integral equation was obtained independently and somewhat differently by Jengo, Krzywicki, and Petersson<sup>23</sup>. Their motivation and treatment of the equation differ from ours. We should also like, at this stage, to thank A.Krzywicki for helpful discussion.



## 2.4 Solution of the integral equation

We now solve the equation (2.39) arrived at in the previous section and discuss some of the properties of the solution. First let us note that if we assume that the vertices shown in diagram 2.3 have the same  $t$  dependence, then comparison of equations (2.31) and (2.39), (neglecting any difference in  $t_{\min}$  for exchanges at different points in the multiperipheral chain), shows us that the only difference between the particle scattering generating function,  $I(s, z)$ , and  $\tilde{I}(s, z)$ , the reggeon-particle scattering generating function for at least two particles in the final state, is a constant factor. Thus the normalised generating functions  $\phi(s, z) = I(s, z)/I(s, 1)$  and  $\tilde{\phi}(s, z) = \tilde{I}(s, z)/\tilde{I}(s, 1)$  are the same and hence so are the multiplicity distributions. We could of course relax this assumption concerning the  $t$  dependence, but we should like to stress that we are interested in minimising the number of free parameters remaining when we come to fit the data, and the above is the most natural assumption to make. The conclusion it leads

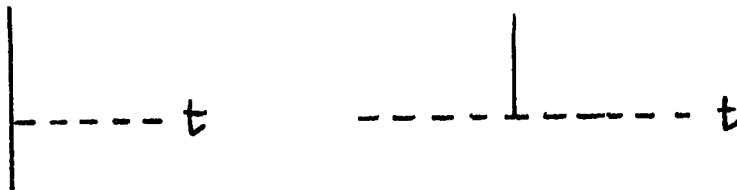


DIAGRAM 2.3 : Dashed lines are reggeons, full lines are particles.

to (i.e. that reggeon-particle and particle-particle multiplicity distributions are the same) is discussed further in the following chapters. Thus we put

$$I(s, z) = C \cdot \tilde{I}(s, z) \quad (2.42)$$

and so (2.39) becomes

$$I(s, z) = z \int_{\frac{s}{2}}^1 \frac{d\rho}{\rho} K(\rho) \left\{ I(\rho s, z) + z \cdot C \cdot \tilde{\sigma}_1(\rho s) \right\} \quad (2.43)$$

Here  $\nu$  is the minimum possible missing mass. Two points should perhaps be noted at this stage. Firstly we did not have to define  $\tilde{\sigma}_1$ . We proceeded as we did because the form (2.27) of  $\tilde{\sigma}_1$  is simple to handle. The other is that  $K(\rho)$  will depend very little on  $s$ . Equation (2.37) shows us that the only  $s$  dependence at fixed  $\rho$  that can enter  $K(\rho)$  does so through the function  $t_{\min}(\rho, s)$ . Let us examine this function. If we consider the process  $a, b \rightarrow c, d$  with  $t = (p_c - p_a)^2$  then

$$t_{\min} = \frac{1}{2s} \left\{ \lambda^{\frac{1}{2}}(s, m_a^2, m_b^2) \lambda^{\frac{1}{2}}(s, m_c^2, m_d^2) - s^2 + 2s(m_a^2 + m_b^2 + m_c^2 + m_d^2) - (m_a^2 - m_b^2)(m_c^2 - m_d^2) \right\} \quad (2.44)$$

If we now expand this in the limit when  $s \gg m_a^2, m_b^2, m_c^2$  and  $m_d = M$  with  $\rho = M^2/s$ , we find

$$t_{\min} \approx - \frac{(m_b^2 - m_a^2)\rho + m_a^2 \rho^2}{1 - \rho} \quad (2.45)$$

where here we have neglected terms smaller by factors of  $m_a^2/s$  etc.

Thus at high energy  $K(\rho)$  depends only on  $\rho = M^2/s$ . We also note that if  $g(t)$  is small for  $|t|$  large, (for example an exponential), then equation (2.37) tells us that if we write

$$K(\rho) = e^{2-2\alpha(\rho)} k(\rho) \quad (2.46)$$

then  $k(\rho)$  cuts off as  $\rho$  approaches 1. Having noted these properties of  $K(\rho)$  we proceed formally to solve (2.43). To do this we first write (2.43) in terms of logarithmic variables which we define by

$$\begin{aligned} Y &= \ln \frac{s}{\nu^2} \\ y &= \ln \frac{M^2}{\nu^2} = \ln \frac{\rho}{\nu^2} \\ \lambda &= -\ln \frac{M^2}{s} = -\ln \rho \\ Y &= y + \lambda \end{aligned} \quad (2.47)$$

Then (2.43) is just

$$\mathbb{I}(e^y, z) = z \int_0^y d\lambda K(e^{-\lambda}) \left\{ \mathbb{I}(y-\lambda, z) + z C \tilde{\sigma}_1(y-\lambda) \right\} \quad (2.48)$$

This convolution integral now suggests the use of a Laplace transform which has the property

$$\mathcal{L} : \int_0^y d\lambda F(\lambda) \cdot G(y-\lambda) = [\mathcal{L} : F] [\mathcal{L} : G] \quad (2.49)$$

Hence defining the Laplace transforms

$$\mathbb{I}_L(\omega, z) = \int_0^\infty e^{-\omega y} \mathbb{I}(e^y, z) dy \quad (2.50)$$

$$K_L(\omega) = \int_0^\infty e^{-\lambda \omega} K(e^{-\lambda}) d\lambda \quad (2.51)$$

$$D(\omega) = \int_0^\infty e^{-\omega y} C \tilde{\sigma}_1(y) dy \quad (2.52)$$

then (2.48) transforms to

$$\mathbb{I}_L(\omega, z) = z K_L(\omega) \left\{ \mathbb{I}_L(\omega, z) + z D(\omega) \right\} \quad (2.53)$$

which upon rearrangement becomes

$$\mathbb{I}_L(\omega, z) = \frac{z^2 D(\omega) K_L(\omega)}{1 - z K_L(\omega)} \quad (2.54)$$

To recover the generating function we invert the transform

$$\mathbb{I}(e^y, z) = \frac{1}{2\pi i} \int_C e^{\omega y} \mathbb{I}_L(\omega, z) d\omega \quad (2.55)$$

$\mathcal{C}$  here is the usual contour parallel to the imaginary axis in the complex  $\omega$  plane. From (2.27) we have

$$D(\omega) = C e^{-\omega y_0} \quad (2.56)$$

where all constant factors have been absorbed into  $C$  and  $y_0 = \ln(s/v^2)$ . We expect  $K_L(\omega)$  to vanish as  $|\omega| \rightarrow \infty$  in the left half of the complex plane, and so we can close the contour  $\mathcal{C}$  in the left half of the complex  $\omega$  plane. (We are of course interested in  $Y > y_0$ ). At high energy (2.55) allows us to take the leading pole contribution from (2.54). This will come from a zero in  $1 - zK_L(\omega)$ . It will become clear in what follows that we expect a simple pole. The total cross-section  $\sigma = I(s,1)$  is thus asymptotically a power of  $s$  and the Froissart bound implies that

$$1 - zK(\omega) = 0 \quad (2.57)$$

can only have a solution  $\omega \leq 0$  when  $z=1$ . (Comparison of the usual  $j$ -plane transformation with the optical theorem (1.7) and equation (2.50) reveals  $\omega = j-1$ ). Letting the solution to (2.57) be

$$\omega = f(z) \quad (2.58)$$

we have  $f(z)$  given by (2.51) and (2.57). We have, then, the implicit equation

$$\int_0^{\infty} e^{-\lambda f(z)} K(e^{-\lambda}) d\lambda = \frac{1}{z} \quad (2.59a)$$

or

$$\int_0^1 \frac{de}{e} e^{f(z)} K(e) = \frac{1}{z} \quad (2.59b)$$

or

$$K_L(f(z)) = \frac{1}{z} \quad (2.59c)$$

We have then

$$I(e^y, z) = \text{Residue at } w=f(z) \left\{ \frac{z^2 D(w) K_L(w) e^{wy}}{1 - z K_L(w)} \right\} \quad (2.60)$$

That is

$$I(e^y, z) = \frac{z^2 D(w) K_L(w) e^{yw}}{\frac{d}{dw}(1 - z K_L(w))} \Big|_{w=f(z)} \quad (2.61)$$

From (2.59c) we observe

$$-\frac{1}{z^2} = \frac{d}{dz} K_L(f(z)) = \frac{df}{dz} \frac{dK_L(w)}{dw} \Big|_{w=f(z)} \quad (2.62)$$

and so we find using (2.56)

$$I(e^y, z) = C z^2 \frac{df}{dz} e^{(y-y_0)f(z)} \quad (2.63a)$$

or

$$I(s, z) = C z^2 \frac{df}{dz} \left(\frac{s}{s_0}\right)^{f(z)} \quad (2.63b)$$

This result defines the multiplicity distribution of the model.

We should like to point out here that although the low multiplicity cross-section appears explicitly in the above derivation, the shape of the multiplicity distribution is insensitive to this. It is determined solely by  $f(z)$  which is dependent on the kernel.

## 2.5 Properties of the multiplicity distribution of the model

### (a) Total cross-section and correlations

We can now discuss features of the multiplicity distribution just derived, even before calculation of  $f(z)$ . We note that the total cross-section must behave like a power of  $s$ . If we denote the intercept of the output trajectory (i.e. that of the singularity in the imaginary part of the elastic amplitude) by  $\alpha_{out}$  then

$$\sigma_t \sim s^{\alpha_{out} - 1} \quad (2.64)$$

Equation (2.29) tells us

$$\sigma_t(s) = I(s, 1) = c \left. \frac{df}{dz} \right|_{z=1} \cdot \left( \frac{s}{s_0} \right)^{f(1)} \quad (2.65)$$

and so

$$f(1) = \alpha_{out} - 1 \quad (2.66)$$

(For the sake of discussion we retain generality here although later we shall choose  $\alpha_{out}$  to be a pomeron singularity ( $\alpha_{out}=1$ ) to obtain an asymptotically non-vanishing cross-section.)

To obtain the correlations we expand  $f(z)$  about  $z=1$  defining constants  $c_n$  by

$$f(z) = \sum_{n=0}^{\infty} c_n \frac{(z-1)^n}{n!} \quad (2.67)$$

We thus have

$$c_0 = \alpha_{out} - 1 \quad (2.68)$$

and the correlations

$$f_n(s) = c_n \ln^n \frac{s}{s_0} + d_n \quad (2.69)$$

where the constants  $d_n$  are also determined by (2.63). The mean multiplicity and the correlations are thus linearly dependent upon  $\ln(s)$ . This is the well known short range correlation property of multi-peripheral models.

(b) n-particle production cross-sections and Regge intercepts.

We now examine equation (2.59) which determines  $f(z)$ . At  $z = 1$  this becomes

$$\int_0^1 \frac{d\rho}{\rho} \rho^{\alpha_{out}-1} K(\rho) = 1 \quad (2.70)$$

Thus the intercept of the output trajectory for a given input singularity determines the overall size of  $K(\rho)$ , that is the strength of the reggeon-reggeon-particle coupling. The definition (2.37) of  $K(\rho)$  suggests that

$$K(\rho) \underset{\rho \rightarrow 0}{\propto} \rho^{2-2\alpha(o)} \quad (2.71)$$

and so the above integral converges if

$$(\alpha_{out}-1) - (2\alpha(o)-2) > 0 \quad (2.72a)$$

and (2.59) converges for  $z$  such that

$$f(z) + 2 - 2\alpha(o) > 0 \quad (2.72b)$$

We shall discuss these inequalities in a moment, but first let us examine the consequences of (2.69) for the  $n$  particle production cross-sections. Looking at the generating function (2.63), we quickly find that

$$\sigma_n \sim \tau_n(\ln s) s^{f(o)} \quad (2.73)$$

where the functions  $\tau_n$  depend at most upon a finite power of  $\ln(s)$ .

Although we cannot evaluate  $f(0)$  from (2.59) directly we have from

(2.67)

$$f(s) = \sum_{n=0}^{\infty} \frac{(-1)^n c_n}{n!} \quad (2.74)$$

These equations show that all the  $\sigma_n$  behave asymptotically like the same power of  $s$ . This criterion is often quoted as characteristic of the multiperipheral model. It is, however, more generally true of any model possessing only short range correlations. As we discussed earlier the short range correlation hypothesis leads to correlations of the logarithmic form (2.69) which in turn leads to (2.73).

Comparison of (2.73) with the power behaviour expected of  $\sigma_2$  from (2.28) gives

$$f(s) = 2\alpha(s) - 2 \quad (2.75)$$

and so now the interpretation of (2.72a) is just that

$$\frac{\sigma_n}{\sigma_t} \underset{s \rightarrow \infty}{\sim} s^{-\epsilon} \quad (2.76)$$

with  $\epsilon$  strictly greater than zero and the same for all  $n$ . This emphasises the difficulty of putting a multiperipheral chain, a difficulty first pointed out by Finkelstein and Kajantie<sup>25</sup>. It is also just the condition discussed earlier, which was shown in reference 9 for models with the property (2.69).

We also note in passing that an alternative way of expressing this is the following. If we were to make a model with the output trajectory the same as the input, that is  $\alpha_{\text{out}} = \alpha(0)$ , then equation (2.72a) becomes

$$\alpha(0) < 1 \quad (2.77)$$

which excludes the pomeron.



(c) A constraint on the model

We now turn to a point drawn attention to by Harari<sup>26</sup>. If we combine equations (2.68), (2.74), and (2.75) we obtain

$$\alpha_{out} = 2\alpha(0) - 1 - \sum_{n=1}^{\infty} \frac{(-1)^n c_n}{n!} \quad (2.78)$$

Thus if we know the trajectory intercepts  $\alpha_{out}$  and  $\alpha(0)$ , then we have a relation amongst the  $c_n$ . This relation is quite general as we have used only the leading power in  $s$  to derive it irrespective of logarithmic terms. The consistency of the data with this relation is tested in a paper of Harari and Rabinovici<sup>22</sup>, who assume a two component model, one of whose components has the short range correlation property (2.69). Their result is that the first two terms of the sum in (2.78) are roughly consistent with  $\alpha_{out}=1$  and  $\alpha(0) = 0.5 \pm 0.1$ . We shall further discuss their model later in the chapter, but we wish to stress here that in the interaction calculated in the previous sections, the relation (2.78) is an in-built constraint. Our viewpoint is that this equation follows for models with only short range correlations, and so consistent with the belief that long range correlations are generated primarily by the two component effect, it should be allowed to constrain the model. Thus, perhaps we shall be able, from the results of comparing the model with the data, to say more about the particular features required of it. This indeed turns out to be the case, as we shall see later.

(d) An explicit solution to the integral equation for the generating function

So far we have presented an integral equation for the multiplicity distribution generating function and provided a solution in terms of a function  $f(z)$  defined implicitly in (2.59) in terms of the kernel of the integral equation. In this section we have discussed some properties of this solution. It will be instructive here to consider an explicit solution in an approximation where one is feasible. Later when we compare our model with the data we shall attempt a more

realistic solution. So for now let us take the approximation that  $t_{\min} = 0$  for the exchange in diagram 2.2, and calculate the consequences for a fixed pole exchange

$$\alpha(t) \equiv \alpha \quad (2.79)$$

Taking the vertex function to be an exponential function of  $t$

$$g(t) = A e^{\beta t} \quad (2.80)$$

(2.37) tells us that

$$K(p) = g^2 e^{2-2\alpha} \quad (2.81)$$

where all the multiplicative constants have been absorbed into  $g^2$ . Our function  $f(z)$  is now defined by

$$\int_0^1 \frac{de}{e} p^{2-2\alpha+f(z)} = \frac{1}{g^2 z} \quad (2.82)$$

from which by performing the integration we find

$$f(z) = g^2 z + 2\alpha - 2 \quad (2.83)$$

We note that the integral converges for  $z > 0$  (c.f. equation (2.72b)). Thus from the solution (2.63) of our integral equation we find

$$I(s, z) = C g^2 z^2 \left(\frac{s}{s_0}\right)^{2\alpha-2+g^2} + g^2(z-1) \quad (2.84)$$

and so

$$\sigma_{tot} \propto \left(\frac{s}{s_0}\right)^{2\alpha-2+g^2} \quad (2.85)$$

and the normalised generating function is

$$\phi(s, z) = z^2 \left( \frac{s}{s_0} \right)^{g^2(z-1)} \quad (2.86)$$

From (2.85) we see that

$$\alpha_{out} = 2\alpha - 1 + g^2 \quad (2.87)$$

and (2.86) will be recognised as the generating function for a Poisson distribution in  $n-2$  particles. The mean of the distribution is just

$$\langle n \rangle = g^2 \ln \frac{s}{s_0} + 2 \quad (2.88)$$

Equation (2.87) is typical of multiperipheral-type models although with a more complicated kernel this will also be more complicated. Equations (2.87) and (2.88) illustrate the constraint (2.78) where in this case it is satisfied by

$$c_1 = g^2 ; \quad c_n = 0 \quad n \geq 2 \quad (2.89)$$

Finally we remark that the model discussed in this sub-section where the multiplicity distribution turns out to be completely uncorrelated (Poisson) is just the well known model of Chew and Pignotti<sup>27</sup>. (This is also nicely summarised in references 1a, 28.)

(e) The need for another mechanism

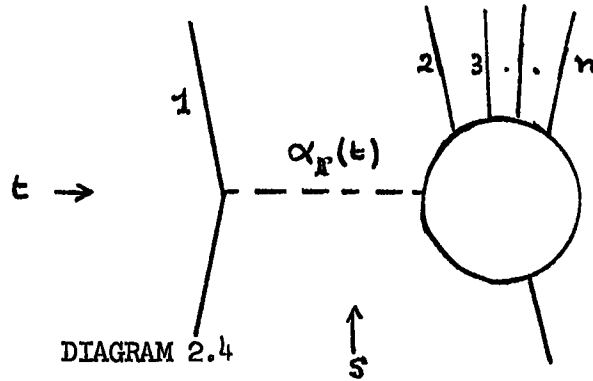
Without discussion of the momentum dependence of correlations and inclusive distributions, the need for a second mechanism is already apparent. Let us calculate  $\bar{n}/D$  in this model and compare with the calculation in section 2.1. For this model we find

$$\frac{\bar{n}}{D} \underset{s \rightarrow \infty}{\sim} \frac{c_1}{\sqrt{c_1 + c_2}} (\ln s)^{1/2} \quad (2.90)$$

(Notice that this displays the property  $D^2 = \bar{n}$  for a Poisson distribution -  $c_2 = 0$ ). The data (see figure 2.1) show no sign of a rise in this quantity at high energy and so we are attracted to the ideas presented in section 2.1. As discussed there we should now be looking for a low multiplicity mechanism to give the required effect. The need for a correction to the low multiplicity end of the distribution is obviated by the fact that  $\sigma_2$  in the model that we have derived so far (and indeed  $\sigma_n$ ) must fall with energy to zero. It seems natural then to base a second component on pomeron exchange in the  $2 \rightarrow n$  amplitude.

## 2.6 Diffraction - a second mechanism

To calculate this mechanism we go back to the basic calculation of section 2.2 and look at pomeron exchange. We redraw diagram 2.2 with a pomeron exchange :



For this diagram equation 2.31 gives us

$$I_D(s, z) = \frac{z}{16\pi^2 u^2} \int dt \frac{dM^2}{M^2} \left(\frac{s}{M^2}\right)^{2\alpha_P(t)-2} |V_P(t)|^2 \tilde{I}_P(M^2, z) \quad (2.91)$$

$V_P$  is just the vertex on the left of diagram 2.4 ;  $\tilde{I}_P$  is the pomeron-particle scattering generating function ;  $I_D$  is the generating function for the (diffractive) process shown in diagram 2.4 .

We now make an assumption which will later prove to be a powerful constraint on any fit to the data. We assume that the multiplicity distribution arising from pomeron-particle collisions is just the same as that arising from reggeon-particle collisions. We allow the total cross-sections of these processes, however, to be different. Thus we have an intuitive picture of the probability of interaction of two objects being dependent upon the nature of the objects, but once they interact, all 'knowledge' of what the original objects were is lost, and thus the relative probabilities of producing  $n$  particles for

various  $n$  is independent of the incident objects. Further consequences of this assumption are discussed in detail later. Continuing with the calculation we have

$$\tilde{I}_p(s, z) = \frac{\tilde{\sigma}_{pp}(s)}{\tilde{\sigma}_{Rp}(s)} \tilde{I}_+(s, z) \quad (2.92)$$

where  $\sigma_{pp}$  and  $\sigma_{Rp}$  are the pomeron-particle and reggeon-particle cross-sections respectively.  $\tilde{I}_+$  is known from the calculation of the previous sections. We perform the  $t$  integration as before defining

$$K_p(\rho) = \frac{1}{16\pi^2 \mu^2} \int_{-\infty}^{t_{\min}(\rho)} dt |V_p(t)|^2 e^{2-2\alpha_p(t)} \quad (2.93)$$

leaving

$$I_D(s, z) = z \int_{\frac{1}{s}}^1 \frac{de}{e} K_p(\rho) \tilde{I}_p(e^s, z) \quad (2.94)$$

in analogy with (2.37) and (2.39). Again we have denoted by  $\nu$  the minimum possible value of the missing mass  $M$ . Using (2.63) and (2.41) we find

$$I_D(s, z) = z^2 \sigma_{p_2}(s) + z^3 \frac{df}{dz} c\left(\frac{s}{s_0}\right) \int_{\frac{1}{s}}^1 \frac{de}{e} \frac{\sigma_{pp}(\rho s)}{\sigma_{Rp}(\rho s)} e^{f(z)} K_p(\rho) \quad (2.95)$$

In the next section we shall calculate the correlations from not only this mechanism but also the multiperipheral mechanism. We shall then examine the features of the resultant two component model and compare with the data.

## 2.7 Calculation of the model

### (a) The non-diffractive component

In constructing the two component model from the mechanisms discussed, it is natural to look for the correlations of each component and to use the equations of section one. We first calculate the non-diffractive, 'pionisation' component, which we shall from now on label with the letter  $\pi$ . We have

$$f_n^\pi = c_n \ln \frac{s}{s_0} + d_n \quad (2.96)$$

where

$$f(z) = \sum \frac{c_n (z-1)^n}{n!} \quad (2.97)$$

We calculate the  $c_n$  from equation (2.59) which was

$$\int_0^1 \frac{de}{e} e^{f(z)} K(p) = \frac{1}{z} \quad (2.98)$$

by expanding about  $z = 1$ . Because this integral must be convergent near  $z = 1$ , it is natural to calculate the correlations  $f_n$  rather than the cross-sections  $\sigma_n$ . As our model is attempting to describe the strong interaction particularly in terms of many-particle final states, we stress that it is an attractive feature of this scheme that the multiplicity distribution is most conveniently calculated by first finding the mean, then the width, and then the more subtle correlations. If we define the integrals

$$Q_j = (-1)^j \int_0^1 \frac{de}{e} (\ln e)^j K(p) \quad (2.99)$$

then equation (2.98) becomes at  $z=1$

$$Q_0 = 1 \quad (2.100)$$

where we now restrict our attention to the case  $\alpha_{\text{out}} = 1$  or  $f(1) = 0$

to give an asymptotically non-vanishing pionisation component.

Successive differentiation with respect to  $z$  at  $z=1$  reveals from (2.98)

using (2.97)

$$c_1 Q_1 = 1 \quad (2.101)$$

$$-c_2 Q_1 + c_1^2 Q_2 = 2! \quad (2.102)$$

$$c_3 Q_1 - 3c_2 c_1 Q_2 + c_1^3 Q_3 = 3! \quad (2.103)$$

$$-c_4 Q_1 + (3c_2^2 + 4c_1 c_3) Q_2 - 6c_1^2 c_2 Q_3 + c_1^4 Q_4 = 4! \quad (2.104)$$

and so on.

Thus the  $c_n$  can be calculated in turn. We find then

$$c_1 = Q_1^{-1} \quad (2.105)$$

$$c_2 = Q_1^{-3} \{ Q_2 - 2! Q_1^2 \} \quad (2.106)$$

$$c_3 = Q_1^{-5} \{ 3Q_2(Q_2 - 2! Q_1^2) - Q_1(Q_3 - 3! Q_1^3) \} \quad (2.107)$$

and

$$c_4 = Q_1^{-7} \{ Q_1^2(Q_4 - 4! Q_1^4) - 4Q_1 Q_2(Q_3 - 3! Q_1^3) \\ + 12Q_2^2(Q_2 - 2! Q_1^2) - 6Q_1 Q_3(Q_2 - 2! Q_1^2) + 3Q_2(Q_2 - 2! Q_1^2)^2 \} \quad (2.108)$$

The normalised generating function for the pionisation component is

$$\Phi_{\pi}(s, z) = z^2 \frac{f'(z)}{f'(1)} \left( \frac{s}{z} \right)^{f(z)} \quad (2.109)$$



and so

$$d_n = \left( \frac{d}{dz} \right)^n \ln \frac{z^2 f'(z)}{f'(1)} \Big|_{z=1} \quad (2.110)$$

(1)  
Thus the constants  $d_n$  are determined in terms of the constants  $c_n$

$$d_1 = 2 + c_2/c_1 \quad (2.111)$$

$$d_2 = -2 + c_3/c_1 - (c_2/c_1)^2 \quad (2.112)$$

$$d_3 = 4 + c_4/c_1 - \frac{3c_2c_3}{c_1^2} + 2 \left( \frac{c_2}{c_1} \right)^3 \quad (2.113)$$

To calculate the integrals  $Q_j$  let us recall the definition and discussion of  $K(\rho)$  from sections three and four. Writing again

$$K(\rho) = \rho^{2-2\alpha(0)} k(\rho) \quad (2.114)$$

$$K_p(\rho) = \rho^{2-2\alpha_p(0)} k_p(\rho) \quad (2.115)$$

we expect  $k(\rho)$  and  $k_p(\rho)$  to become small as  $\rho \rightarrow 1$ . This followed from the assumption of a strong dominance of the small  $|t|$  region. Rather than making an ansatz for  $V(t)$  and calculating  $K(\rho)$ , we make an ansatz directly for  $K(\rho)$  embodying the features discussed. We put then

$$K(\rho) = \rho^{2-2\alpha(0)} A \cdot [1 - b\rho] \Theta(1 - b\rho) \quad (2.116)$$

and similarly

$$K_p(\rho) = \rho^{2-2\alpha_p(0)} A_p [1 - b_p\rho] \Theta(1 - b_p\rho) \quad (2.117)$$

where  $A, A_p, b, b_p$  are constants and the  $\Theta$  step functions ensure that

$K$  and  $K_p$  are positive. We now evaluate the constants  $Q_j$  from (2.99) and determine  $A$  from (2.100). Thus

$$Q_j = \frac{j!}{[2-2\alpha(s)]^j} \frac{[1 - b \left[ \frac{2-2\alpha(s)}{3-2\alpha(s)} \right]^{j+1}]}{[1 - b \left[ \frac{2-2\alpha(s)}{3-2\alpha(s)} \right]^{j+1}]} \quad \text{if } b \leq 1 \quad (2.118)$$

and

$$Q_j = \frac{j! [3-2\alpha(s)]}{[2-2\alpha(s)]^j} \left\{ e_j([2-2\alpha(s)] \ln b) - \left[ \frac{2-2\alpha(s)}{3-2\alpha(s)} \right]^{j+1} e_j([3-2\alpha(s)] \ln b) \right\} \quad \text{if } b > 1 \quad (2.119)$$

where

$$e_j(x) = \sum_{i=0}^j \frac{x^i}{i!} \quad (2.120)$$

Thus the constants  $c_n$  can now be obtained from equations (2.105)-(2.108) and hence the constants  $d_n$ . The non-diffractive component of our model is thus calculated in terms of the parameter  $b$ . (We note that as  $b \rightarrow 0$  we find  $Q_j = j!(2-2\alpha(0))^{-j}$  and hence  $c_n = 0$  for  $n \geq 2$ . This is, as expected, just the Chew-Pignotti model again.)

(b) The diffractive component

The diffractive component is now simply calculable in terms of the already known constants  $c_n$  from equation (2.95). To do this we let

$$\frac{\sigma_{Pp}(s)}{\sigma_{Rp}(s)} \sim \left( \frac{s}{s_0} \right)^{-\gamma} \quad ; \quad \gamma \geq 0 \quad (2.121)$$

As we have taken  $\sigma_{Rp}$  to be constant,  $\gamma$  will measure the  $s$  dependence of the forward elastic pomeron-particle scattering amplitude. In

triple Regge language  $\gamma = 0$  corresponds to a non-zero triple pomeron coupling. We also wish to normalise to the inelastic part of the total cross-section and we do this simply by approximating the elastic cross-section to be just the two particle diffractive cross-section at high energies. We shall return to these points in later discussion. Equation (2.95) now becomes

$$\bar{I}_D(s, z) = z^3 \frac{df}{dz} c \left( \frac{s}{s_0} \right)^{-\gamma + f(z)} \int_{\frac{\sqrt{s}}{s_0}}^1 \frac{de}{e} c [1 - b_p \rho] \theta(1 - b_p e)^{f(z) - \gamma} \quad (2.122)$$

As  $f(1)=0$  this integral is very much determined by the behaviour of the integrand as  $\rho \rightarrow 0$ , and the lower limit of integration. Here we assume a diffractive contribution due to a pomeron-pomeron-reggion coupling and postpone discussion of the triple pomeron case. Taking  $\gamma > 0$  then we have

$$\bar{I}_D(s, z) = z^3 \frac{df}{dz} \frac{c \left( \frac{\sqrt{s}}{s_0} \right)^{f(z) - \gamma}}{\gamma - f(z)} \quad (2.123)$$

to leading order in  $s$ . Thus at high energy this diffractive contribution produces a constant inelastic (and total) cross-section and also a multiplicity distribution which is asymptotically independent of  $s$ . (c.f. references 20-22). The multiplicity distribution given by (2.123) can now be calculated in terms of  $f(z)$  and the new parameter  $\gamma$ . The correlations are most simply calculated in the following form. The normalised generating function is

$$\Phi_D(s, z) = z^3 \frac{f'(z)}{f'(1)} \left( \frac{\sqrt{s}}{s_0} \right)^{f(z)} \frac{\gamma}{\gamma - f(z)} \quad (2.124)$$

We thus observe from (2.109) that

$$\frac{\Phi_{\pi}(s, z)}{\Phi_D(s, z)} = \frac{\gamma - f(z)}{\gamma z} \left(\frac{s}{v^2}\right)^{f(z)} \quad (2.125)$$

And so we can calculate more easily

$$f_n^{\pi} - f_n^D = \left(\frac{\partial}{\partial z}\right)^n \ln \frac{\Phi_{\pi}}{\Phi_D} \Big|_{z=1} \quad (2.126)$$

and substitute these expressions directly into the two component model.

We then find

$$f_1^{\pi} - f_1^D = c_1 \ln \frac{s}{v^2} - [1 + c_1/\gamma] \quad (2.127)$$

$$f_2^{\pi} - f_2^D = c_2 \ln \frac{s}{v^2} + [1 - \frac{c_1^2}{\gamma^2} - c_2/\gamma] \quad (2.128)$$

$$f_3^{\pi} - f_3^D = c_3 \ln \frac{s}{v^2} - [2 + \frac{2c_1^3}{\gamma^3} + \frac{3c_1c_2}{\gamma^2} + \frac{c_3}{\gamma}] \quad (2.129)$$

We rewrite equations (2.9)-(2.11) in the form

$$f_1 = f_1^D + p_{\pi} (f_1^{\pi} - f_1^D) \quad (2.130)$$

$$f_2 = f_2^D + p_{\pi} (f_2^{\pi} - f_2^D) + p_{\pi} p_D (f_1^{\pi} - f_1^D)^2 \quad (2.131)$$

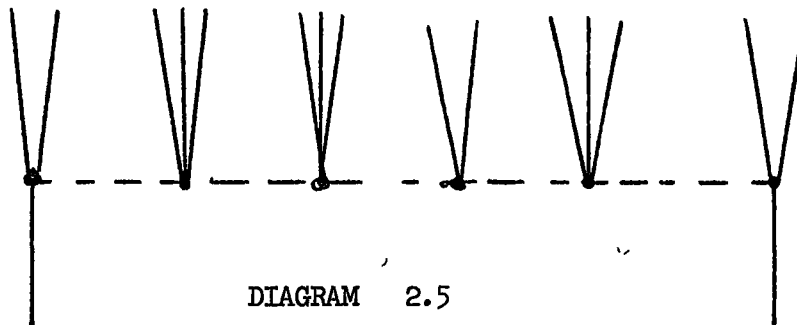
$$f_3 = f_3^D + p_{\pi} (f_3^{\pi} - f_3^D) + 3p_{\pi} p_D (f_1^{\pi} - f_1^D)(f_2^{\pi} - f_2^D) - p_{\pi} p_D (p_{\pi} - p_D) (f_1^{\pi} - f_1^D)^3 \quad (2.132)$$

so that all the energy dependence is now in the terms involving differences between the mechanisms. We have also written the strengths of the components as  $p_{\pi}$  and  $p_D$  where of course  $p_{\pi} + p_D = 1$ .

## 2.8 Comparison with the data

We are now in a position to discuss the model in direct comparison with the data. The parameters which we have available at the moment are  $b$ ,  $\gamma$ ,  $p_\pi$ ,  $\nu$ ,  $s_0$ , and  $\alpha(0)$ . The constants  $c_n$  and  $d_n$  are determined entirely by  $b$  and  $\alpha(0)$ , which together with  $s_0$  determine the non-diffractive multiplicity distribution ;  $\gamma$  and  $\nu$  determine the diffractive distribution ;  $p_\pi$  determines their relative contributions.

As neutral particles are not observed, to compare with the data we must find the multiplicity distribution for charged particles. We choose, in fact, to do it for negatively charged particles. Conservation of charge will then tell us about correlations between positives or all charged particles if we wish. The multiplicities and correlations which have been calculated are those which apply to the number of rungs in the multiperipheral ladder. We can think of the objects emitted at each vertex of the chain as clusters of particles with similar momenta, each cluster having a small sub-energy  $s_0$ . (c.f. equation (2.27)). It is clear in this case that the average mass squared  $s_0$  of a cluster should not necessarily be the same as the minimum mass squared  $^2$ . We certainly expect, however, that  $s_0 \geq \nu^2$  and that neither should be too large. We have in mind then an amplitude



The multiperipheral model with clustering

---

corresponding to diagram 2.5. We can very easily estimate the number of negatively charged particles per cluster from the mean multiplicity

data. A logarithmic parameterisation of this gives it roughly to be

$$\langle n^- \rangle \sim 0.9 \ln s + \text{constant} \quad (2.133)$$

(  $\langle n^- \rangle$  is the mean number of negatively charged particles .) Therefore we expect from (2.127) and (2.130)

$$N \cdot c_1 \cdot p_\pi \approx 0.9 \quad (2.134)$$

$N$  here is the average number of negative particles per vertex in the multiperipheral chain. We know that  $p_\pi \leq 1$ . In the Poisson-Chew-Pignotti limit  $c_1 = 2 - 2\alpha(0)$ . However we have argued that small  $|t|$  dominance implies that the function  $K(\rho)$  is cut off as  $\rho \rightarrow 1$ , while its overall normalisation is kept the same to ensure a constant total cross-section. We are thus stressing small missing mass production relative to high missing mass production as the latter of necessity involves large  $|t|$ . Thus we expect the mean multiplicity and hence  $c_1$  to be smaller than in the Poisson distribution case. Examination of the  $b$  dependence of (2.118) for  $j=1$  with equation (2.105) does in fact demonstrate this to be the case as  $Q_1$  increases with  $b$  as  $b$  increases from zero. We should also like to point out that, as  $b$  increases from zero  $Q_1^2$  becomes greater than  $\frac{1}{2}Q_2$  and so  $c_2$  becomes negative. Examination of the general form (2.99) for the  $Q_j$  leads us to believe strongly that any function  $k(\rho)$  as defined in (2.114) which has the cut off property as  $\rho \rightarrow 1$ , and normalised such that  $Q_0=1$  will give  $Q_1^2 \geq \frac{1}{2}Q_2$  and hence  $c_2 \leq 0$ , producing an asymptotically negative two particle correlation in the multiperipheral model. In (2.134) we then have

$$c_1 \leq 2 - 2\alpha(0) \quad (2.135)$$

We shall constrain  $\alpha$  to be the leading meson trajectory ( $\rho, f, \omega, A_2$ ) that

we expect in elastic proton-proton collisions, putting  $\alpha(0) \approx \frac{1}{2}$  and thus finding  $c_1 \leq 1$ . Equation (2.134) thus tells us that

$$N \geq 1 \quad (2.136)$$

We expect, then, at least one negatively charged particle per vertex of the multiperipheral chain. To make a more detailed comparison we must discuss the structure of these clusters. We are not concerned with the momenta of particles within the cluster as a whole, but we are forced to say something about the distribution of negatively charged particles within the cluster. The generating function again provides an elegantly simple technique. Let the generating function for the production of clusters be

$$\Phi(s, z) = z^2 \Phi^*(s, z) \quad (2.137)$$

The cross-section for the production of  $n+2$  clusters is

$$\begin{aligned} \frac{\sigma_{n+2}}{\sigma_{tot}} &= \frac{1}{(n+2)!} \left( \frac{\partial}{\partial z} \right)^{n+2} \Phi(s, z) \Big|_{z=0} \\ &= \frac{1}{n!} \left( \frac{\partial}{\partial z} \right)^n \Phi^*(s, z) \Big|_{z=0} \end{aligned} \quad (2.138)$$

We now also introduce the generating function for the distribution of negatively charged particles within a cluster. Let this be  $\Psi(z)$ . Then

$$\tau_n = \frac{1}{n!} \left( \frac{\partial}{\partial z} \right)^n \Psi(z) \Big|_{z=0} \quad (2.139)$$

defines the probability that a cluster contains  $n$  negatively charged particles. We also have

$$N = \frac{\partial \Psi}{\partial z} \Big|_{z=1} \quad (2.140)$$

The generating function for production of negatively charged particles then turns out<sup>29</sup> to be

$$\Phi^-(s, z) = \Phi(s, \Psi(z)) \quad (2.141)$$

We thus have

$$\frac{\sigma_n^-}{\sigma_{tot}} = \frac{1}{n!} \left( \frac{\partial}{\partial z} \right)^n \Phi(s, \Psi(z)) \quad (2.142)$$

for the production cross-section for negatives. As we shall be considering only proton-proton interactions we make one small modification to the above remarks. We assume that in general the protons are the leading particles (or at least in the leading clusters) and therefore observe that it is less likely that a negatively charged particle will occur in the leading clusters. We therefore put the distribution  $\Psi(z)$  in only for the non-leading clusters. We thus write

$$\Phi^-(s, z) = \Phi^*(s, \Psi(z)) \quad (2.143)$$

with  $\Phi^*$  defined in (2.137).

We define the reduced cluster production (i.e. that with the leading particles subtracted) generating function and moments by

$$\Phi^*(s, z) = \exp \left\{ \sum_{n=1}^{\infty} \frac{(z-1)^n f_n^*(s)}{n!} \right\} \quad (2.144)$$

and so

$$f_n^*(s) = f_n(s) + 2(n-1)! (-1)^n \quad (2.145)$$

We also define

$$\Phi^+(s, z) = \exp \left\{ \sum_{n=1}^{\infty} \frac{(z-1)^n f_n^+(s)}{n!} \right\} \quad (2.146)$$



and

$$\begin{aligned} \Psi(z) &= \exp \left\{ \sum_{n=1}^{\infty} \frac{(z-1)^n}{n!} g_n \right\} = \sum_{n=0}^{\infty} z^n \tau_n \\ &= 1 + \sum_{n=1}^{\infty} \frac{(z-1)^n}{n!} \psi_n \end{aligned} \quad (2.147)$$

The  $f_n^-$  are then the correlations between negatively charged particles and the  $g_n$  are the correlations between the negatively charged particles within a single cluster (with  $g_1 \equiv N$ ). The quantities  $\psi_k$  are just the moments  $\langle n(n-1)(n-2)\dots(n-k+1) \rangle$  of the composition of a cluster. Combination of (2.144), (2.146), and (2.147) then gives

$$f_1^- = \psi_1 f_1^* \quad (2.148)$$

$$f_2^- = \psi_1^2 f_2^* + \psi_2 f_1^* \quad (2.149)$$

$$f_3^- = \psi_1^3 f_3^* + 3\psi_1 \psi_2 f_2^* + \psi_3 f_1^* \quad (2.150)$$

or alternatively

$$f_1^- = g_1 f_1^* \quad (2.151)$$

$$f_2^- = g_2 f_1^* + g_1^2 (f_2^* + f_1^*) \quad (2.152)$$

$$f_3^- = g_3 f_1^* + 3g_1 g_2 (f_2^* + f_1^*) + g_1^3 (f_3^* + 3f_2^* + f_1^*) \quad (2.153)$$

In addition to the parameters discussed at the beginning of this subsection we now have the unknown function  $\Psi(z)$ . In accord with our aim of reducing the number of free parameters, we look only at possibilities which can be simply described in terms of a single parameter.

Our procedure for comparison with the observed correlations is then to choose a likely distribution of negatively charged particles in a cluster, and to calculate the multiplicity distribution of negatively charged particles according to (2.148)-(2.150) from the two component model already constructed in terms of the parameters outlined above\*

A first guess for the cluster structure might be that the cluster always contains exactly  $N$  negatively charged particles. If this ansatz is taken, then no satisfactory fit is found for integral  $N$ . If  $N$  is then allowed to vary continuously, however, a reasonably good fit is found with  $N=1.38$ . The other parameters take the values:  $p_D=0.31$ ,  $\gamma = 1.2$ ,  $s_0 = 4.0 \text{ GeV}^2$ ,  $v^2 = 2.6 \text{ GeV}^2$ ,  $b = 1.0$ ,  $\alpha(0) = 0.5$ . In this and following fits we restrict the input trajectory, except where stated, to have intercept in the range  $0.4 - 0.6$ . The situation here with  $N=1.38$  is, of course, not satisfactory, and it is necessary to introduce a distribution with some width. We shall, however, take this fit as an indication that the mean number of negatives in a cluster is likely to lie between one and two.

Our next attempt is to take  $\Psi(z)$  to be the generating function of a Poisson distribution.

$$\Psi(z) = e^{N(z-1)} \quad (2.154)$$

The fit now obtained is singularly unsuccessful. The reason which rules out this distribution is that when a suitable mean  $N$  is taken, the possibility of producing three or more negatively charged particles from a cluster is quite large. (The probability of three or more is roughly  $\frac{1}{3}$  for  $N \approx 1.4$ , or alternatively  $\psi_3 \approx 2.7$ ). This produces a strong positive contribution to  $f_3^-$ , directly contrary to the data.

---

\*For fits to the data the CERN minimisation program 'MINUIT' was used, both on N.U.M.A.C. and the R.H.E.L 360 computer.

A somewhat narrower distribution seems to be needed.

### FIT I

We thus take a distribution in which one negative charge appears with frequency  $(2-N)$  and two appear with frequency  $(N-1)$ . With this distribution a fit to the data is found which is shown in figures 2.3, 2.4, and 2.5. No sharply defined minimum of the  $\chi^2$  parameter used to compare the theoretical distribution with the data was found and so the values found for the parameters can only be regarded as typical and not in any way definitive. These were :  $N = 1.27$  (negatives per cluster on average) ;  $b = 1.1$  ,  $s_0 = 3.35 \text{ GeV}^2$  ;  $v^2 = 2.8 \text{ GeV}^2$  ;  $\alpha(0) = 0.41$  ;  $p_D = 0.31$  ; and  $\gamma = 1.48$ . The only two of these which perhaps deserve particular comment are  $p_D$  and  $\gamma$ .

The parameter  $p_D$  is larger than in many two component models. The parameter  $\gamma$  is also larger than one might at first have expected, corresponding to a Regge singularity in elastic Pomeron-proton scattering with intercept of  $-.48$ . This is a typical value in our fit. Fits can be found with this intercept as high as zero but no acceptable fit is found with an intercept higher than this. Physically the large value of  $\gamma$  is restricting the diffractive multiplicity to small values by keeping the missing mass low. An advantage of this is that we do not now have to consider the possibility of pomeron exchange in the centre of a long multiperipheral chain, as the presence of the pomeron would keep the chain short. The diffractive interaction that we have already calculated will therefore suffice. The underlying feature of both these effects, large  $p_D$  and large  $\gamma$ , is that they tend to make the two component effect more dominant. Consider the form (2.10) of  $f_2$ . That is

$$f_2 = p_\pi f_2^\pi + p_D f_2^D + p_\pi p_D (\bar{n}_\pi - \bar{n}_D)^2 \quad (2.155)$$

The last term is going to dominate most effectively if  $p_D \rightarrow \frac{1}{2}$  and

$\bar{n}_\pi - \bar{n}_D$  becomes large as discussed in section 2.1 . The necessity for this is now more marked as  $f_2^\pi$  is, as we have discussed, asymptotically negative owing to the effects of momentum conservation (in the form of the  $t_{\min}$  effect) and small  $t$  dominance. (We also remark that the clustering effect helps to alleviate this problem). A non-diffractive mechanism with  $f_2 > 0$  would admit considerably fewer difficulties in describing the data in terms of two components.

The last possibility we consider for the cluster structure is a binomial distribution allowing zero, one, or two negatively charged particles. Constraining, as before,  $\alpha(0)$  to lie between 0.4 and 0.6 we arrive at identical conclusions from very similar parameter values and a very similar fit.

#### FIT II

We finally remark that if we allow  $\alpha(0)$  to be a little lower we can improve the fit slightly as shown in figures 2.6, 2.7, and 2.8 . The parameters are now as follows : clusters contain a binomial distribution of negatives of mean  $N = 0.2$  ;  $\alpha(0) = 0.05$  ;  $b = 1.2$  ;  $\gamma = -0.5$  ;  $p_D = 0.34$  ;  $s_0 = 9 \text{ GeV}^2$  ;  $v^2 = 7.5 \text{ GeV}^2$  .  $\alpha(0)$  may perhaps be interpreted as an effective trajectory intercept. Other than this our conclusions are as before.

## 2.9 The pomeron as a projectile

The basic ingredient of our model is that the multiplicity distribution of the interaction is assumed to be independent of the nature of the projectile. We shall investigate this further in the next chapter but at this stage it is perhaps worthwhile to note how restrictive this is to our fit to the multiplicity distribution.

If we relax the assumption that pomeron-proton collisions produce the same multiplicity distribution as reggeon-proton collisions, then for a diffractive interaction which can be described by a triple Regge term of the form pomeron-pomeron-reggeon, we find from (2.94) that the multiplicity distribution is independent of energy. We have here retained the assumption that the pomeron-proton interaction has only short range correlations and thus  $f_n^{Pp} \sim r_n \ln(s)$ . The freedom that this arbitrary distribution gives to the two component fit is considerable. If we take the Poisson limit of the non-diffractive part and assume (ad hoc) that the diffractive multiplicity distribution is also Poisson, the data are easily fitted. This two Poisson fit we label FIT III. It is shown in figures 2.9, 2.10, and 2.11. We stress that a very large number of similar fits are possible depending on what one assumes for the diffractive distribution. The parameters in this fit are:  $\alpha(0)=0.45$ ;  $p_D=0.17$ ;  $s_0=17 \text{ GeV}^2$ ; and the clusters were restricted, each to contain only one negatively charged particle. The means of the two component distributions are  $\bar{n}_D=2.94$  and  $\bar{n}_\pi=1.1 \ln(s)+2$ . Thus we would stress that the assumption that the multiplicity distributions are independent of the nature of the projectile provides a considerable constraint on the model.

## 2.10 Other two component models

In this section we should like to mention other models based on the two component prescription outlined in section 2.1 .

The approach of Fialkowski and Miettinen<sup>20</sup> is to make a Poisson distribution ansatz for one component and to subtract it from the observed multiplicity distribution to find the other. The second component, they find, is significant only for fewer than eight charged particles produced and has  $\sigma_n$  independent of energy.

Van Hove<sup>21</sup> observes the attractiveness of the two component model in connection with the Wroblewski plot (figure 2.1) and his fit to this indicates  $p_D$  to be roughly 26% .

Harari and Rabinovici<sup>22</sup>, as discussed earlier, parameterise the data with a similar two component model to test the relation (2.78) for the non-diffractive part. Fitting  $\bar{n}$  and  $f_2$  they observe that this relation is satisfied for reasonable  $\alpha_R$  by the sum taking only the first two terms  $c_1$  and  $c_2$ . Our model having (2.78) built in clearly has a lot to say about this. Whereas their fit has  $c_2 > 0$ , our model has difficulty in producing this, as we discussed earlier in this chapter. Our fits labelled I and II, when one calculates the first four terms, only satisfy the relation respectively to 88% and 78%. This emphasises the non-Poisson nature of our pionisation component. We must conclude then that the series in (2.78) may not be so rapidly convergent as is hoped by these authors.

Frazer and Snider<sup>30</sup> propose a mechanism for diffraction into high masses based on a triple pomeron term and calculate its mean multiplicity and total cross-section, using the assumption that the pomeron-particle scattering multiplicity distribution is the same as that for non-diffractive particle-particle scattering. They do not attempt a fit to the data. We shall discuss such mechanisms in chapter four.

Berger and Fox<sup>31</sup> also introduce a triple pomeron diffractive term but note that their fit to the data is more dependent on their non-diffractive component which they take to be a multiperipheral cluster model. It is interesting to note that although their fit is primarily to inclusive distribution data, they find that the clusters should on average contain approximately four pions. This is nicely consistent with our estimate of 1.3 negatively charged particles. Their difficulty in producing a good fit to the multiplicity distribution for  $s < 200 \text{ GeV}^2$ , we should to the lack of any suitable mechanism for low mass diffraction which our analysis (in agreement with references 20 and 22) indicates to be crucially important in this respect.

Roberts and Roy<sup>32</sup> discuss only the diffractive interaction. They allow this two components corresponding to triple pomeron and pomeron-pomeron-meson terms, and calculate an approximate form for the diffractive multiplicity distribution.

## FIGURES FOR CHAPTER TWO

The Roman numerals labelling figures 2.3 to 2.11  
refer back to those used in the text in sections  
2.8 and 2.9



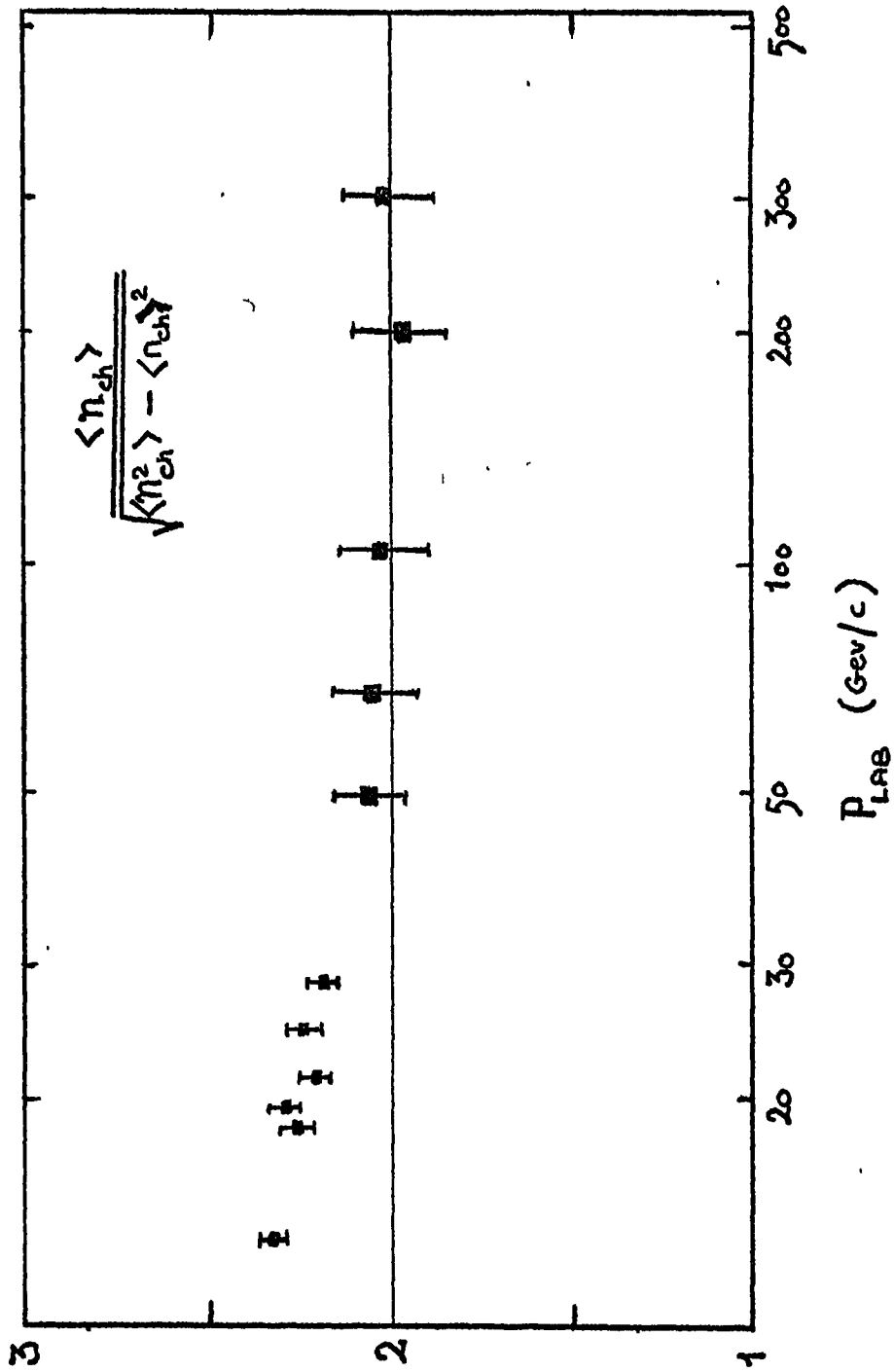


FIGURE 2.1. : The MEAN/STANDARD DEVIATION for the charged particle multiplicity distribution in proton-proton scattering plotted against the laboratory beam momentum.

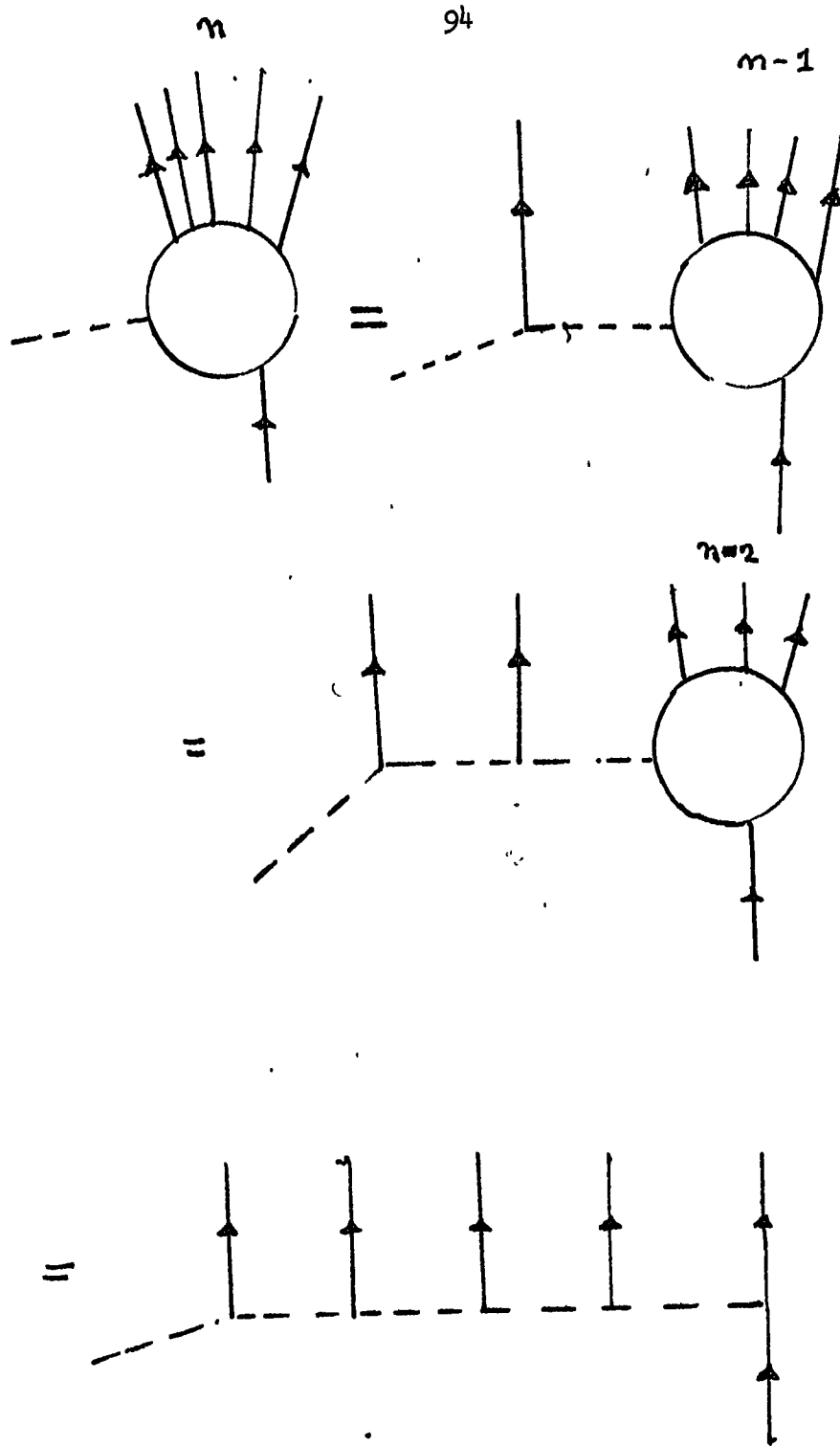


FIGURE 2.2

iterative derivation of the  
multiperipheral model.

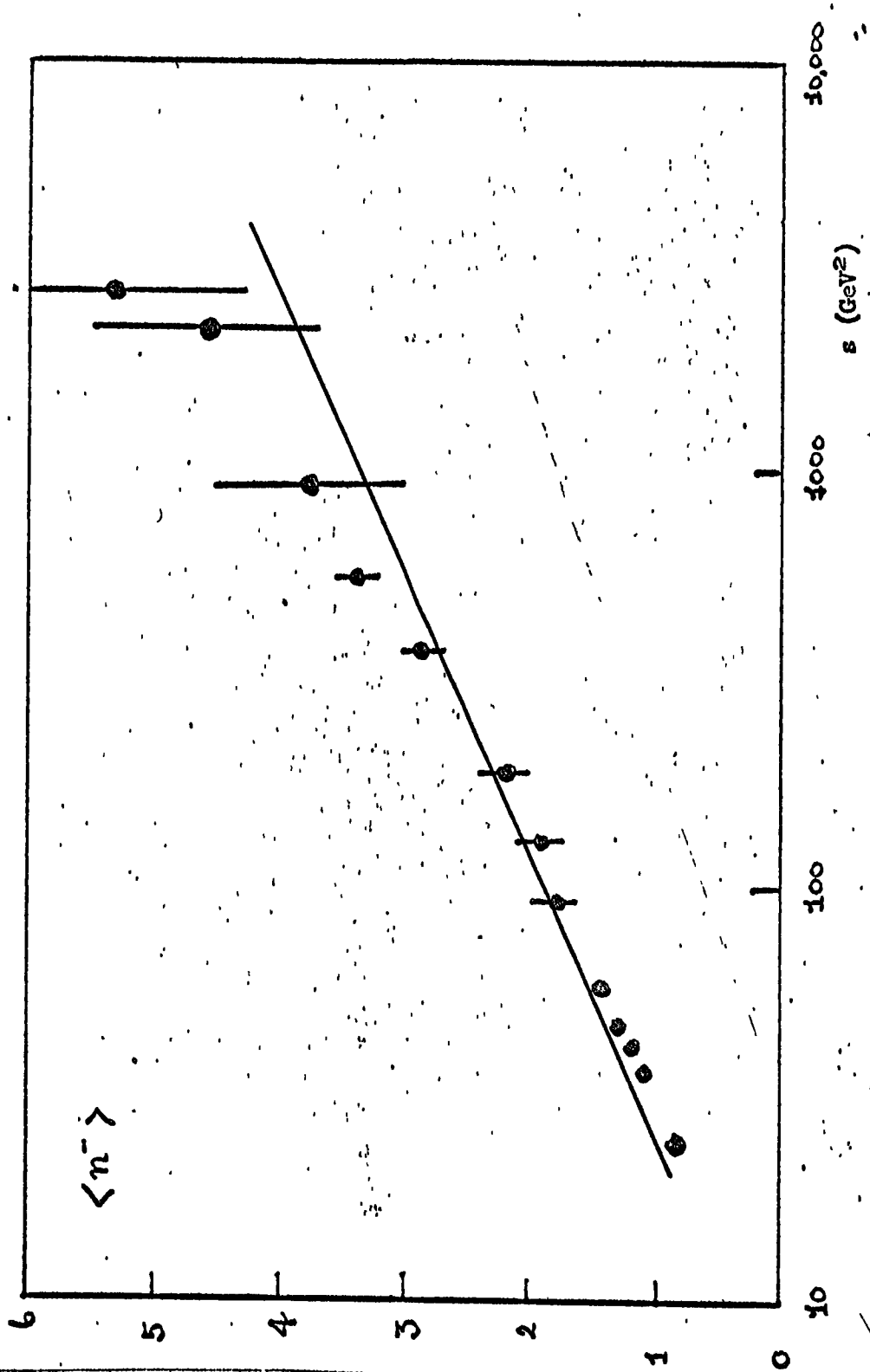


FIGURE 2.3 : The mean multiplicity. (I)

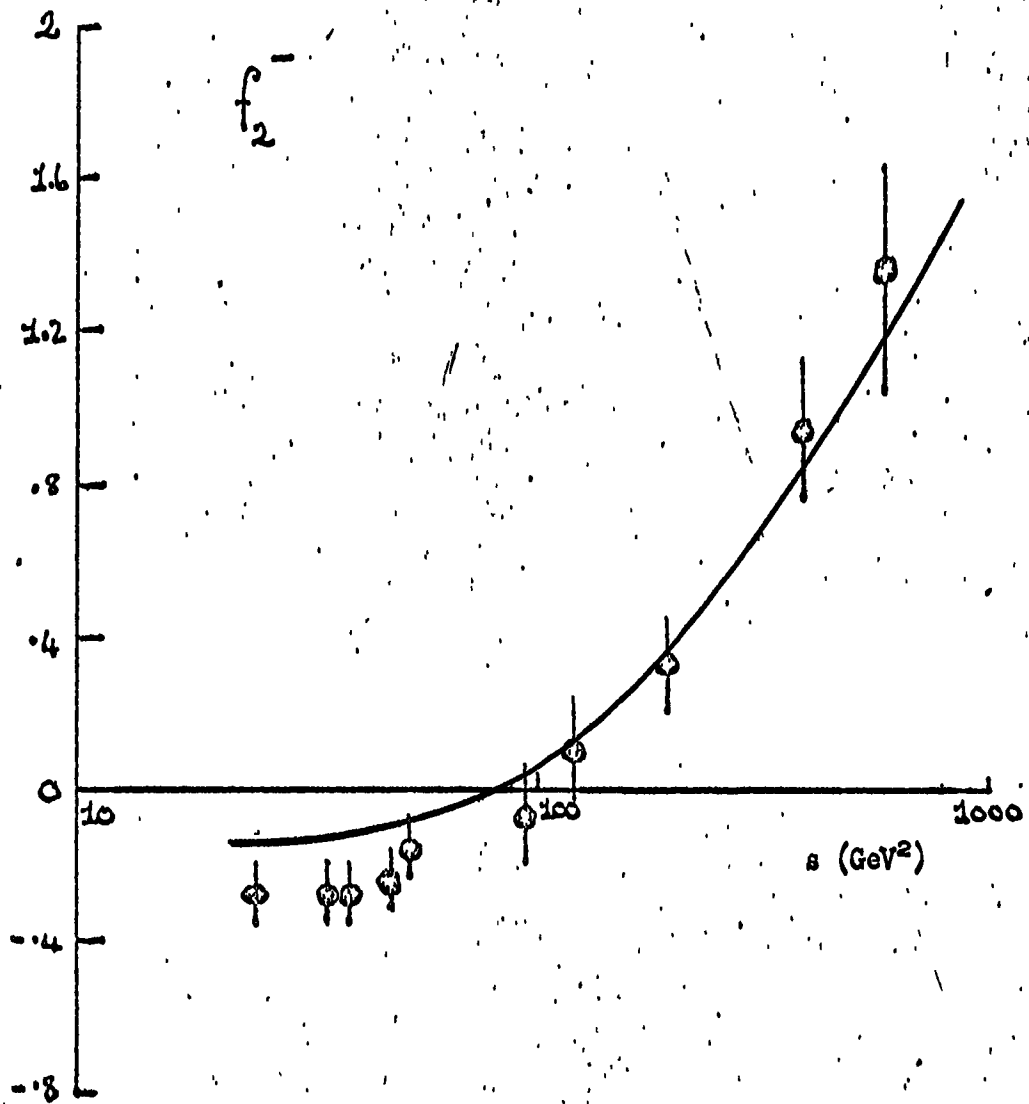


FIGURE 2.4 - The two particle correlation. (I)

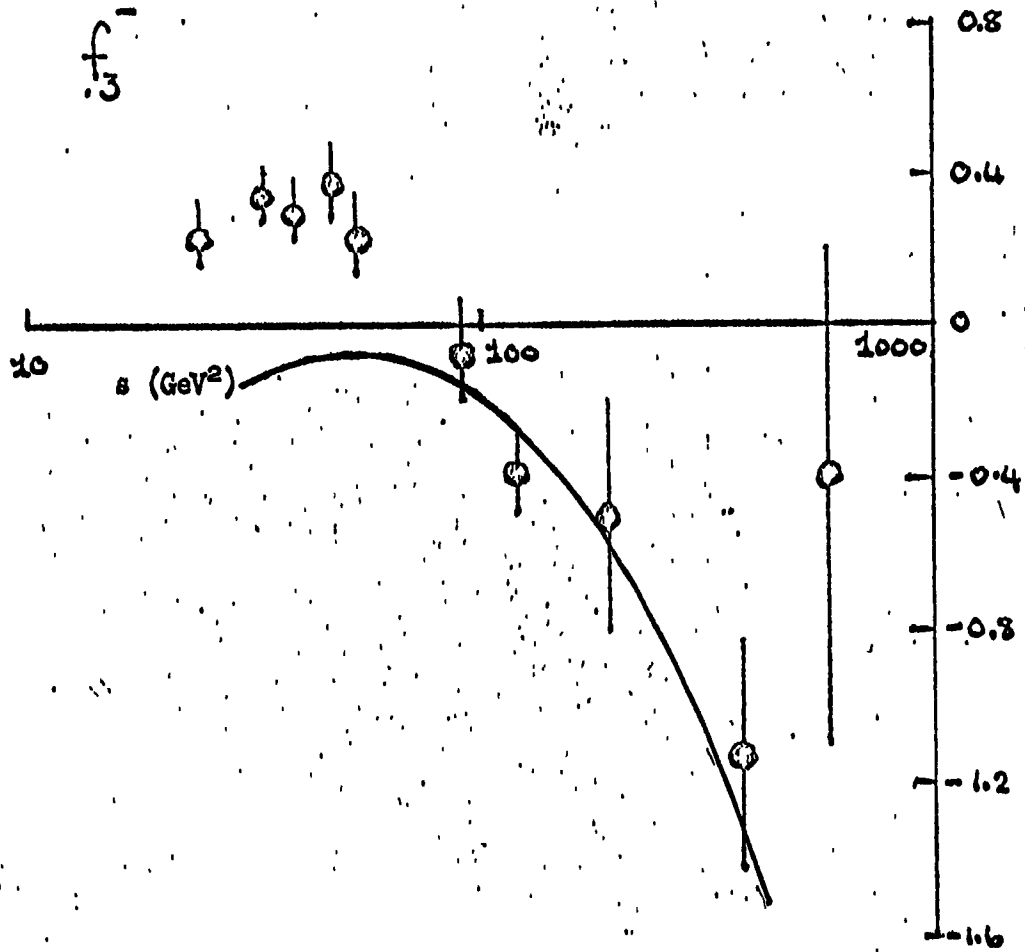


FIGURE 2.5 : The three particle correlation (I)

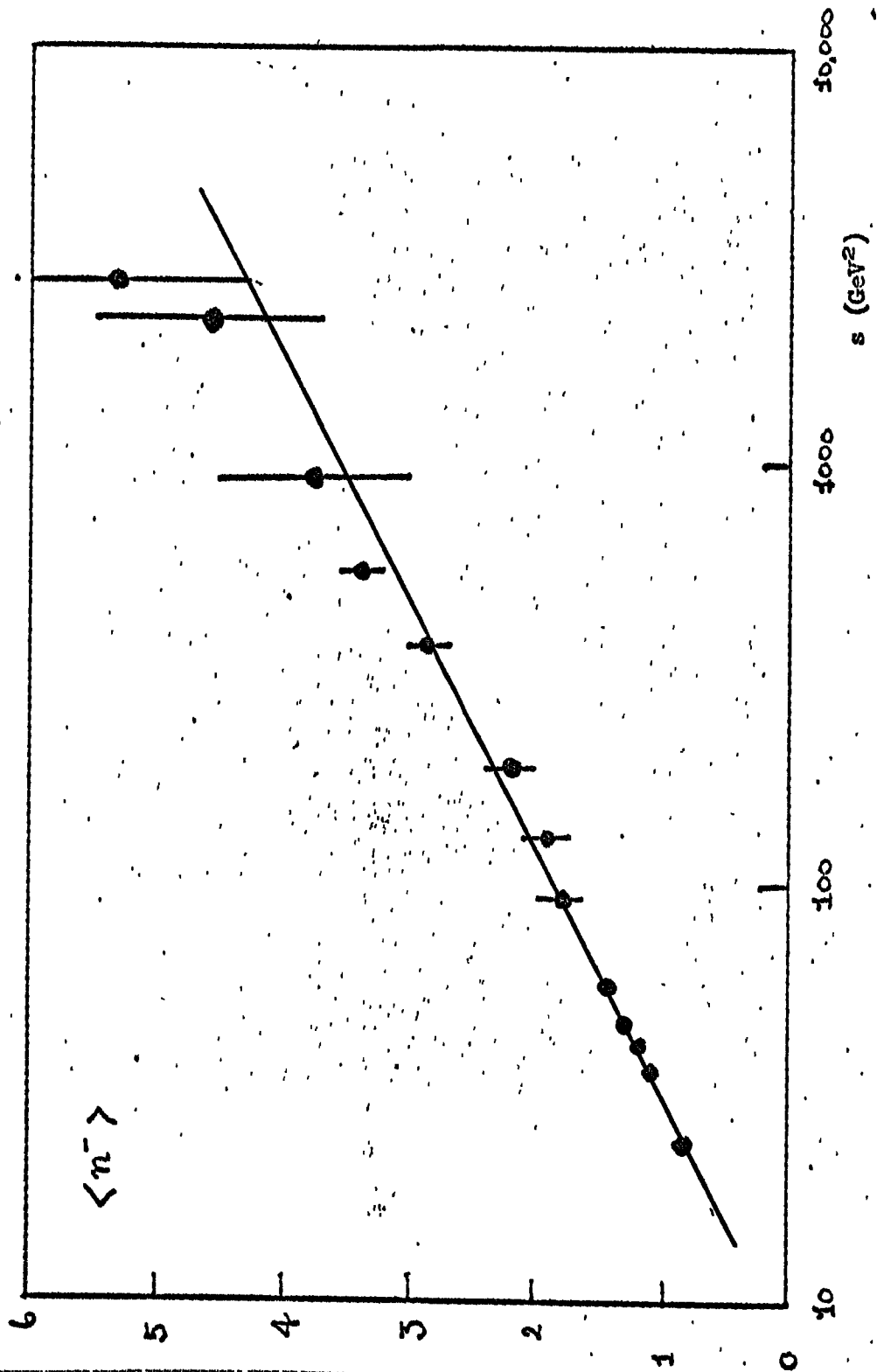


FIGURE 2.6 : The mean multiplicity (II)

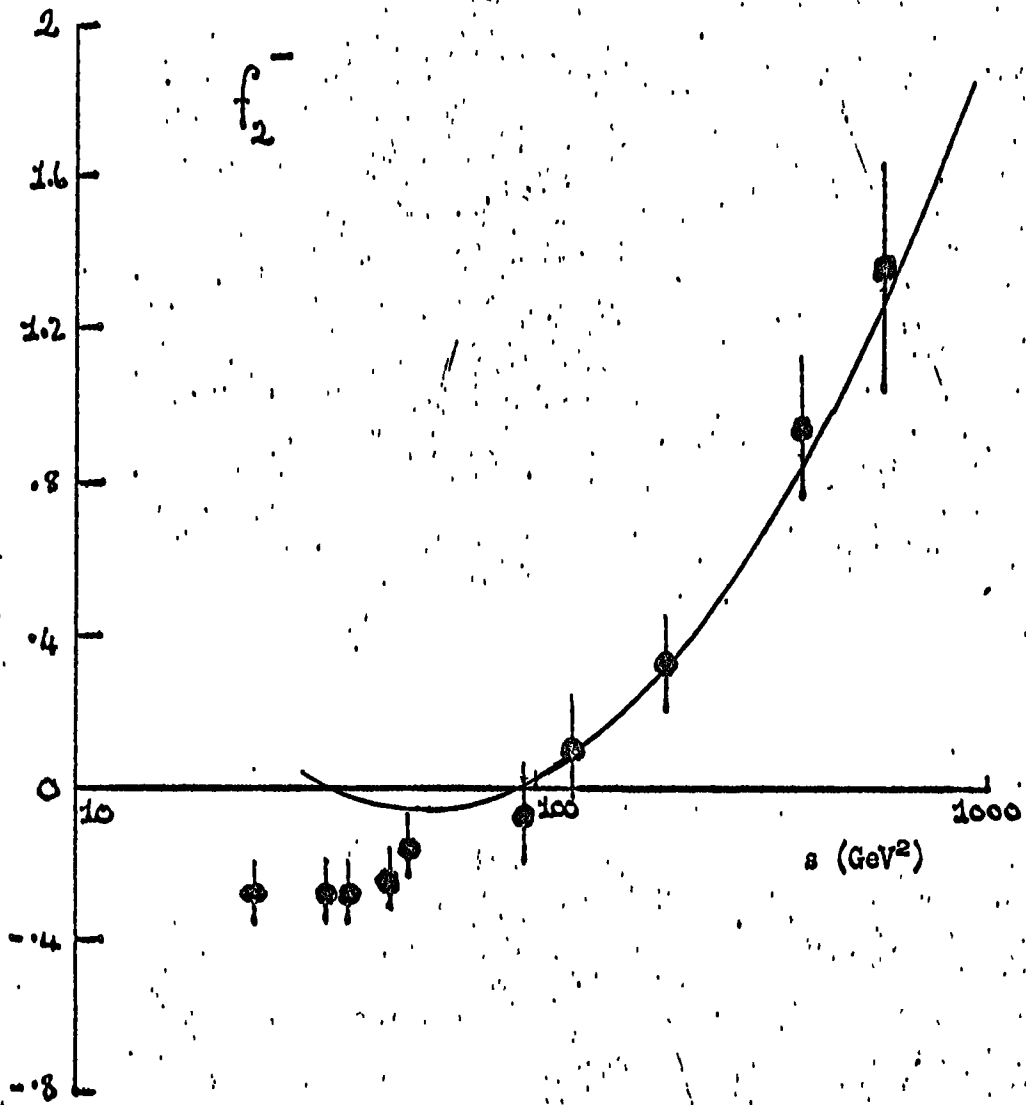


FIGURE 2.7 : The two particle correlation. (II)

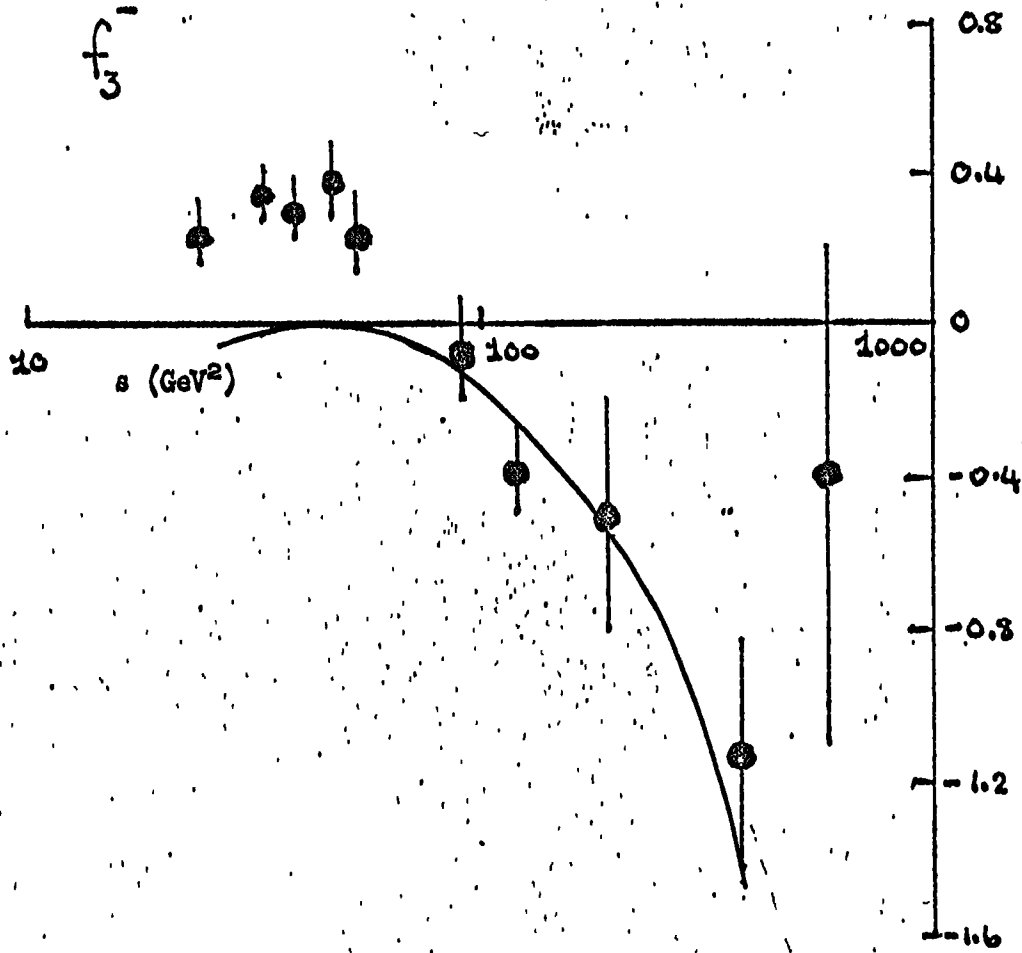


FIGURE 2.8 : The three particle correlation (II).



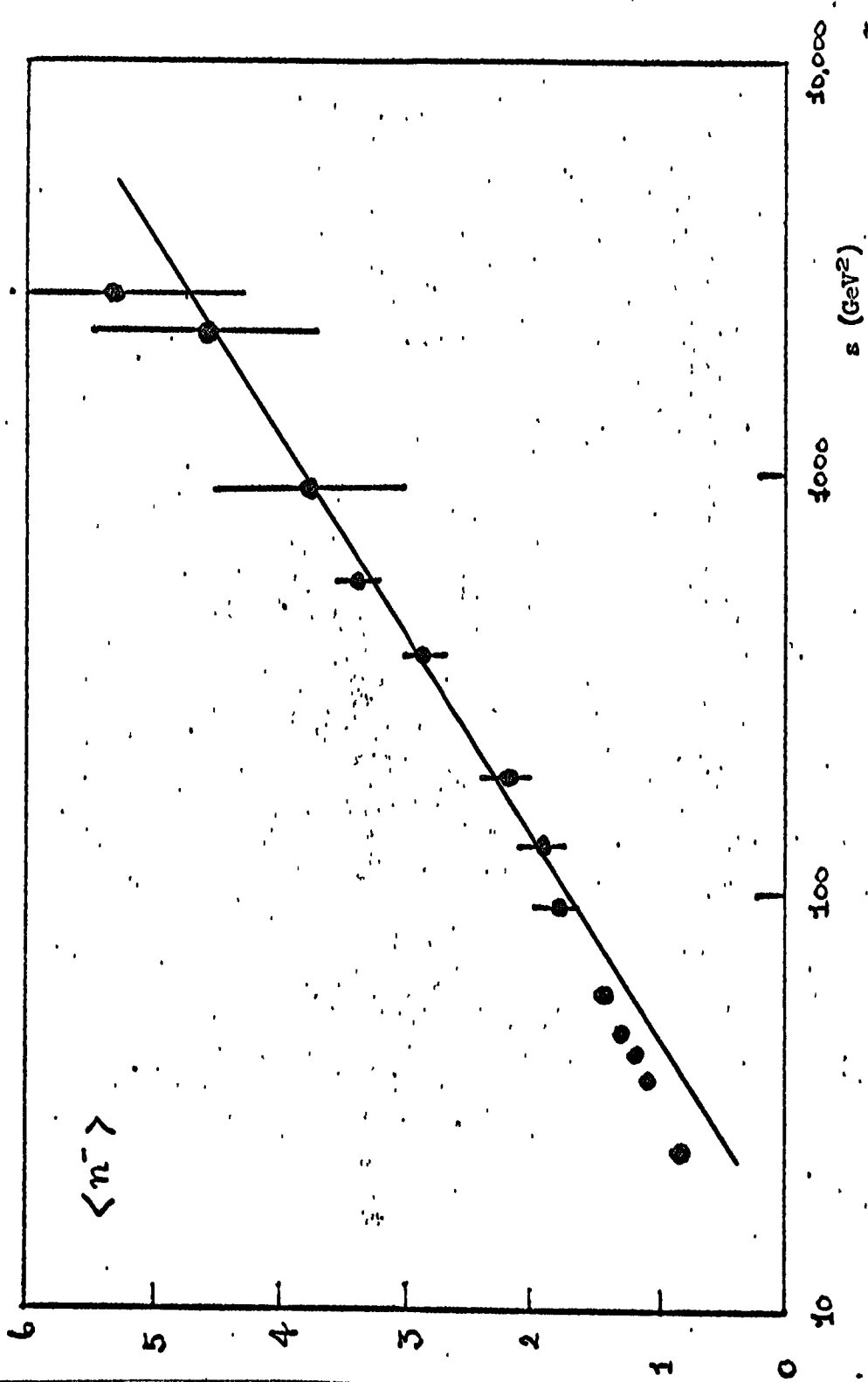


FIGURE 2.9 : The mean multiplicity (III)

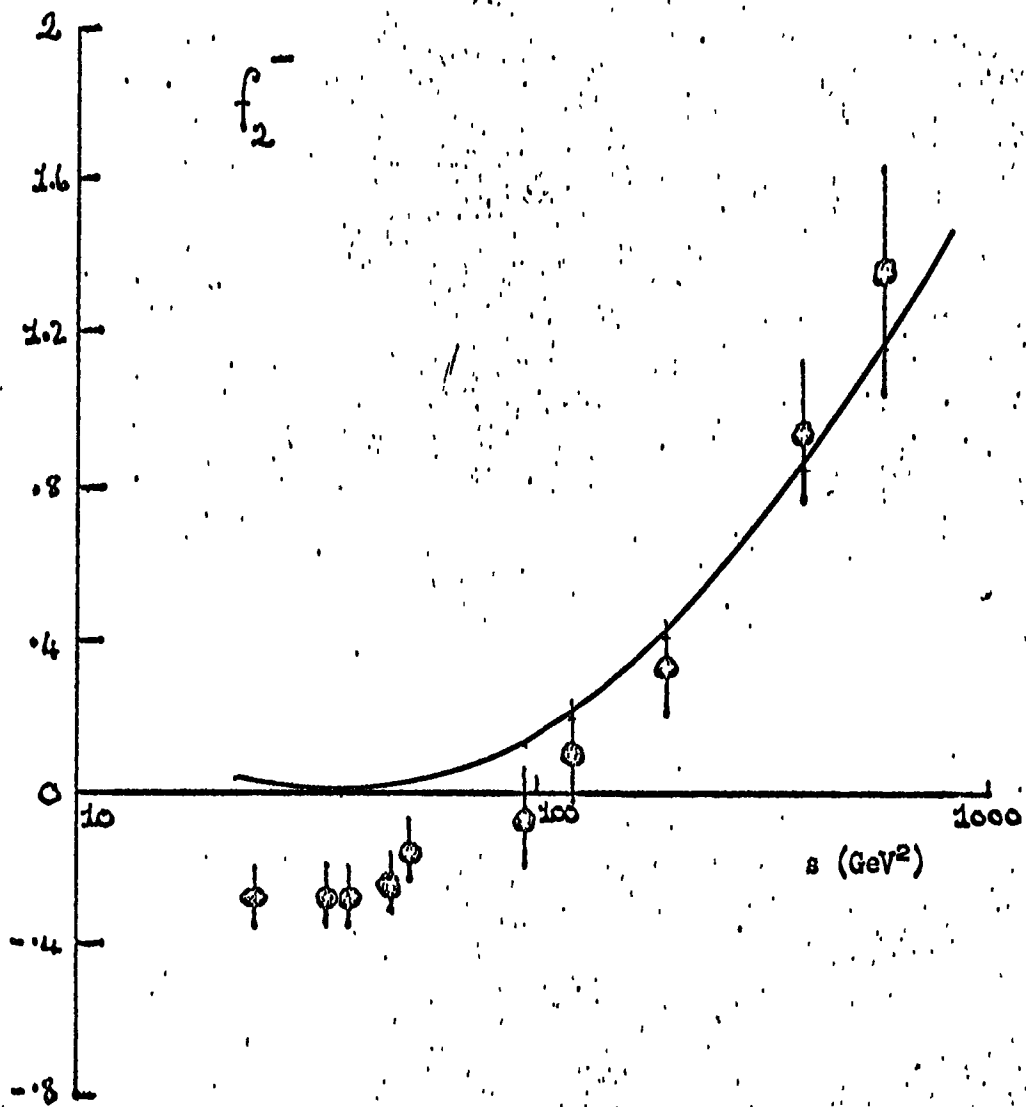


FIGURE 2.10.: The two particle correlation (III)

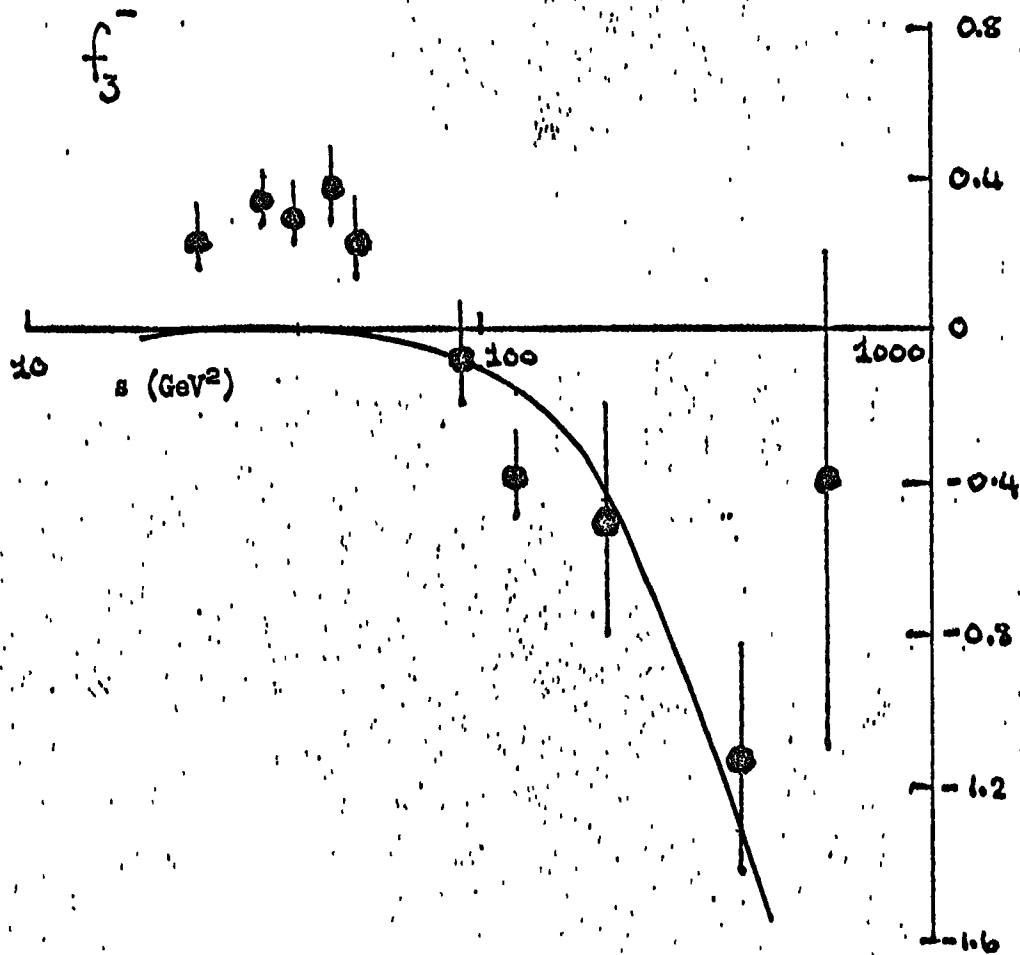


FIGURE 2.11 : The three particle correlation (III)

## CHAPTER THREE

### Inclusive distributions and correlations

#### INTRODUCTION

This chapter is, in a way, complementary to the preceding one in that we now go on to examine the features of the two component model in general and our model in particular, which unlike those features discussed in the previous chapter, depend on the momenta of the observed particles. In section one we discuss inclusive distributions and correlations from two component models. We show in particular that the two component model with a low mass diffraction component gives a good description of the two particle correlation. The second section discusses the semi-inclusive process  $pp \rightarrow p + n \text{ charged particles} + \text{any}$ . The remainder of the chapter is devoted to discussion of the reaction  $pp \rightarrow p, q, X$ , where  $q$  is a charged particle. The ideas leading to the model of chapter two are again found to describe the data well. In the final two sections of this chapter, predictions of the model are outlined which might prove useful in testing it further when more inclusive and semi-inclusive data are available.

### 3.1 The two component model

Here we shall study, in the same way as in the first section of the preceding chapter, the basic construction of the two component model. We are now interested in the inclusive distributions and the momentum dependence of the correlations. We use again the shorthand notation

$$dp \equiv \frac{d^3p}{2E} \quad (3.1)$$

and

$$N_k = \frac{1}{\sigma} \frac{d\sigma^{inc}}{dp_1 \dots dp_k} \quad (3.2)$$

For our two mechanisms (which we again denote here a and b) we expect

$$\frac{d\sigma^{inc}}{dp_1 \dots dp_k} = \frac{d\sigma^{inc}(a)}{dp_1 \dots dp_k} + \frac{d\sigma^{inc}(b)}{dp_1 \dots dp_k} \quad (3.3)$$

and so in the notation of section 2.1

$$N_k(p_1 \dots p_k) = \alpha_a N_k^{(a)}(p_1 \dots p_k) + \alpha_b N_k^{(b)}(p_1 \dots p_k) \quad (3.4)$$

with

$$\alpha_a + \alpha_b = 1 \quad (3.5)$$

We now construct the correlations defined in the introductory chapter

$$C_2(1, 2) = N_2(1, 2) - N_1(1)N_1(2) \quad (3.6)$$

$$\begin{aligned} C_3(1, 2, 3) = & N_3(1, 2, 3) - N_1(1)N_2(2, 3) - N_1(2)N_2(3, 1) \\ & - N_1(3)N_2(1, 2) - N_1(1)N_1(2)N_1(3) \end{aligned} \quad (3.7)$$

Precisely as in section 2.1 , we find equation (3.4) to be in terms of these correlations

$$C_2(1,2) = \alpha_a C_2^{(a)}(1,2) + \alpha_b C_2^{(b)}(1,2) + \alpha_a \alpha_b (N_1^a(1) - N_1^b(1))(N_1^a(2) - N_1^b(2)) \quad (3.8)$$

and

$$C_3(1,2,3) = \alpha_a C_3^a(1,2,3) + \alpha_b C_3^b(1,2,3) + \alpha_a \alpha_b \{ [C_2^a(1,2) - C_2^b(1,2)] [N_1^a(3) - N_1^b(3)] + \text{cyclic terms} \} - \alpha_a \alpha_b (\alpha_a - \alpha_b) (N_1^a(1) - N_1^b(1)) (N_1^a(2) - N_1^b(2)) (N_1^a(3) - N_1^b(3)) \quad (3.9)$$

Equation (3.4) for  $k=1$  , (3.8), and (3.9) upon integration over all momenta involved clearly reduce to (2.9), (2.10), and (2.11). The situation for higher correlations will become rapidly more complicated but fortunately as there are no relevant data we need not discuss them. The two component terms are again clearly displayed in equations (3.8) and (3.9). As in the previous chapter we can look at these terms on their own. (Technically  $C_2^a$  and  $C_2^b$  cannot be zero owing to conservation of momentum constraints, although they can be much smaller than  $N_1^a$  ,  $N_1^b$ ). We take mechanism a to be the short range correlation mechanism, discussed in the first chapter in the context of the Mueller-Regge analysis, having a plateau in the central region of the single particle inclusive rapidity distribution. This will correspond to our non-diffractive mechanism in chapter two. The low mass diffraction mechanism in chapter two should provide an inclusive distribution which is peaked at either end of the rapidity plot and approximately zero in the central region. Thus as  $s$  increases its peaks merely move out with the kinematic limits of the rapidity variable. (See figure 3.1). Thus taking the two component term in equation (3.8) we have

$$C_2 \approx \alpha_a \alpha_b (N_1^a(1) - N_1^b(1))(N_1^a(2) - N_1^b(2)) \quad (3.10)$$

We can now examine the behaviour of this correlation. Figure 3.2a shows where we expect this function to be positive, negative or zero. In this case the correlation is definitely of long range. In figure 3.2b this correlation is plotted against one of its variables with the other fixed. The short range correlations present in either of the two components will of course be superimposed on the features shown. (For example as shown in figure 3.2c.)

We should also like to remark that the data are often presented in terms of a normalised correlation. In our notation this is

$$R_2(1,2) = \frac{C_2(1,2)}{N_1(1)N_1(2)} \quad (3.11)$$

This has the advantage that it compares the size of the correlation with the size of the uncorrelated production distributions.  $R_2$  clearly also satisfies

$$N_1(1,2) = N_1(1)N_1(2) \{ R_2(1,2) + 1 \} \quad (3.12)$$

If the total  $N_1$  is roughly constant as figure 3.1 suggests it might be, then the shape of  $R$  from the two component model will look just like  $C_2$ . Data for the two particle correlations are shown in figure 3.3. The form given by the two component model that we have been discussing looks qualitatively good, as has been discussed by various authors<sup>33,34</sup>.

As data are now available over a considerable energy range (the I.S.R. data alone span a factor of five or so in  $s$ ), we should like here to examine one particular distinctive feature of the two component model. Examination of equation (3.8) shows that  $C_2(y_1, y_2)$  for

any  $y_2$  has a zero as a function of  $y_1$  whose position does not depend upon  $y_2$ . (We have assumed here that  $C_2^a$  and  $C_2^b$  are small - this will be the case if our two components have only short range correlations and  $y_2$  is kept more than a correlation length away from where we expect the zero in  $C_2$ .) Furthermore a low mass diffraction contribution which has constant multiplicity and cross-section, and which provides a non-zero contribution to the inclusive distribution only within a fixed range of the end of the rapidity plot, will imply that the zero of  $C_2$  will be at fixed  $|Y-y|$  where  $Y = \frac{1}{2}\ln(s/s_0)$ . We have here assumed limiting fragmentation of the pionisation component. We take  $s_0 = m_\pi^2$  - this is arbitrary and does not affect the result. In figure 3.4 we show  $|Y-y_0|$  where  $y_0$  is the position of the zero in  $C_2$  found empirically and defined in our model by

$$N_1^a(y_0) = N_1^b(y_0) \quad (3.13)$$

We take only the very high energy data where one can more optimistically separate long and short range correlations. We display the data for  $|y_2 - y_0| > 2$  where we expect short range effects to be negligible, choosing also the data where the position of the zero is reasonably well defined. The results are in excellent agreement with the two component model prediction although the error bars would permit a slight variation in the position of the zero with respect to the energy. Figure 3.3 also shows that when both the particles 1 and 2 are well in the central region, then the correlation is independent of energy, just as we should expect from equation (3.8) if each component has scaling behaviour. This is shown more clearly in figure 3.5 . .



### 3.2 A simple semi-inclusive measurement

Before turning our attention to the form of further inclusive measurements predicted by our model, we should like to examine the recently published data on the experiment where the multiplicity of the event is measured, as well as the momentum of a proton in the final state. This is the simplest experiment in a class denoted semi-inclusive. A thorough study of this experiment is performed in reference 35 where references to earlier such analyses (with more limited data) are given.

Our model of chapter two tells us that the mean multiplicity in reggeon-particle channels should be the same, when the available energy is the same, as the mean multiplicity in non-diffractive particle-particle scattering, independent of which Regge singularity we choose. (In the spirit of the model we should have liked to have said that reggeon-particle multiplicity distributions should be the same as the overall particle-particle distribution, but the existence of the pomeron with  $\alpha(0)=1$  forced us to add diffractive terms in separately.) In figure 3.6 the mean multiplicities of particles are plotted against the available energy,  $E=M-m$  in the  $M^2$  channel, and  $E=\sqrt{s}-2m$  in the  $s$  channel.  $\langle n_{ch} - 1 \rangle$  is plotted in the case of the  $M^2$  channel owing to the smaller initial charge. The authors of reference 35 make explicit comments that there appears to be no change in behaviour of  $\bar{n}(M^2)$  as  $M^2$  rises from the (pomeron dominated) region where there is strong  $M^2$  dependence in the pp pX inclusive distribution, to the region (presumably non-diffractively dominated) where there is very little  $M^2$  dependence in this quantity. This, as well as the similarity to the mean multiplicity in the  $s$  channel, is very natural to our model where the multiplicity distribution in reggeon-particle collisions is independent of whether the reggeon is a meson or the pomeron. The multiplicity distributions in  $s$  and  $M^2$  channels are shown in figure 3.7 at various energies. This

experimental result we regard as excellent justification for the underlying philosophy of our model.

### 3.3 The reaction $pp \rightarrow p + \text{charged particle} + \text{any}$

In this section we shall calculate the form for the two particle correlation when one of the particles is a proton<sup>III</sup>. The prime motivation for this is that whereas the proton distribution in the reaction  $pp \rightarrow pX$  displays a peak when the proton is observed near  $x=1$ , when a charged particle is observed simultaneously in the central region the peak is no longer present. This feature occurs very naturally in our

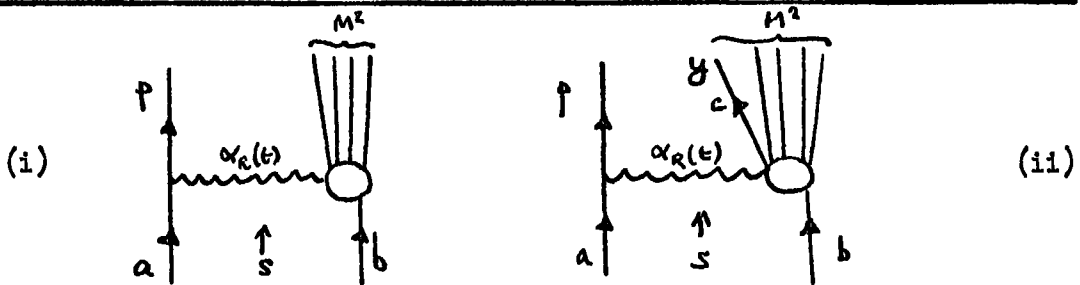


DIAGRAM 3.1 : Pictorial representation of amplitudes for (i) a proton ; (ii) a proton and another charged particle , produced in proton-proton interactions.

model. We first take equation (2.31) at  $z=1$  , (derived from an amplitude factorised as is in diagram 3.1.i), and sum over  $n$ , rewriting it as

$$\frac{d\sigma}{dt dx} = \sum_R \frac{1}{16\pi^2} |V_R(t)|^2 (1-x)^{1-2\alpha_R(t)} \tilde{\sigma}_{Rp}((1-x)s) \quad (3.14)$$

$t$  is the invariant momentum transfer to the proton and  $x$  is the longitudinal Feynman variable of the proton. The sum we expect to include as in chapter two notably the pomeron and leading meson term. We neglect interference between the two on the grounds mentioned earlier. Equation (3.14) is just that which leads to the triple Regge expansion when Regge behaviour is taken for  $\tilde{\sigma}_{Rp}$ . It may be expected to be valid for

$$\frac{s}{M^2} = \frac{1}{1-x} \gg \frac{1}{1-x_0} \quad (3.15)$$

where  $x_0$  is some constant. (For example if Regge analysis is good for  $s/M^2 > 2$  then  $x_0 \sim \frac{1}{2}$ . We shall discuss this point later in connection with the data.)

The second particle, labelled  $c$  in diagram 3.1.ii, is in the central region and so rapidity is a more convenient variable than  $x$ . The simple Lorentz transform properties of the rapidity variable will also be of use to us. The expression from diagram 3.1.ii analogously to equation (3.14) is

$$\frac{d\sigma}{dt dx dy_c} = \sum_R \frac{1}{16\pi^2} |V_R(t)|^2 (1-x)^{1-2\alpha_R(t)} \frac{d\sigma_{RP}}{dy'_c} ((1-x)s) \quad (3.16)$$

$y_c$  is the rapidity of particle  $c$  in the centre of mass and  $y'_c$  is the rapidity of particle  $c$  in the rest frame of the missing mass  $M^2$ , the centre of mass of the reggeon-proton interaction. We must now relate  $y'_c$  to  $y_c$ . Considering the reaction represented in diagram 3.2 with

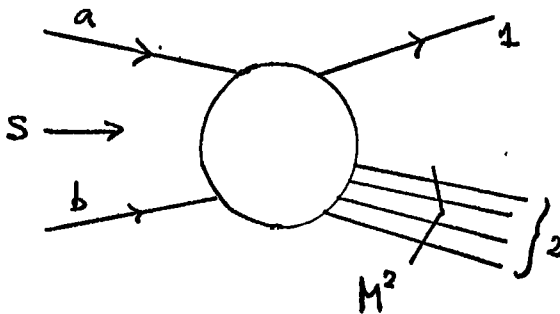


DIAGRAM 3.2

the momenta given by

$$p_1 = m_1 \cosh y_1, \vec{p}_1, m_1 \sinh y_1$$

and

$$p_2 = M_1 \cosh y_2, -\vec{p}_1, M_1 \sinh y_2 \quad (3.17)$$

one finds that if  $y_1 > 0$

$$y_2 = \frac{1}{2} \ln(1-x) \quad (3.18)$$

where  $x$  is the Feynman variable of 1 or is  $(1-M^2/s)$ . Using the

linearity property of the Lorentz transform in terms of the rapidity variable we have

$$y_c = y'_c + \frac{1}{2} \ln(1-x) \quad (3.19)$$

For convenience we define the following notation\*.

Let

$$G_R = \frac{1}{16\pi^2} |V_R(t)|^2 (-x)^{1-2\alpha_R(t)} \quad (3.20)$$

As before

$$N_2(s; x, t, y_c) = \frac{1}{\sigma_c(s)} \frac{d\sigma(s)}{dx dt dy_c} \quad (3.21)$$

$$N_1(s; x, t) = \frac{1}{\sigma_c(s)} \frac{d\sigma(s)}{dx dt} \quad (3.22)$$

$$\tilde{N}_1(M^2; y'_c; R) = \frac{1}{\tilde{\sigma}_R(M^2)} \frac{d\sigma_{Rp}(M^2)}{dy'_c} \quad (3.23)$$

The tilde we again use to denote reggeon-particle scattering (including pomeron-particle scattering). Then equations (3.14) and (3.16) become

$$N_1(s; x, t) = \frac{1}{\sigma_T(s)} \sum_R G_R \tilde{\sigma}_{Rp}(M^2) \quad (3.24)$$

$$N_2(s; x, t, y_c) = \frac{1}{\sigma_T(s)} \sum_R G_R \tilde{\sigma}_{Rp}(M^2) \tilde{N}_1(M^2; y'_c; R) \quad (3.25)$$

---

\* When the arguments  $x, t$  are used we shall always be referring to the final state proton. When the rapidity variable is used we are referring to the meson. Thus, for example,  $N_1(s; x, t)$  is the single particle inclusive distribution for  $pp \rightarrow pX$ .  $N_1(s; y_c)$  is for  $pp \rightarrow \text{meson} + X$ . They are not the same function. ( $\tilde{N}_1(M^2; y'_c)$  is for  $Rp \rightarrow \text{meson} + X$ .)

where

$$M^2 = (1-x)s \quad (3.26)$$

and

$$y_c' = y_c - \frac{1}{2} \ln(1-x) \quad (3.27)$$

So far we have only assumed that a number of factorisable exchanges are present (c.f. section 2.2). Next we shall compute the form of the correlations in our particular model.

We do this by noting again that our model hinges on the assumption that multiplicity distributions from reggeon-particle collisions do not depend on whether the reggeon is a pomeron or a lower lying trajectory. Indeed simplifications introduced in the non-diffractive mechanism made these distributions the same as the non-diffractive particle-particle scattering multiplicity distribution. The total cross-section was, however, allowed to depend upon the nature of the interacting objects. Here again we say nothing about the total cross-sections. To test the assumption concerning the multiplicity distributions against momentum dependent data we must make it considerably stronger. We assume that

$$\tilde{N}_k(s; p_1 \dots p_k, R) = \frac{1}{\sigma} \frac{d\tilde{\sigma}_{Rp}^{\text{inc.}}}{dp_1 \dots dp_k}$$

is independent of the incident reggeon  $R$ . This of course implies the assumption above through

$$\int N_k(s; p_1 \dots p_k) dp_1 \dots dp_k = \langle n(n-1) \dots (n-k+1) \rangle \quad (3.28)$$

as the moments  $\langle n(n-1) \dots (n-k+1) \rangle$  determine the generating function completely through

$$\phi(s, z) = \sum_{k=1}^{\infty} \frac{(z-1)^k}{k!} \langle n(n-1) \dots (n-k+1) \rangle \quad (3.29)$$

and hence determine the multiplicity distribution. This assumption is

thus sufficient (but not necessary) to imply the earlier one. In any case we only actually test the assumption for  $k=1$  here. To do more than this would require fairly detailed data on three and more particle correlations.

If  $\tilde{N}_1(M^2; y'_c, R)$  is independent of the reggeon  $R$  we can remove it from the summation in equation (3.25) obtaining

$$N_2(s; x, t, y_c) = \tilde{N}_1(M^2; y'_c) \frac{1}{\sigma_1(s)} \sum_R G_R \tilde{\sigma}_{R_f}(M^2) \quad (3.30)$$

which from (3.24) becomes

$$N_2(s; x, t, y_c) = N_1(s; x, t) \tilde{N}_1(M^2, y'_c) \quad (3.31)$$

The steps necessary to achieve this result are recounted pictorially in terms of generalised optical theorem diagrams in figure 3.8 .

We can now construct the two particle correlation

$$C_2(s; x, t, y_c) = N_1(s; x, t) \left\{ \tilde{N}_1(M^2; y'_c) - N_1(s; y_c) \right\} \quad (3.32)$$

or alternatively

$$R_2(s; x, t, y_c) = \frac{\tilde{N}_1(M^2; y'_c)}{N_1(s; y_c)} - 1 \quad (3.33)$$

Notice that  $R$  is particularly simple as explicit dependence on the observed proton is not present. The dependence upon the baryon momentum only enters through equations (3.26) and (3.27).

Before making a comparison with the data we should remark upon a point relevant to the measurement of inclusive processes. Often only the angle  $\vartheta$  at which a particle emerges is measured and used in the form

$$\eta = - \ln \tan^{1/2} \theta \quad (3.34)$$

which is the same as

$$\sinh \eta = \frac{1}{\tan \theta} \quad (3.35)$$

hence

$$p_{\parallel} = \frac{p_{\perp}}{\tan \theta} = p_{\perp} \sinh \eta = m_{\perp} \sinh y \quad (3.36)$$

and so if a particle's mass is much smaller than its average transverse momentum ( which is the case for a pion ), then  $p_{\perp} \approx m_{\perp}$  and so

$$y \approx \eta \quad (3.37)$$

Thus for particles observed in the central region, the difference between  $y$  and  $\eta$  is often neglected by phenomenologists. We shall do so here. In reference 31 it is noted that in a Monte-Carlo program it makes little difference which of  $y$  and  $\eta$  are used.



### 3.4 Comparison with the data - global structure

The data for the correlation  $R$  over the range  $0 < x < 1$  are shown in figure 3.9 for I.S.R. energies and  $\eta_c = 0$  and  $-0.88$ . The general trends that one can see in this data are a roughly zero correlation in the region  $0.5 < x < 0.9$  with a negative correlation for a very much forward proton. There is also an indication of a positive correlation at small  $x$ . To see what sort of prediction we get from the model let us consider a very simple form for  $N_1(s; y_c)$  and take  $\tilde{N}_1(s; y_c) = N_1(s; y_c)$ . The form we take is shown in figure 3.10. This is just the Mueller-Regge picture with a central plateau in  $y$  being independent of  $s$ , and with limiting fragmentation within a range  $\Delta$  of the end of the plot. That is

$$N_1(s, y) = \frac{1}{2} \quad : \quad |y| \leq |Y/2 - \Delta| \quad (3.38)$$

$$N_1(s, y) = \frac{1}{\Delta} (Y/2 - y) \quad : \quad |y| > |Y/2 - \Delta| \quad (3.39)$$

where  $Y/2 = y_{\max}$  and  $y_{\min} = -Y/2$ . We take a linear form in the fragmentation region purely for simplicity - we shall perform a more detailed comparison as  $x \rightarrow 1$  in the following section. From (3.33), (3.26) and (3.27) we thus have

$$R = \frac{N_1(s(1-x); y - \frac{1}{2} \ln(1-x))}{N_1(s; y)} - 1 \quad (3.40)$$

If a particle of mass  $m$  is observed then  $Y = \ln(s/m^2)$ . We also need the length of the rapidity plot in the missing mass channel. This is

$$Y' = \ln \frac{M^2}{m^2} = Y + \ln(1-x) \quad (3.41)$$

Thus the form we have for  $R$  becomes (when  $y$  is in the central region

in the s channel) :

$$R \doteq 0 \quad ; \quad x \leq x_c \quad (3.42)$$

and

$$R = \frac{[\ln \sqrt{\frac{s}{m^2}} - y + \ln(1-x)]}{\Delta} - 1 \quad (3.43)$$

;  $x > x_c$

The x dependence enters owing to the fact that while y can be in the central region as far as the initial interaction (s channel) is concerned, it may well be near to its kinematic limit and hence in the fragmentation region in the reggeon-particle collision ( $M^2$  channel). If one particle is seen with momentum x then another cannot be seen with more than (1-x). The point where the form of the correlation changes is given by

$$-\ln(1-x_c) = \frac{1}{2} \gamma - y - \Delta \quad (3.44)$$

or

$$x_c = 1 - \exp\left\{-\left[\frac{1}{2}\gamma - y - \Delta\right]\right\} \quad (3.45)$$

and the kinematic limit on x when a particle with rapidity is observed is

$$x_{\max} = 1 - \exp\left\{-\left[\frac{1}{2}\gamma - y\right]\right\} \quad (3.46)$$

The form of R is plotted in figure 3.11 taking  $\Delta=2$  and  $m=\frac{1}{2}$  GeV/c<sup>2</sup>. (This latter we take to represent an average transverse mass for the centrally observed particle.) For x greater than roughly 0.4, the discrepancies between model and data may perhaps be judged to be owing more to the data than to inherent deficiencies in the model. However

the model does not give a positive correlation for small  $x$  which the data do seem to indicate. This discrepancy is not surprising when one recalls that for factorisable Regge poles to be a good approximation  $s/M^2 = (1-x)^{-1}$  should be large. The fact that  $R$  is roughly zero down to  $x \approx 0.4$  ( $s/M^2 \approx 1.6$ ) is encouraging as the sum of terms in (3.25) which simplifies so neatly in this model to (3.31) should surely not be dominated by a single term down to  $x \approx 0.4$ .

### 3.5 Detailed comparison with the data as $x \rightarrow 1$

In the previous section we took a global view of the two particle correlation. In this section we shall examine the behaviour of the correlation when the proton is observed very close to the forward direction. We take again equation (3.31) and compare it with the more detailed data near  $x=1$ . We take  $N_1(s;x,t)$  from the data (see figure 3.12), and in order to make a parameter free comparison we take  $\tilde{N}_1(y_c)$  to be the same as the particle-particle interaction inclusive distribution. We use data (see figure 3.13) for the processes  $p \xrightarrow{\pi^-} \pi^-$ ;  $\pi^+ \xrightarrow{p} \pi^-$ ;  $p \xrightarrow{\pi^+} \pi^-$ ; and  $p \xrightarrow{p} \pi^-$ . We choose these as none of them should have a diffractive peak and we expect none in  $R^0 \xrightarrow{p}$  charged particle, which is effectively the process described by  $\tilde{N}$  as  $x \rightarrow 1$ .

We again neglect the difference between the variables  $y$  and  $\eta$  and so

$$\left. \begin{aligned} \Theta = 90^\circ \pm 14^\circ &\Rightarrow y = 0 \pm 0.25 \\ \Theta = 117.5^\circ \pm 12.5^\circ &\Rightarrow y = -0.5 \pm 0.25 \end{aligned} \right\} \quad (3.47)$$

The correlation data are at  $s=929.5 \text{ GeV}^2$ . We thus take the low energy data at energy  $M^2$  and calculate  $x=1-M^2/s$ . For each of the two values of  $y$  we calculate  $y'$  knowing  $x$  and hence read off  $\tilde{N}_1(M^2; y')$  from the low energy data\*. The integral over the small size of the detector we approximate by

$$\int_{y_0-\epsilon}^{y_0+\epsilon} \tilde{N}_1(M^2; y') dy' = 2\epsilon \cdot \tilde{N}_1(M^2; y_0) \quad (3.48)$$

Here  $\epsilon = 0.25$ . This value is then multiplied by  $N_1(s;x,t)$  for proton production to find the double differential cross-section.

---

\* We also use the data for the relevant  $\sigma_{\text{tot}}$  to get the normalised distribution  $N$ . (See figure 3.14)

The resulting parameter free prediction is shown in figure 3.15 . There is now no diffractive peak in the double differential cross-section. The model predicts, if anything, a too rapid decrease as  $x \rightarrow 1$  . This may be due to the  $x$  resolution of the experiment. To see the model's prediction for  $M^2 > 50 \text{ GeV}^2$  where there is very little suitable low energy data, we can extrapolate using a scaling approximation. We assume that for  $M^2 > 50 \text{ GeV}^2$  the distribution  $\tilde{N}_1(M^2; y')$  does not depend upon  $M^2$ . Dependence on  $x$  will still come in through  $y'$  . In each case ( $\vartheta = 90^\circ$ ,  $\vartheta = 117.5^\circ$ ) we extrapolate from the largest  $M^2$  point that we have into the central region where we expect the scaling approximation to work best. These lines are also shown in figure 3.15 . Errors on them will clearly be at least as large as on the points from which the extrapolation is made. Within this error the description they give of the shape of the data is excellent.

### 3.6 The correlation as $x \rightarrow 0$

The exact nature of the correlation when the proton is produced at small  $x$  is difficult to ascertain from the data. (Figure 3.9) There does, however seem to be a positive correlation. Our model in this region is inappropriate. However we can make some remarks concerning this region. First let us examine the baryon-meson correlation under the assumption that one and only one baryon is found with  $x > 0$  in proton-proton interactions. If this assumption is correct, then from

$$C_2^{H.B.}(p_B, p_M) = N_2^{H.B.}(p_B, p_M) - N_1^B(p_B) N_1^M(p_M) \quad (3.49)$$

we have

$$\int C_2^{H.B.}(p_B, p_M) dp_B dp_M = \langle n_B n_M \rangle - \langle n_B \rangle \langle n_M \rangle = 0 \quad (3.50)$$

and also

$$\int C_2^{H.B.}(p_B, p_M) dp_B = 0 \quad (3.51)$$

If the relative production cross-sections for the various possible baryons are independent of the number of mesons produced, then can substitute 'proton' for 'baryon' in this discussion. If now there is a short range

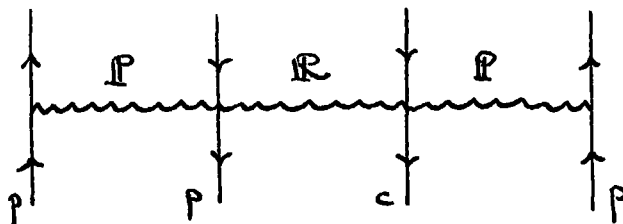


DIAGRAM 3.3

---

correlation between the proton and particle  $c$ , (the Mueller-Regge

approach - diagram 3.3 - gives us no reason to suppose (there isn't), then the long range correlation will have to have the opposite sign to satisfy (3.51). This can simply be effected in our model by taking

$$\tilde{N}_1 = (1 + \delta) N_1 \quad (3.52)$$

where  $\delta$  can be positive or negative as required.

On the other hand it may be that the short range correlation (if this is what is observed as  $x \rightarrow 0$ ) is associated with antibaryon production and hence a violation of (3.51).

### 3.7 Beyond two particle correlations

The ease with which our model can be generalised makes it worthwhile to predict further quantities which have yet to be measured. We take here the case where one proton and two centrally produced particles which we refer to as c and d are observed.

Instead of equation (3.31) we now have analogously

$$N_3(s; x, t, y_c, y_d) = N_1(s; x, t) \tilde{N}_2(M^2; y_c', y_d') \quad (3.53)$$

The three particle correlation we wish to find is from (1.14)

$$\begin{aligned} C_3(s; x, t, y_c, y_d) = & N_3(s; x, t, y_c, y_d) - N_1(s, x, t) N_2(s; y_c, y_d) \\ & - N_1(s; y_c) N_2(s; x, t, y_d) - N_1(s; y_d) N_2(s; x, t, y_c) \\ & - N_1(s, x, t) N_1(s; y_c) N_1(s; y_d) \end{aligned} \quad (3.54)$$

Equations (3.51) and (3.53) now give

$$\begin{aligned} C_3(s; x, t, y_c, y_d) = & N_1(s; x, t) \left\{ \tilde{N}_2(M^2, y_c', y_d') \right. \\ & - N_2(s; y_c, y_d) - N_1(s; y_c) \tilde{N}_1(M^2, y_d') \\ & \left. - N_1(s; y_d) \tilde{N}_1(M^2, y_c') - N_1(s; y_c) N_1(s; y_d) \right\} \end{aligned} \quad (3.55)$$

We again define in a similar way to  $R_2$

$$R_3(1, 2, 3) = \frac{C_3(1, 2, 3)}{N_1(1) N_1(2) N_1(3)} \quad (3.56)$$

and so this quantity becomes



$$R_3(s; x, t, y_c, y_d) = \frac{\tilde{C}_2(M^2; y_c', y_d') - C_2(s; y_c, y_d)}{N_2(s; y_c) N_1(s; y_d)} + \left[ 1 - \frac{\tilde{N}_2(M^2; y_c')}{N_2(s; y_c)} \right] \left[ 1 - \frac{\tilde{N}_1(M^2; y_d')}{N_1(s; y_d)} \right] - 3 \quad (3.57)$$

The quantities  $C_2$  here are the two particle correlations between the two observed particles other than the proton. Although this formula looks complicated, in the central region it is fairly easy to see what it will look like. For  $y_c'$  and  $y_d'$  to be in the central region, we must have analogously to (3.42) and (3.45)

$$x \leq \text{Min}(x_c, x_d) \quad (3.58)$$

where

$$x_c = 1 - \exp\left\{-\left[\frac{1}{2} - y_c - \Delta\right]\right\}$$

$$x_d = 1 - \exp\left\{-\left[\frac{1}{2} - y_d - \Delta\right]\right\} \quad (3.59)$$

The term involving the product in (3.57) vanishes in this region (that is  $R_2=0$ ). The short range component of  $C_2$  will, as discussed in the first chapter, only depend upon  $y_c - y_d$  and so, as

$$y_c' - y_d' = y_c - y_d \quad (3.60)$$

then

$$\tilde{C}_2(\text{short range}) - C_2(\text{short range}) = 0 \quad (3.61)$$

If the long range correlations are of the form (3.10) with the mechanism b being negligible in the central region and mechanism a scaling and

having a plateau in its single particle distribution, as discussed previously, then

$$\tilde{C}_2(\text{long range}) - C_2(\text{long range}) = 0 \quad (3.62)$$

leaving

$$R_2 = -3 \quad (3.63)$$

as the prediction of our model. Furthermore if the first term of (3.57) can be neglected, then we expect, using the behaviour of  $R_2$ , that

$$R_3 \xrightarrow{x \rightarrow 1} -2 .$$

Four and higher particle correlations (involving the leading proton and  $n-1$  others) can be similarly calculated with increasing degrees of complexity.

### 3.8 Semi-inclusive quantities

An approach to long range correlations which differs strikingly from ours is that of reference 36. This model generates long range correlations between protons and pions by relating the pion multiplicity to the momentum of the forward proton. By the assumption that a pion at  $90^\circ$  implies a high multiplicity event which implies large  $M^2$  which a slow proton, the authors of reference 36 are able to generate a positive correlation as  $x \rightarrow 0$ . It is very difficult to see whether their model has any Regge factorisable structure even as  $x \rightarrow 1$ . It does, however, draw attention to semi-inclusive quantities. Here again we can gain some insight into the properties implied by our factorisable model. Although, again, data here are not available we shall write down a typical prediction of the model for two reasons. Firstly we are encouraged by the success of the model so far (in particular in the semi-inclusive property discussed in section 3.2) and secondly the results are perhaps not quite what one might expect.

Let  $n$  be the number of charged pions in the event. The semi-inclusive cross-section for  $pp \rightarrow p + n$  charged pions + anything else is

$$N_p^{(n)}(s; x, t) = \frac{1}{\sigma_n(s)} \frac{d\sigma^{(n)}}{dx dt} \quad (3.64)$$

That for  $pp \rightarrow \pi + n-1$  other charged pions + anything else is

$$N_\pi^{(n)}(s, y_\pi) = \frac{1}{\sigma_n(s)} \frac{d\sigma^{(n)}}{dy_\pi} \quad (3.65)$$

and the double inclusive spectrum is

$$N_2^{(n)}(s; x, t, y_\pi) = \frac{1}{\sigma_n(s)} \frac{d\sigma^{(n)}}{dx dt dy_\pi} \quad (3.66)$$

Denoting

$$\alpha_n(s) = \frac{\sigma_n(s)}{\delta(s)} \quad (3.67)$$

we have

$$\sum \alpha_n(s) = 1 \quad (3.68)$$

$$\sum \alpha_n(s) N_p^{(n)}(s; x, t) = N_1(s; x, t) \quad (3.69)$$

$$\sum \alpha_n(s) N_\pi^{(n)}(s, y_\pi) = N_1(s, y_\pi) \quad (3.70)$$

and

$$\sum \alpha_n(s) N_2^{(n)}(s; x, t, y_\pi) = N_2(s; x, t, y_\pi) \quad (3.71)$$

We also define the semi-inclusive correlations

$$C_2^{(n)}(s; x, t, y_\pi) = N_2^{(n)} - N_p^{(n)}(s; x, t) N_\pi^{(n)}(s, y_\pi) \quad (3.72)$$

from which it follows (see also reference 36) that

$$C_2 = \sum \alpha_n C_2^{(n)} + \sum \alpha_n \left( N_p^{(n)}(s; x, t) - N_1(s; x, t) \right) \left( N_\pi^{(n)}(s, y_\pi) - N_1(s, y_\pi) \right) \quad (3.73)$$

We also define

$$R_2^{(n)} = \frac{C_2^{(n)}(s; x, t, y_\pi)}{N_p^{(n)}(s; x, t) N_\pi^{(n)}(s; y_\pi)} \quad (3.74)$$

So far we have defined the semi-inclusive quantities and written down the equations which follow from the definitions. In exact analogy with equation (3.31) our model gives us

$$N_2^{(n)}(s; x, t, y_\pi) = N_p^{(n)}(s; x, t) \tilde{N}_\pi^{(n)}(M^2, y_\pi') \quad (3.75)$$

Thus exactly as before we obtain

$$R_2^{(n)} = \frac{\tilde{N}_\pi^{(n)}(M^2; y_\pi')}{N_\pi^{(n)}(s; y_\pi)} - 1 \quad (3.76)$$

In this case we cannot resort to the scaling argument that gave  $R_2=0$  in the central region. Instead we assume that the ratio  $N_\pi^n(s; y)/N_1(s; y)$  is independent of  $y$ . This implies through (1.10) that

$$\frac{N_\pi^{(n)}(s, y_\pi)}{N_1(s, y_\pi)} = \frac{n}{\bar{n}(s)} \quad (3.77)$$

and so we find

$$R_2^{(n)}(s; x, t, y_\pi) = \frac{\bar{n}(s)}{\bar{n}(s(x))} \left\{ R_2(s; x, t, y_\pi) + 1 \right\} - 1 \quad (3.78)$$

Here we have a rather strange result. If we measure the correlation  $R_2$  without noting how many pions are produced we get zero (at least in a certain region). If we measure the same thing knowing that exactly  $n$  pions are produced we find a number greater than zero and independent of  $n$  ! Not only that, it varies with the momentum of the proton as shown in figure 3.16. This result also implies that  $\sum \alpha_n C_2^n > 0$  contrary to what is assumed in reference 36.

Finally we should like to note that to write down the correlation  $C_2^n$  we must work out  $N_p^n$ . Following the notation of section 3.3 we have

$$\frac{d\sigma^{(n)}}{dx dt dy_\pi} = \sum_R G_R \frac{d\tilde{\sigma}_{R_p}^{(n)}}{dy_\pi} \quad (3.79)$$

$$\frac{d\sigma^{(n)}}{dx dt} = \sum_R G_R \tilde{\sigma}_{R_p}^{(n)} \quad (3.80)$$

These with the assumption that  $N_\pi^n(M^2; y)$  is independent of the nature

of the reggeon projectile, give (3.75). Equation (3.80) with (3.24) also implies that

$$N_p^{(n)}(s; x, t) = N_1(s, x, t) \frac{\sigma(s)}{\alpha_n(s)} \frac{\sum_R G_R \tilde{\sigma}_{R_T}^{(n)}(M^2)}{\sum_R G_R \tilde{\sigma}_{R_P}^{(n)}(M^2)} \quad (3.81)$$

Our assumption of the previous chapter that  $\tilde{\sigma}_{R_P}^{(n)}/\tilde{\sigma}_{R_T}^{(n)}$  is independent of the reggeon R is now sufficient to give

$$\tilde{N}_p^{(n)}(s; x, t) = N_1(s; x, t) \frac{\tilde{\alpha}_n(M^2)}{\alpha_n(s)} \quad (3.82)$$

With this (3.69) follows from (3.68) and (3.71) follows from (3.75) and (3.70). (This is just the statement that our factorising model describes the n dependent quantities consistently.) Hence

$$C_2^{(n)} = N_1(s; x, t) \frac{\tilde{\alpha}_n(M^2)}{\alpha_n(s)} \left\{ \tilde{N}_T^{(n)}(M^2; y_T) - N_T^{(n)}(s; y_T) \right\} \quad (3.83)$$

To examine (3.82) we should write  $\alpha_n(s)$  as a weighted sum of diffractive and non-diffractive parts, and consistent with the model of chapter two put  $\tilde{\alpha}_n(M^2)$  equal to the non-diffractive part. However as data are not yet available we regard it as sufficient, to find a rough prediction, to set  $\tilde{\alpha}_n(M^2)$  and  $\alpha_n(s)$  to the same distribution (as indicated in section 3.2) and write a Poisson ansatz

$$\alpha_n(s) = \frac{[\bar{n}(s)]^n}{n!} e^{-\bar{n}(s)} \quad (3.84)$$

with mean

$$\bar{n}(s) = \lambda e^{s/s_0} \quad (3.85)$$

Thus we find

$$\frac{N_p^{(n)}(s; x, t)}{N_1(s; x, t)} = (1-x)^{-\lambda} \left\{ 1 + \frac{\ln(1-x)}{\ln \frac{s}{s_0}} \right\}^n \quad (3.86)$$

This prediction is shown in figure 3.17 for various values of  $n$ .

Although in the absence of data these last two sections have been speculative, they do provide some interesting predictions on which our model (which seems successful as far as existing data go) could be tested.

FIGURES FOR CHAPTER THREE



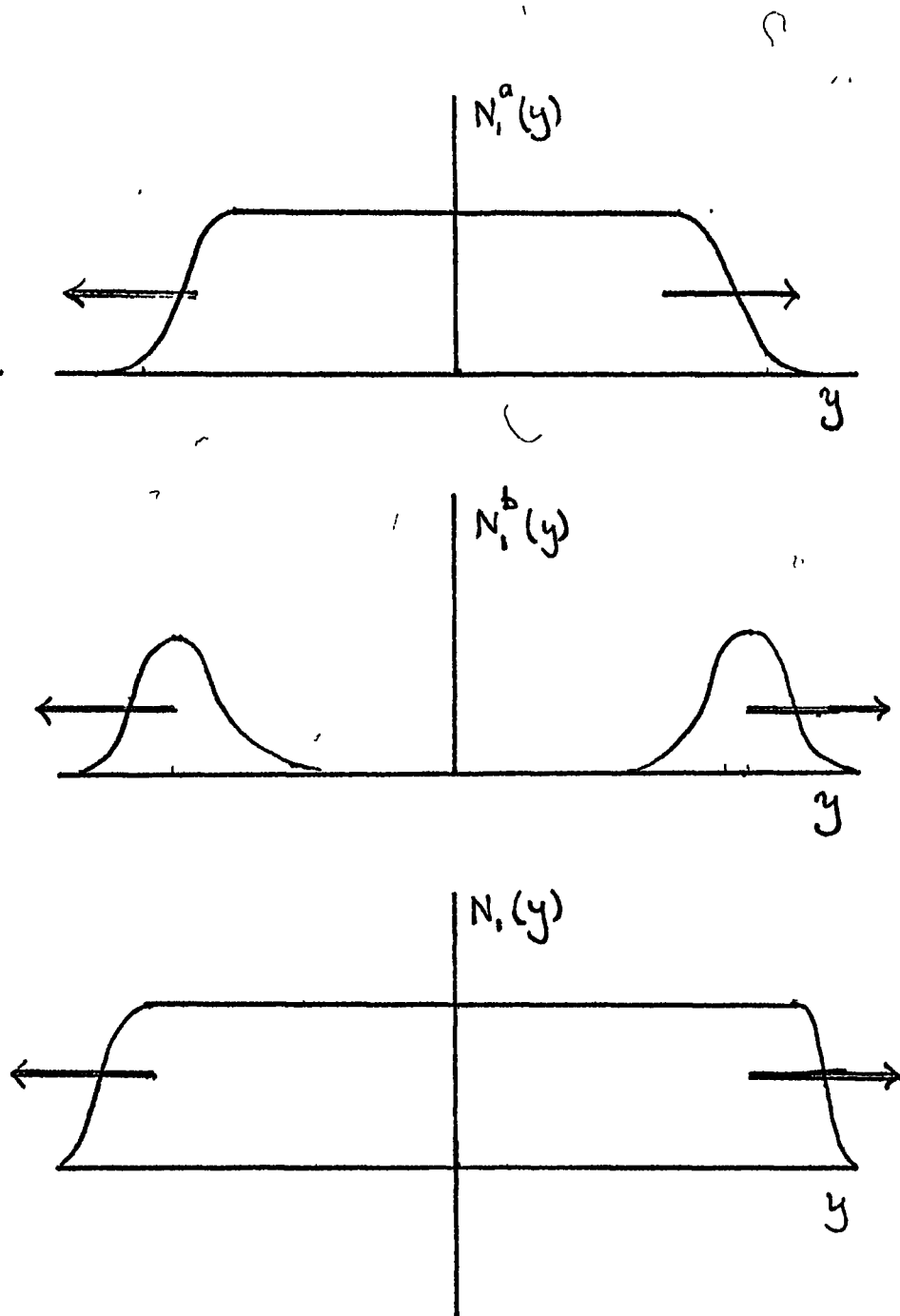


FIGURE 3.1 : Diagrammatic representation of addition of inclusive distributions in the two component model. The arrows represent the behaviour as energy increases. The second component (b) is a typical low mass diffraction term with a large rapidity gap and constant multiplicity.

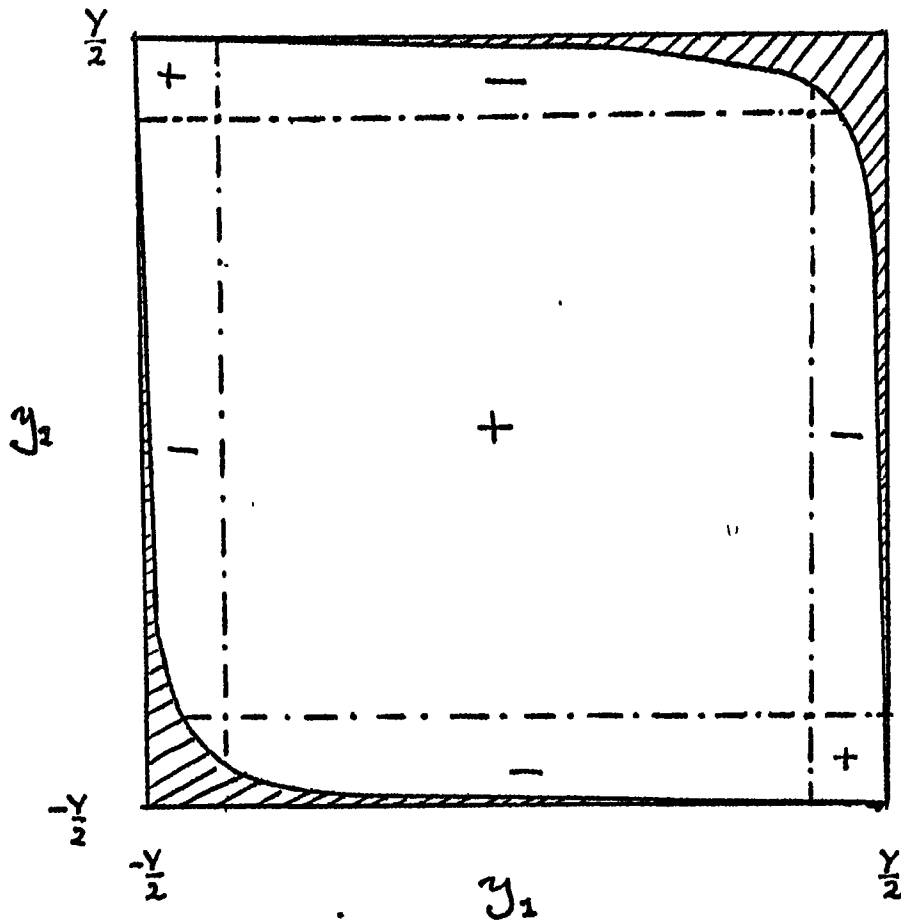


FIGURE 3.2.a : The sign of the long range two particle correlation as a function of the two rapidities. The broken lines represent the positions of zeros . The shaded region lies outside the kinematic limit.

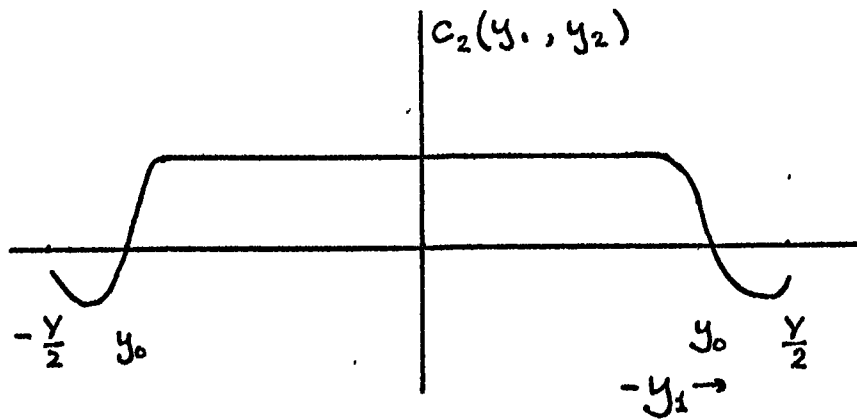


FIGURE 3.2.b : The two component model's long range correlation plotted against one of the rapidities.

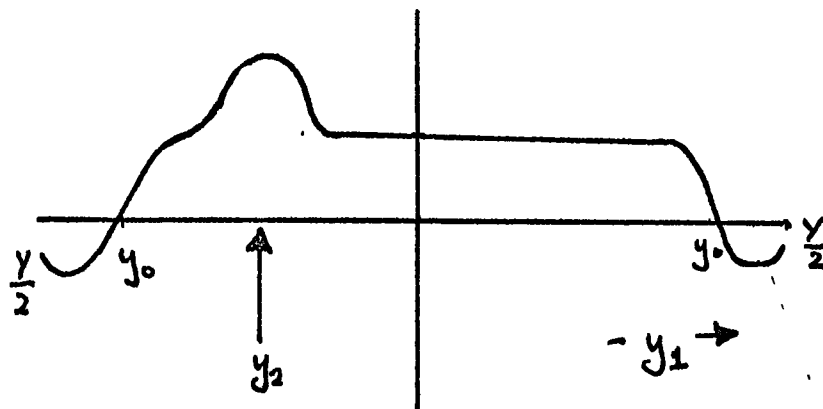


FIGURE 3.2.c : As above but with a typical short range correlation superimposed.

In both these illustrations the position of the zero, labelled  $y_0$ , remains a fixed distance from the end of the plot as  $Y$  becomes large. (See section 3.1)

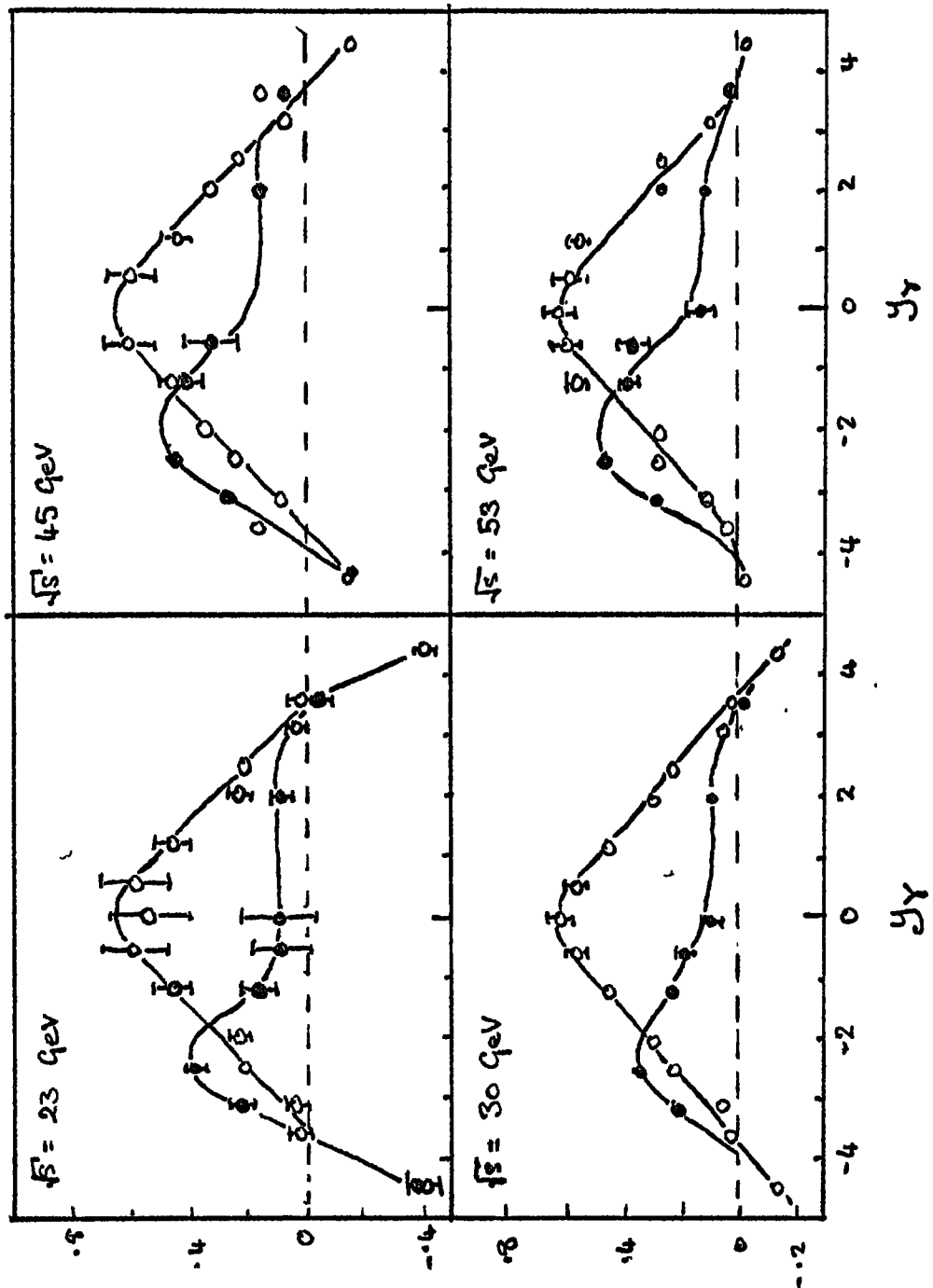


FIGURE 3.3.a : Data for the two particle correlation in the reaction  $pp \rightarrow \gamma + \text{hadron} + \text{anything}$  plotted against the photon rapidity. The white dots are for  $y_h = 0$ , black dots are for  $y_h = -2.5$ . Data are from reference 48.

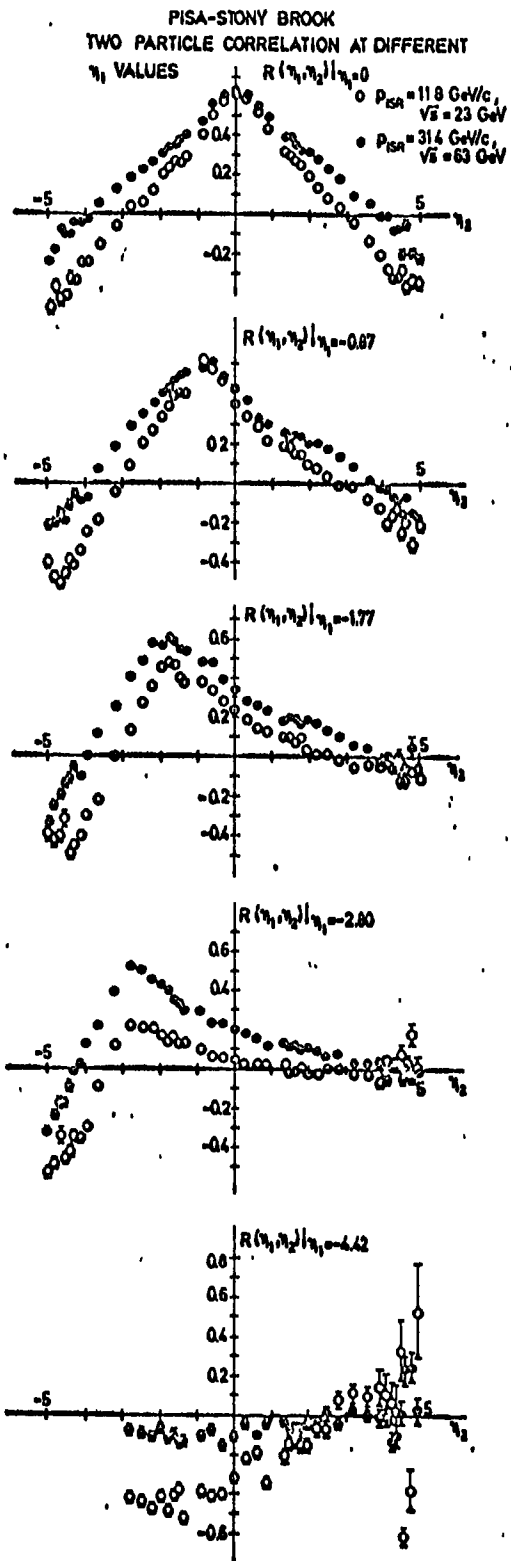


FIGURE 3.3.b : Data for the normalised two particle correlation  $R$ . (See reference 49).

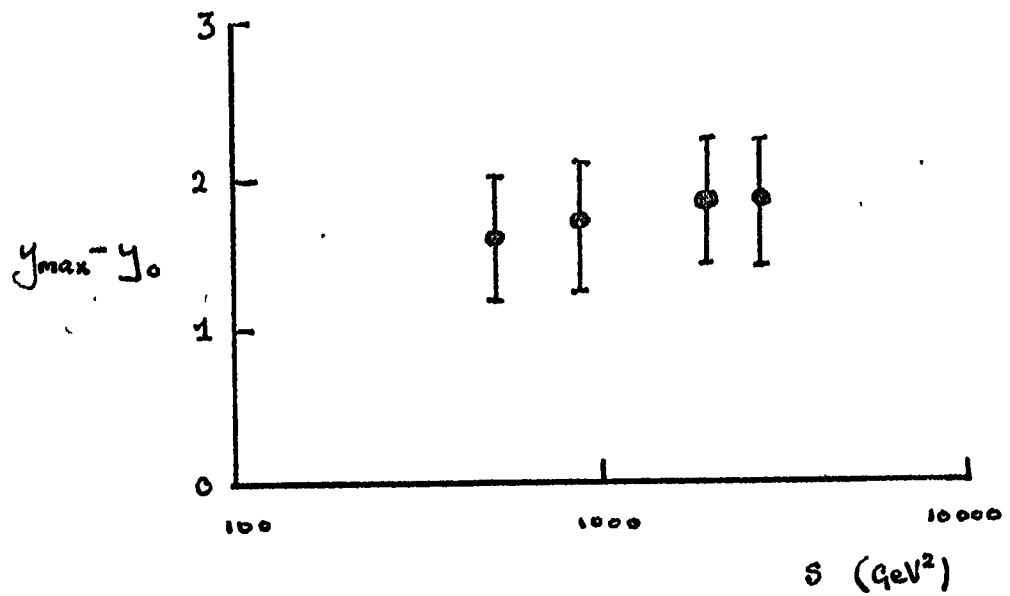


FIGURE 3.4.a : The distance of the zero in the correlation from the end of the rapidity plot as a function of energy. (Data from fig. 3.3a)

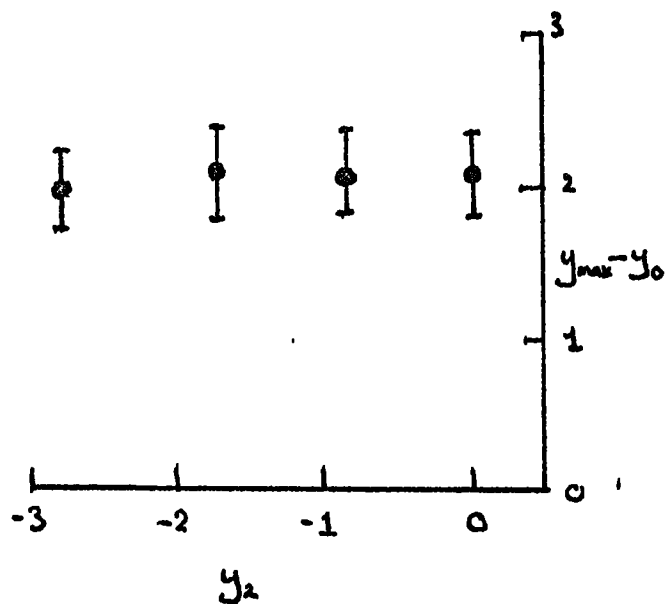


FIGURE 3.4.b : The distance of the zero in the correlation from the end of the rapidity plot as a function of the rapidity of the second particle. (Data from fig 3.3b)

The constant behaviour indicated in each case is in accord with our model.

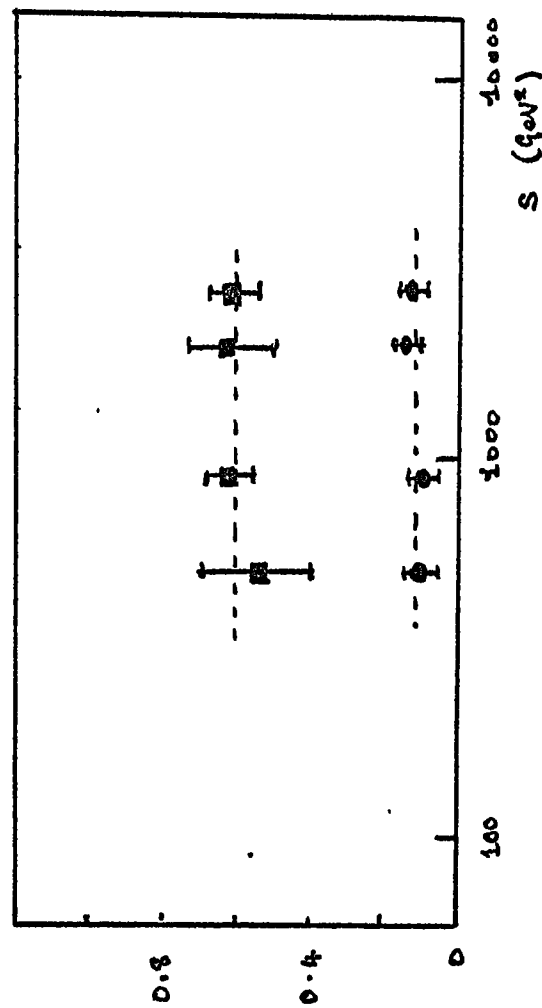


FIGURE 3.5 : The two particle correlation as a function of energy. Data from figure 3.3.a .

Upper points :  $y_1 = y_2 = 0$

Lower points :  $y_1 = 2 ; y_2 = -2.5$

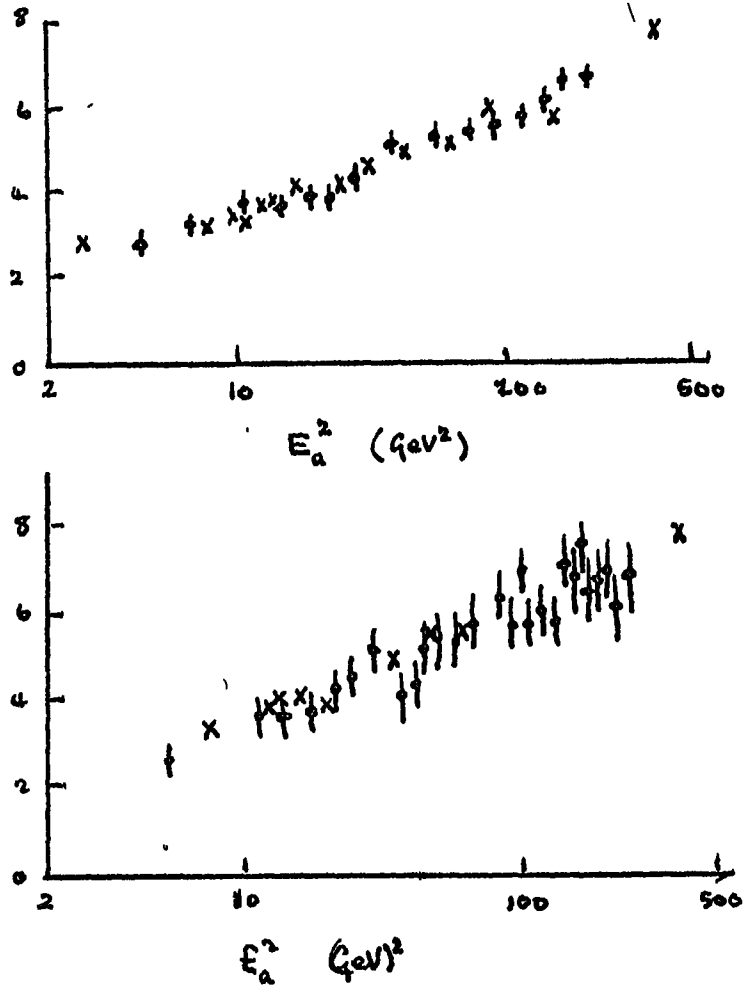


FIGURE 3.6 :

Upper graph: The average multiplicity in pp interactions  
(crosses)

The average multiplicity in pp → pX (points)

Lower graph: The average multiplicity in πp interactions  
(crosses)

The average multiplicity in πp → pX (points)

For the points on each plot,  $\langle n_{ch} \rangle - 1$  is plotted against the available energy  $E_a$  in the  $M^2$  channel.



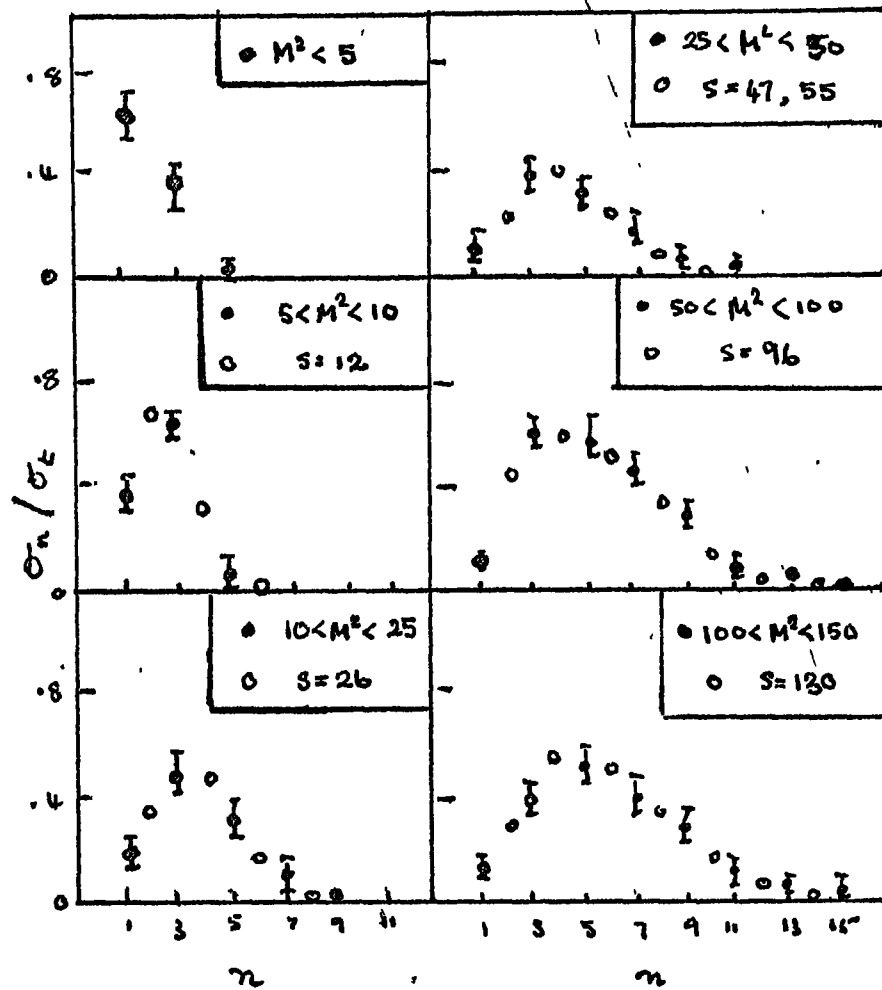


FIGURE 3.7 : The multiplicity distributions from pp interactions in  $s$  and  $M^2$  channels. (The figures for  $s$  and  $M^2$  are in  $\text{GeV}^2$ ).

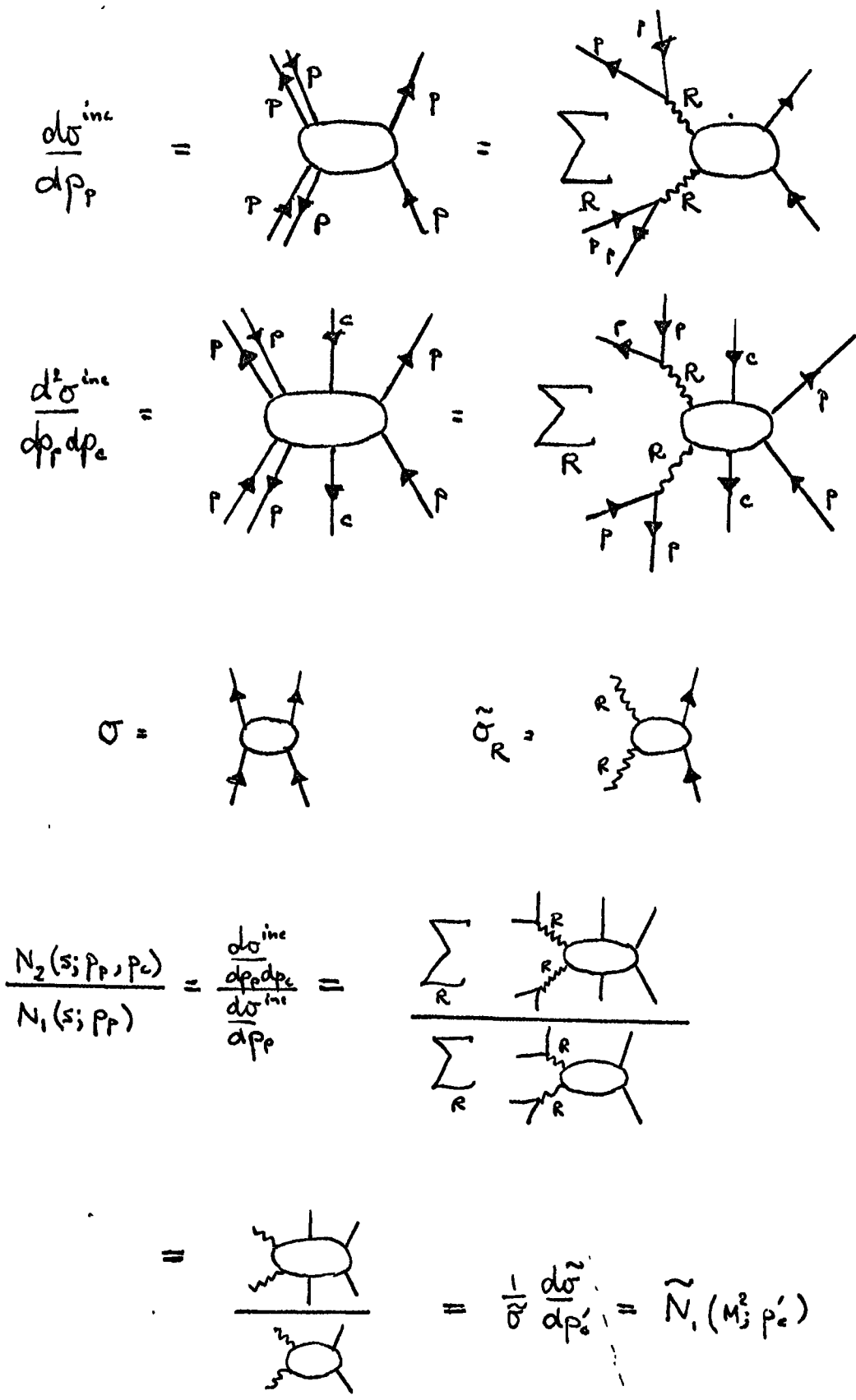


FIGURE 3.8 : Calculation of the two particle inclusive distribution with one particle in the fragmentation region. The blobs represent Mueller discontinuities of forward elastic amplitudes.

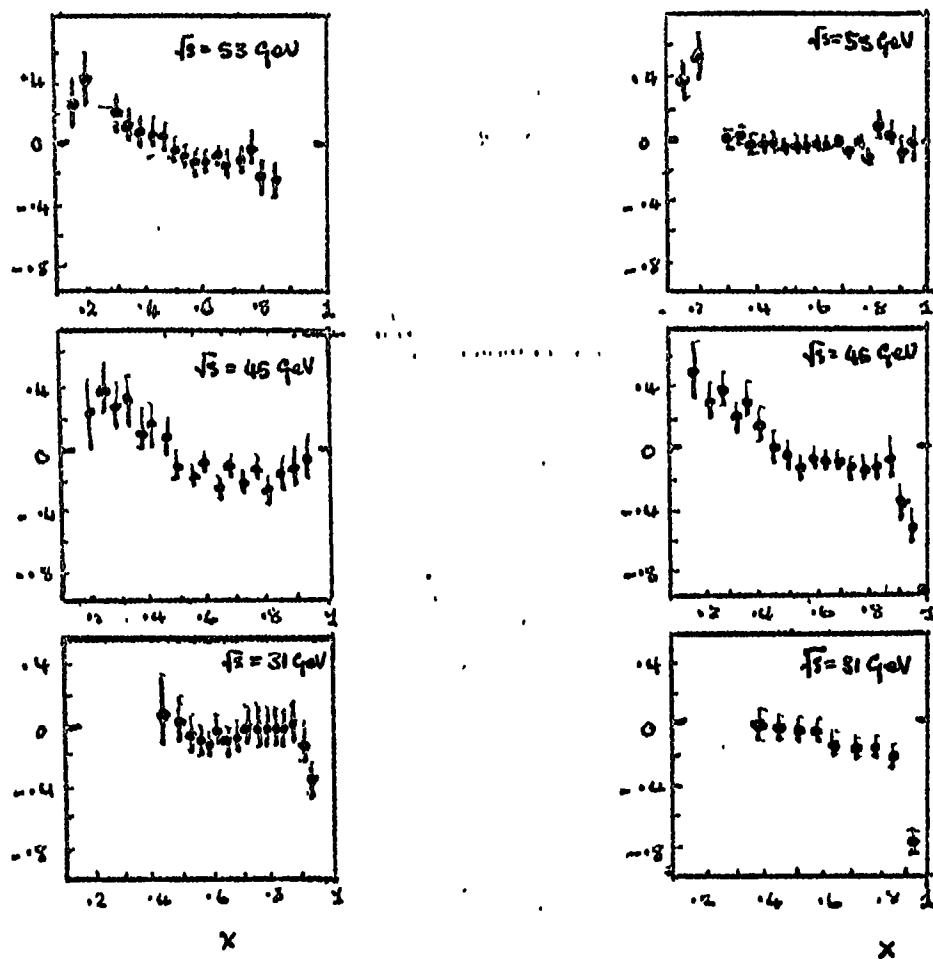


FIGURE 3.9 : The correlation  $R_2$  between a proton (characterised by the Feynman variable  $x$ ) and a charged particle with rapidity  $y$ .

Left :  $y=0$

Right :  $y = -.87$

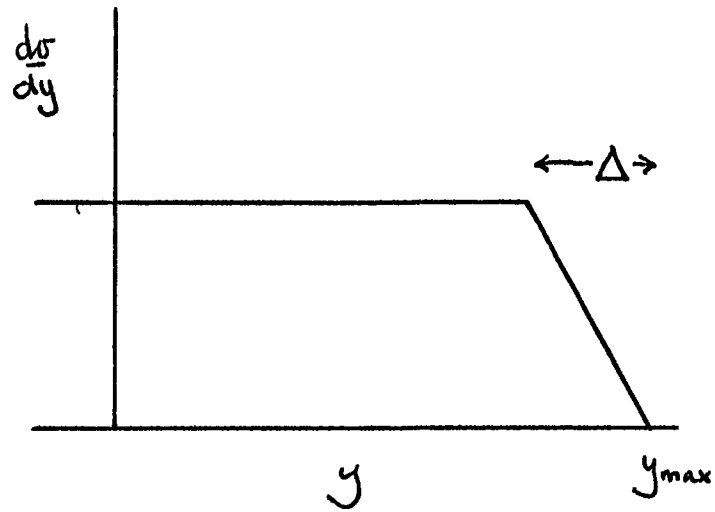


FIGURE 3.10 : An approximate parameterisation of the single particle inclusive distribution.

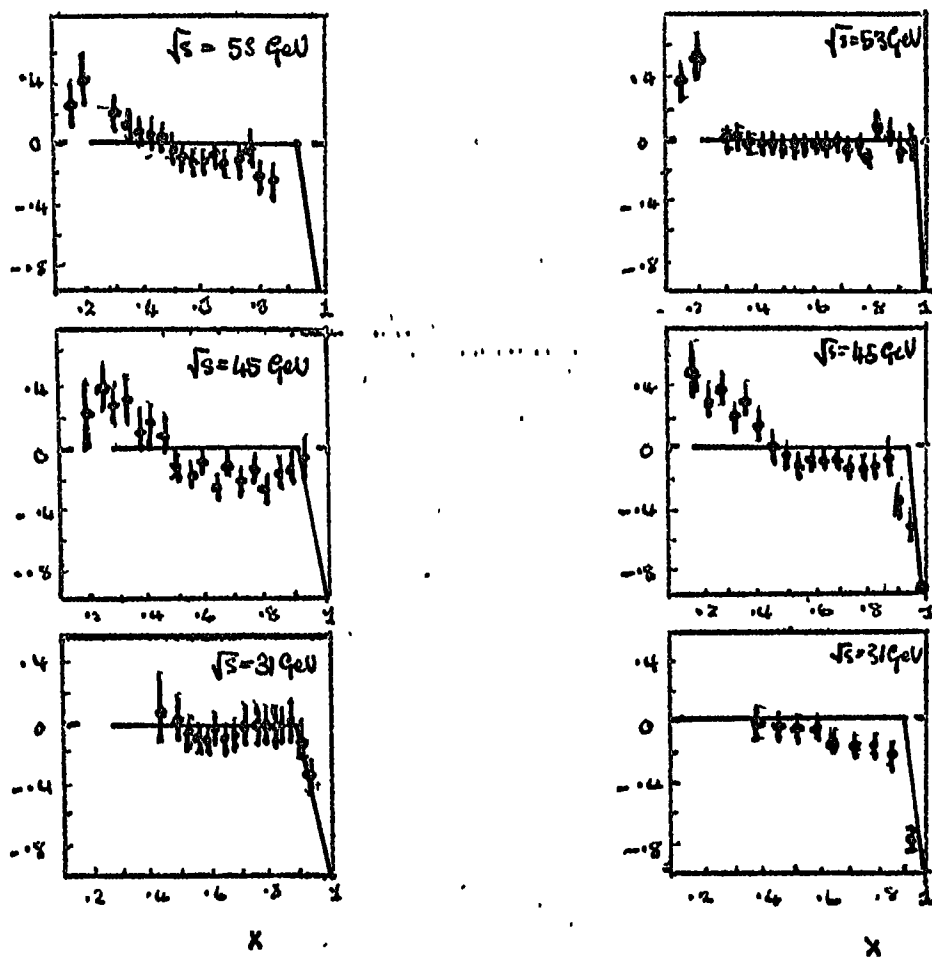


FIGURE 3.11 : As for figure 3.9 but with a typical result from our model superimposed.

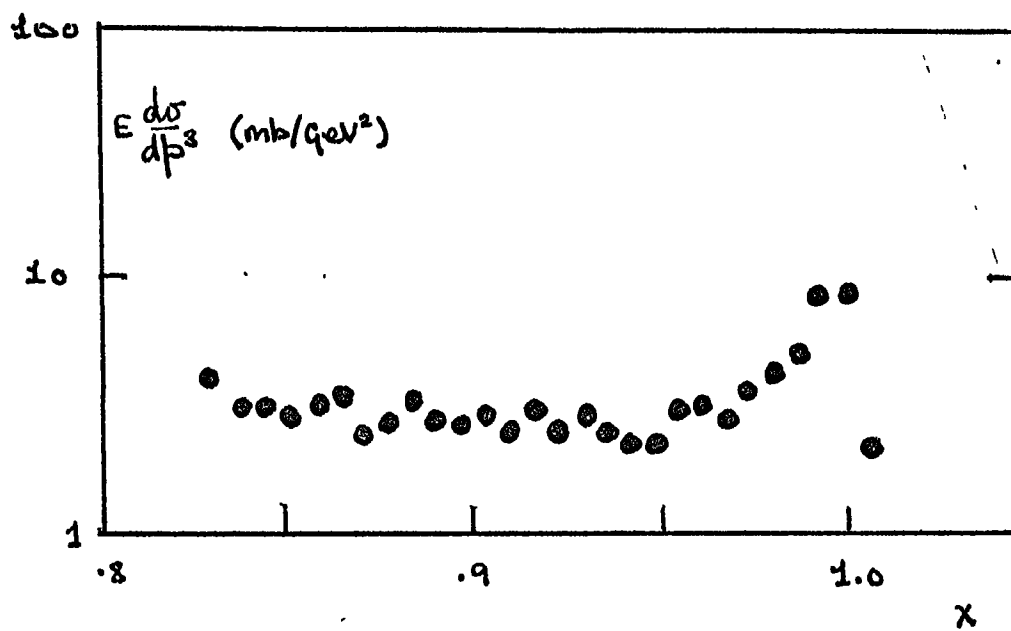


FIGURE 3.12 : The inclusive distribution for the reaction  $pp \rightarrow pX$  showing the diffractive peak.

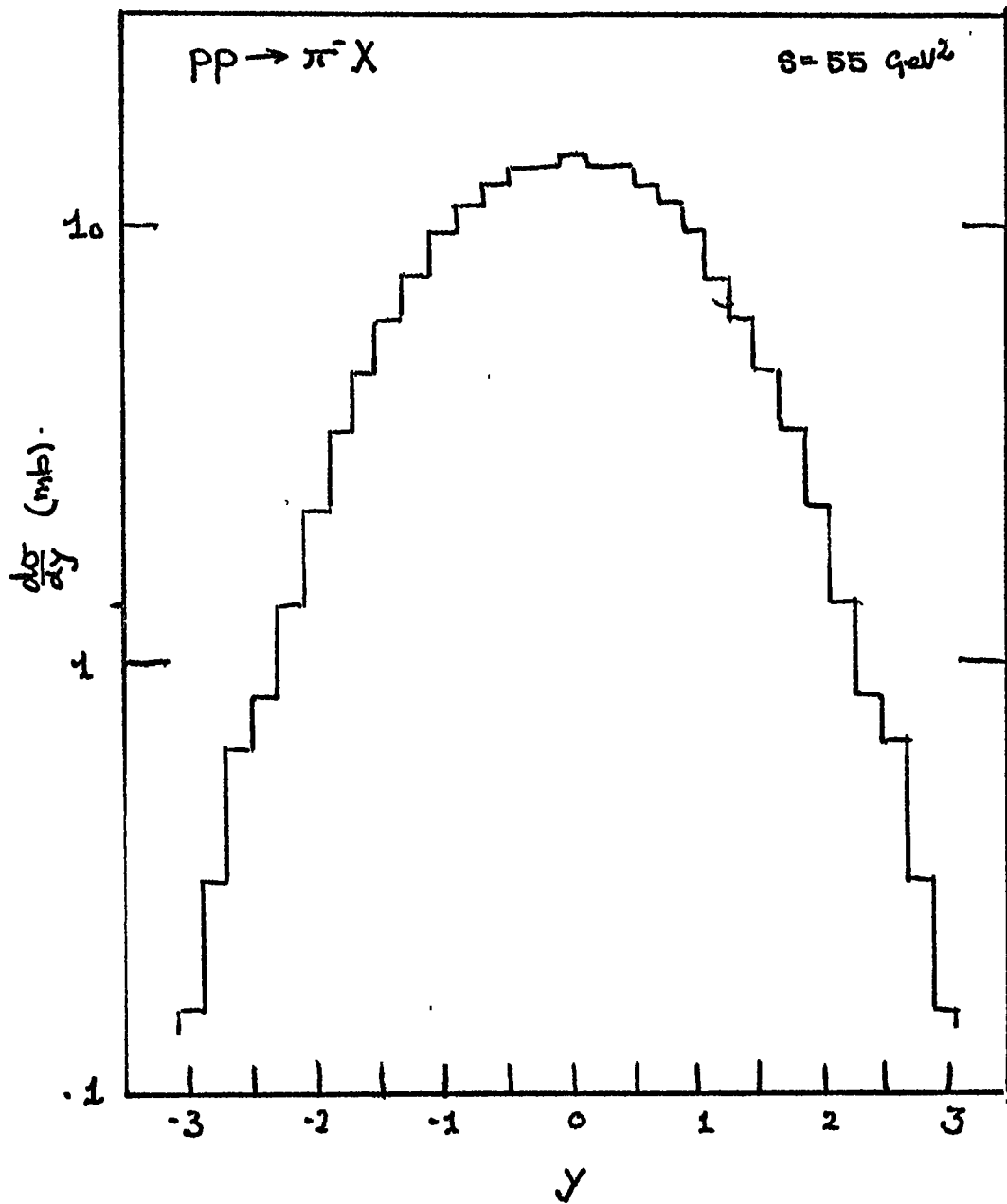


FIGURE 3.13a : The inclusive rapidity distribution of a pion in proton-proton interactions. (c.f. following three figures)

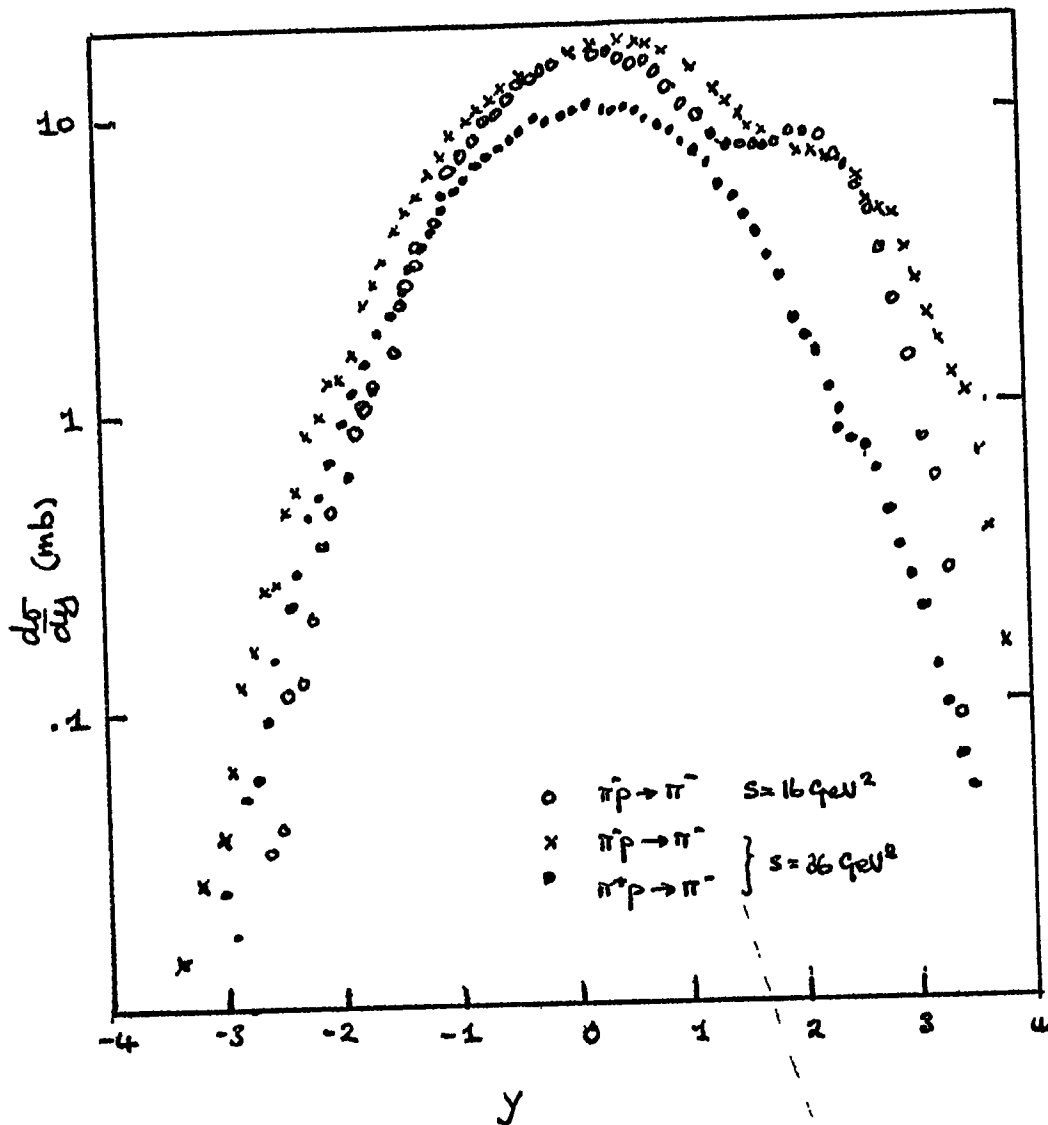


FIGURE 3.13b



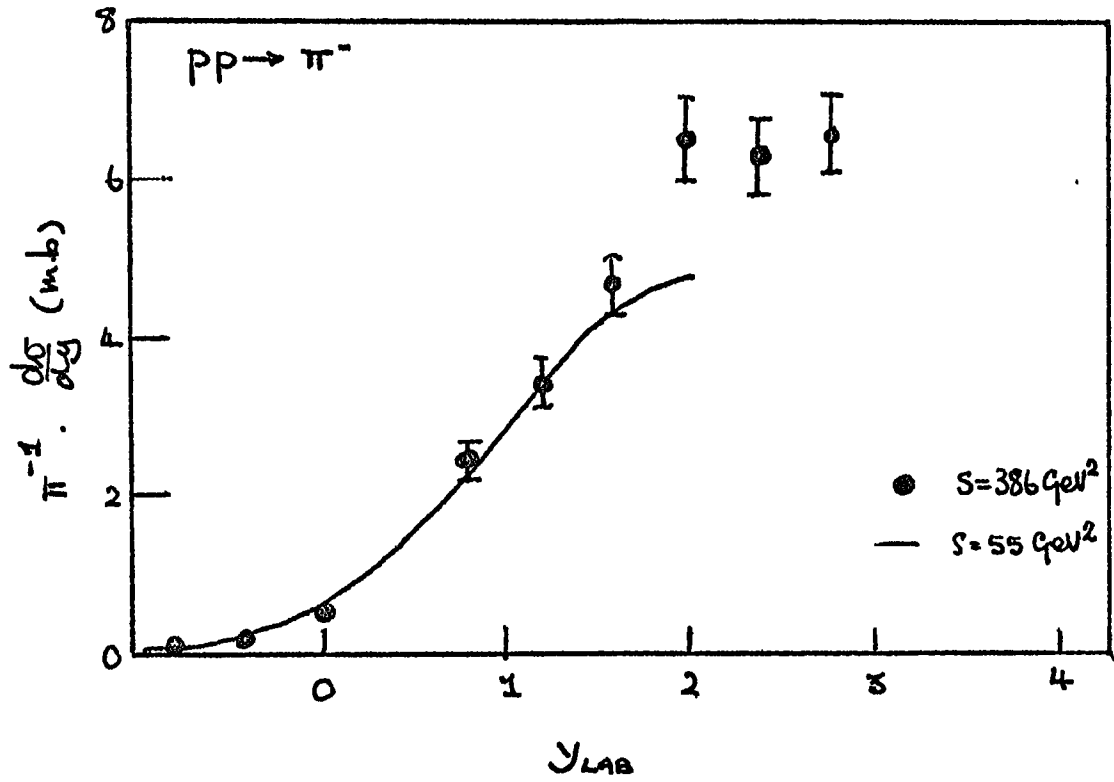


FIGURE 3.13c

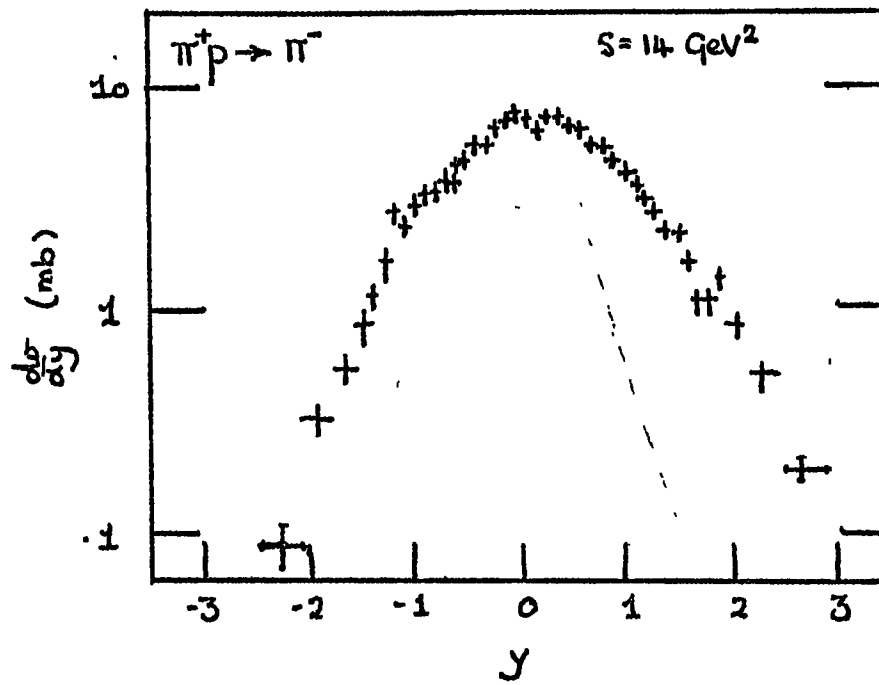


FIGURE 3.13d

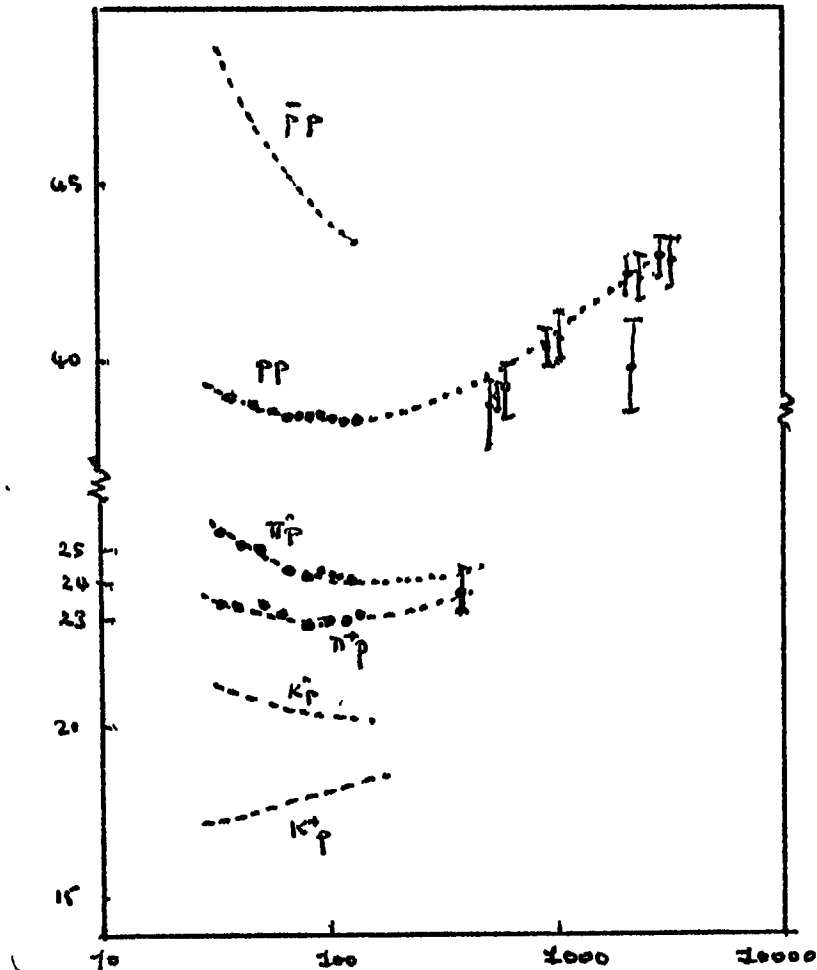
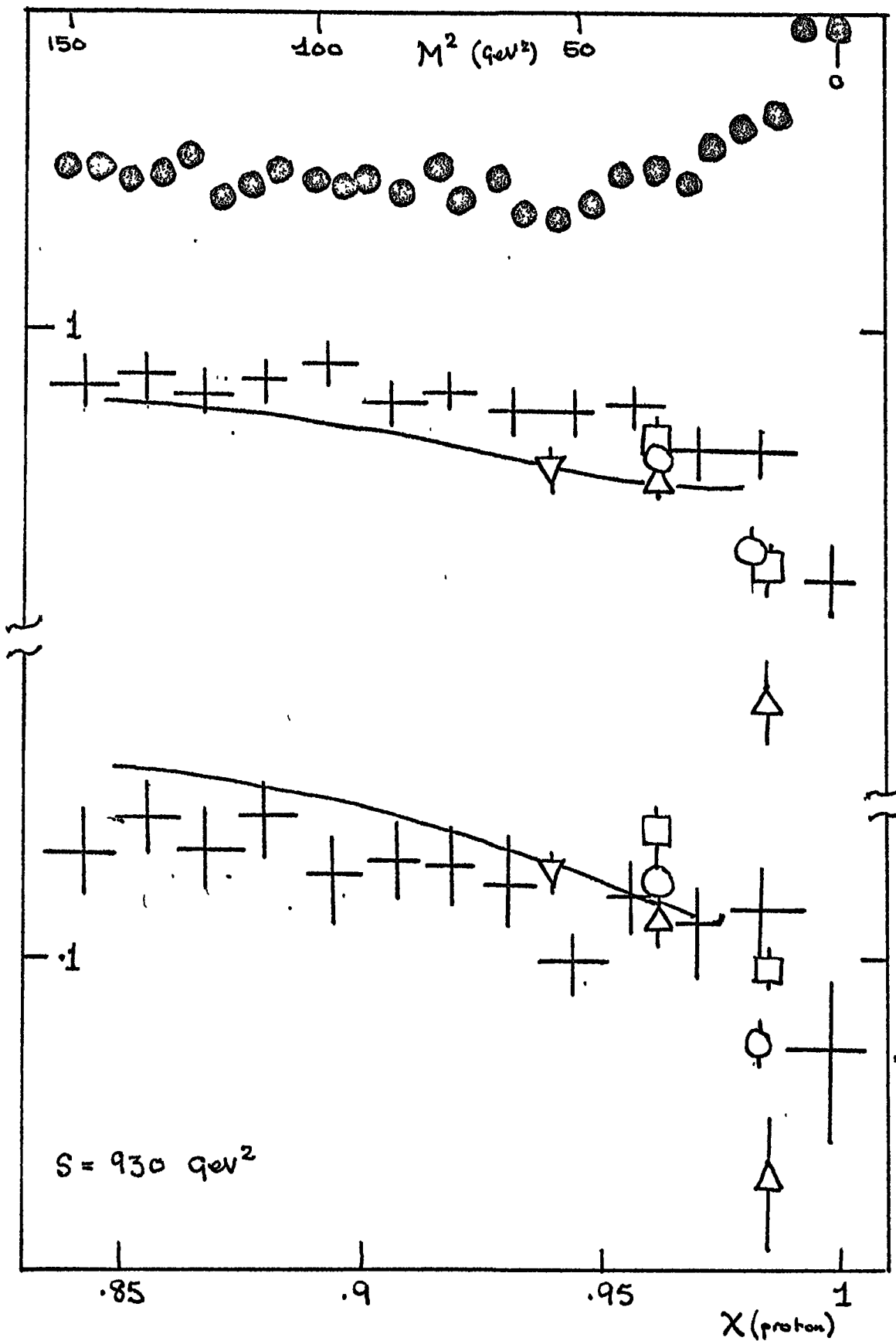


FIGURE 3.14 : Total cross-sections used to normalise inclusive distributions.

FIGURE 3.15 :

(overleaf →

The top set of points represent data for the inclusive reaction  $pp \rightarrow pX$ . The large crosses are the inclusive spectrum at the same energy ( $s=930 \text{ GeV}^2$ ) when a charged particle is observed near  $117.5^\circ$  (upper graph) or  $90^\circ$  (lower graph) in the centre of mass. The open points and the curves represent the result of our model as described in the text. To obtain these results data from lower energy inclusive experiments were used as follows :  $\circ$   $p \rightarrow \pi^-$  ;  $\square$   $\pi^+ p \rightarrow \pi^-$  ;  $\triangle$   $p \rightarrow \pi^+$  ;  $\nabla$   $p \rightarrow \pi^-$ .



← caption overleaf)

FIGURE 3.15

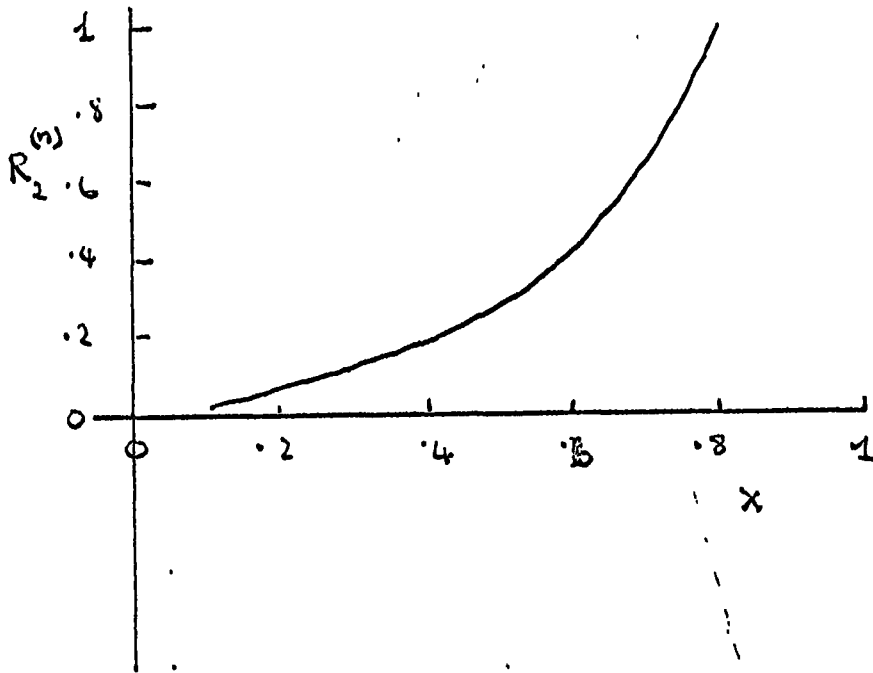


FIGURE 3.16 : The semi-inclusive cross-section  $R_{p\pi}^{(n)}$  in our model, as a function of the proton momentum.

This is independent of  $n$ .

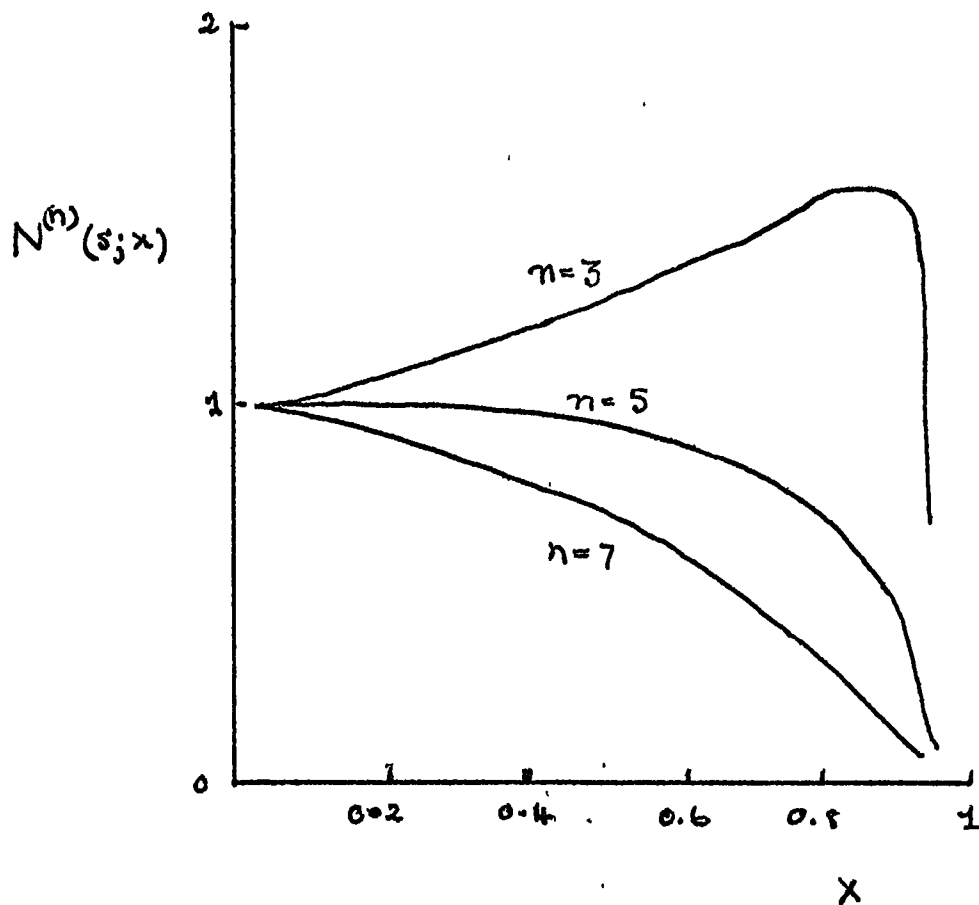


FIGURE 3.17 : The semi-inclusive proton distribution in our model for various numbers of negatively charged particles observed plotted against the proton momentum. The energy here is such that  $\langle n^- \rangle = 5$ .

## CHAPTER FOUR

### The triple pomeron coupling

#### INTRODUCTION

In this chapter we discuss the effects of the triple pomeron coupling. In section one we note its presence in the reaction  $pp \rightarrow pX$  and discuss with reference to recent literature its properties as  $t \rightarrow 0$ . We then discuss the properties of many-particle final states which are implied by the phenomenological triple pomeron model. Finally we briefly review some of the difficulties associated with the pomeron.

4.1 The reaction  $pp \rightarrow pX$  in the triple Regge region

As we briefly mentioned earlier, the more recent high energy accelerators and storage ring apparatus have allowed experiments on inclusive processes to reach the region where the missing mass  $M$  is large and where the ratio  $s/M^2$  is also large. This has stimulated a great deal of phenomenological and theoretical interest in the triple Regge limit. The discovery that cross-sections rise at such high energies has added yet more interest. Phenomenological fits centre around the triple Regge form

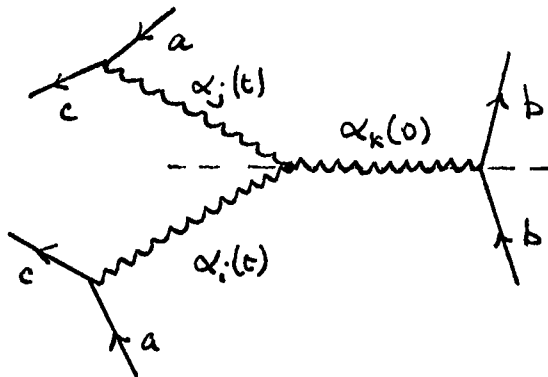
$$\frac{d\sigma}{dxdt} = \sum_{ijk} G_{ijk}(t) \cos \phi_{ij}(t) (1-x)^{\alpha_k(0) - \alpha_i(t) - \alpha_j(t)} s^{\alpha_k(0) - 1} \quad (4.1a)$$

or alternatively

$$s \frac{d\sigma}{dM^2 dt} = \sum_{ijk} G_{ijk}(t) \cos \phi_{ij}(t) (M^2)^{\alpha_k(0) - \alpha_i(t) - \alpha_j(t)} s^{\alpha_i(t) + \alpha_j(t) - 1} \quad (4.1b)$$

which correspond to diagram 4.1.  $G_{ijk}$  is the effective triple Regge coupling (including the external vertices),  $\phi_{ij}$  is the phase from the

DIAGRAM 4.1



Regge signature factors ( $\phi_{ii} = 0$ ), and  $x = 1 - M^2/s$ . The usual trajectories included are the pomeron (P) and a leading meson (R) with  $\alpha(0) \sim \frac{1}{2}$ . Interference terms ( $i=P$  and  $j=R$ ) are usually neglected. We write these trajectories as



$$\alpha_p(t) = 1 + \alpha_p' t \quad (4.2a)$$

$$\alpha_R(t) = \alpha(0) + \alpha_R' t \quad (4.2b)$$

The various terms in the expansion are then

$$\text{PPP : } G_{\text{PPP}}(t) (1-x)^{-1-2\alpha_p' t} \quad (4.3)$$

$$\text{PPR : } G_{\text{PPR}}(t) (1-x)^{\alpha(0)-2-2\alpha_p' t} S^{\alpha(0)-1} \quad (4.4)$$

$$\text{RRP : } G_{\text{RRP}}(t) (1-x)^{1-2\alpha(0)-2\alpha_R' t} \quad (4.5)$$

$$\text{RRR : } G_{\text{RRR}}(t) (1-x)^{-\alpha(0)-2\alpha_R' t} S^{\alpha(0)-1} \quad (4.6)$$

$$\text{PRP : } G_{\text{PRP}}(t) \cos \phi_{\text{RP}}(t) (1-x)^{-\alpha(0)-\alpha_p' t - \alpha_R' t} \quad (4.7)$$

$$\text{RPR : } G_{\text{RPR}}(t) \cos \phi_{\text{RP}}(t) (1-x)^{-1-\alpha_p' t - \alpha_R' t} S^{\alpha(0)-1} \quad (4.8)$$

Terms with the pomeron in the  $M^2$  channel scale whereas those with a lower singularity do not. The first two of these (the ones that we refer to as 'diffractive') are sharply peaked as  $x \rightarrow 1$ , thus giving a pronounced leading particle effect.

Much of the recent interest in the triple Regge region has centred around the triple pomeron (4.3) term. A factorisable pomeron pole ( $\alpha(0)=1$ ) in (4.3) gives an asymptotically rising contribution to the cross-section if  $G_{\text{PPP}}(0) \neq 0$ , which of course is inconsistent with the constant behaviour expected from a factorisable pole in the elastic amplitude. Thus certainly if  $G_{\text{PPP}}(0)$  is not zero, then we can

no longer hope to treat the pomeron as a factorisable pole. The form of  $G_{PPP}(t)$  is, then, of primary interest in fits to the data in the triple Regge region. The phenomenological situation is no more resolved than the theoretical one. Roberts and Roy<sup>37</sup> in a very thorough analysis find no evidence for any vanishing of the triple pomeron coupling, but rather find that the data prefer a sharp peak as  $t$  tends to zero. On the other hand Siotis<sup>38</sup> finds that 'contrary to a common belief all present experimental data are consistent with a triple pomeron coupling which vanishes as  $t$  tends to zero'. Field and Fox<sup>47</sup> agree with this conclusion.

By way of illustration we should like, here, to make a simple parameterisation of the triple Regge couplings and compare with some of the experimental data. We take

$$G_{ijk}(t) = A_{ijk} e^{b_{ijk}t} \quad (4.9)$$

with the exception

$$G_{PPP}(t) = -A_{PPP} t \cdot e^{b_{PPP}t} \quad (4.10)$$

where we put in a prejudice about the triple pomeron coupling at  $t=0$ . We allow the Regge intercept as before to vary between 0.4 and 0.6 and the slope between 0.9 and 1.1  $\text{GeV}^{-2}$ . The pomeron slope we allow to vary between 0 and 0.5  $\text{GeV}^{-2}$ . Assuming exchange degenerate mesons, the interference terms (4.7) and (4.8) have, owing to the phase factor, too small a magnitude to be relevant to the fit. (We put them in initially but it rapidly became clear that they weren't making any difference.) It also became clear that our parameterisation was not free enough to fit all the data. The fit could not produce a deep enough dip in the  $x$  dependence of the N.A.L. data (see for example figure 4.1). Other triple Regge analyses have also had this problem<sup>39</sup>. We can fit the

I.S.R. data well, out to  $t = -.65$  (see figure 4.2). Larger  $|t|$  is difficult just because of the form of equation (4.10). To allow for the rising factor  $(t)$ , the parameter  $b_{PPP}$  must be large and thus we find that this form drops too rapidly as  $|t|$  becomes large. The form of the  $G_{PPP}$  corresponding to the fit in figure 4.2 is shown in figure 4.3. The analyses in references 38,39 perform a fit at each  $t$  value separately and so do not encounter this difficulty. These authors do find one solution where  $G_{PPP}$  seems to dip at small  $|t|$ . The fit in reference 37 allows much greater freedom in the forms for the  $G_{ijk}$  and the trajectories. We can then only state that although all fits to the data require a positive triple pomeron term for  $t$  away from zero, whether it vanishes or not is a very open question. Our parameterisation, which we regard as the simplest that one might think of, requires just a little coercion to fit a limited amount of data, but we hope that it illustrates the controversy around this aspect of the data.

#### 4.2 Particle production from a triple pomeron model

In chapter two we discussed a two component picture of particle production. Our first (non-diffractive) component was one in which the reggeon-particle cross-section was constant : a mechanism corresponding to the RRP term (4.5) . The second (diffractive) mechanism had a pomeron-particle cross-section behaving like  $s^{-\gamma}$  . Our fit to the multiplicity distribution required  $\gamma > 0$  , which one might interpret as an effective trajectory in Pp interactions having intercept considerably below one. (That is a PPR term). In this section we shall discuss the form of the resulting diffractive multiplicity distribution had we kept  $\gamma = 0$  . (That is a triple pomeron mechanism). This has already been done in part in reference 30, where the mean multiplicity and total cross-section are calculated, and in reference 32 where explicit forms for the correlations are not presented.

We follow again the model of the previous two chapters and assume that the multiplicity distribution in pomeron-proton collisions is the same as that in reggeon-proton collisions. In the notation of chapter two then, the correlations in pomeron-proton collisions are

$$f_n = c_n \gamma + d_n \quad (4.11)$$

We write then from (2.94)

$$I_{ppp}(s, z) = z \int \frac{de}{e} K_p(e) \tilde{I}_p(e^s, z) \quad (4.12)$$

where now the condition

$$I_p(s, 1) = \text{constant} \quad (4.13)$$

ensures a mechanism having a non-zero triple pomeron coupling. Again we take  $\tilde{\phi}_p(s,z) = \tilde{I}_p(s,z)/\tilde{I}_p(s,1)$  to be the same as  $\phi_\pi(s,z)$ . Perhaps the simplest way of calculating the correlations in  $I_{PPP}$  is to expand  $I_p$  in powers of  $z^{-1}$  before performing the integrals. One then finds it useful to define the integrals

$$R_e = \int_{-\gamma}^0 d\ln e \, K_p(e) [Y + \ln e]^e \quad (4.14)$$

somewhat in analogy with (2.99). The expansion then gives

$$\sigma_{PPP} \propto R_0 \quad (4.15)$$

$$f_1^{PPP} = c_1 \frac{R_1}{R_0} + (1+d_1) \quad (4.16)$$

$$f_2^{PPP} = c_1^2 \left[ \frac{R_2}{R_0} - \frac{R_1^2}{R_0^2} \right] + c_2 \frac{R_1}{R_0} + d_2 - 1 \quad (4.17)$$

and

$$f_3^{PPP} = c_1^3 \left\{ \frac{R_3}{R_0} - \frac{3R_1 R_2}{R_0^2} + \frac{2R_1^3}{R_0^3} \right\} + 3c_1 c_2 \left\{ \frac{R_2}{R_0} - \frac{R_1^2}{R_0^2} \right\} + c_3 \frac{R_1}{R_0} + d_3 + 2 \quad (4.18)$$

By calculating the asymptotic behaviour of the integrals  $R_e$ , we now have an idea of the multiplicity distribution produced by this mechanism. The form (4.14) immediately suggests that

$$R_e \sim Y^{e+1} \quad (4.19)$$

and so perhaps

$$f_n^{PPP} \sim Y^n \quad (4.20)$$

This, in fact, turns out to be not quite true, although the long range correlations in this interaction suggested by (4.20) will still be present. Let us first calculate the correlations for the simplest approximation. We take (as in the case which led us to the Poisson non-diffractive distribution)  $\alpha'_P=0$  and  $|t|_{\min}=0$ . In this approximation from (2.37) we get

$$K_P = \int_{-\infty}^0 c e^{\beta t} dt = c/\beta \quad (4.21)$$

and hence

$$R_\ell = c/\beta \frac{y^{\ell+1}}{\ell+1} \quad (4.22)$$

We thus have asymptotically

$$\sigma_{PPP} \sim \ln s \quad (4.23)$$

$$f_1^{PPP} \sim \frac{1}{2} c_1 \ln s \quad (4.24)$$

$$f_2^{PPP} \sim \frac{1}{12} c_1^2 (\ln s)^2 \quad (4.25)$$

$$f_3^{PPP} \sim \frac{1}{4} c_1 c_2 (\ln s)^2 \quad (4.26)$$

Equation (4.24) is derived in reference 30. The following two equations, however, also have a lot to say about this mechanism. Their form indicates inherent long range correlations (which we also note are necessary to satisfy the theorem of Le Bellac as  $\sigma_n/\sigma_{\text{tot}}$  does not decrease like a power of  $s$ ). We find positive  $f_2$  asymptotically and negative  $f_3$  as  $c_2 < 0$ . It is interesting to note that the possible  $(\ln(s))^3$  term in  $f_3$  has a vanishing coefficient.

The effect of the  $t_{\min}$  kinematic cut off on the above equations can be estimated in the following manner. From the discussion of section 2.4 we recall that  $t_{\min}$  effectively cuts off  $K(\rho)$  at some fixed value of  $\rho$ . Thus although the correct region of integration is  $|t| > |t_{\min}(\rho)|$  and  $\rho < 1$ , we can approximate the  $t_{\min}$  cut off by  $|t| > 0$  and  $\rho < r$  (or  $\ln(\rho) < -\epsilon = \ln(r)$ ). This procedure is adopted in references 30,32. In the above this merely results in the substitution  $Y \rightarrow Y-\epsilon$  in equation (4.22) for the function  $R_l$ . Hence the asymptotic forms (4.23) - (4.26) are unaltered. As we are not, at this stage, interested in making a quantitative estimate of the behaviour of this mechanism at lower energies, we need not discuss this effect further.

As the asymptotic form of some of these quantities is slightly different if  $\alpha'_p \neq 0$ , we should also discuss this case. For  $g(t) \sim e^{\beta t}$  in (2.37) we find

$$K(e) = \frac{c}{\beta - \alpha'_p \ln e} e \quad (4.27)$$

and so

$$R_e = c \int_{-Y}^0 d \ln e \frac{(Y + \ln e)^p}{(\beta - \alpha'_p \ln e)} \quad (4.28)$$

Expansion in powers of the variable  $\beta/\alpha'_p - \ln(\rho)$  then gives

$$R_e = \frac{1}{\alpha'_p} \left[ Y + \frac{\beta}{\alpha'_p} \right]^p \left\{ \ln \frac{\alpha'_p Y + \beta}{\beta} + \sum_{n=1}^p \frac{(-1)^n}{n} \binom{p}{n} \left[ 1 - \left( \frac{\beta}{\alpha'_p Y + \beta} \right)^n \right] \right\} \quad (4.29)$$

The asymptotic behaviour as  $Y \rightarrow \infty$  with  $\alpha'_p > 0$  gives

$$\sigma_{ppp} \sim \ln \left( 1 + \frac{\alpha'_p}{\beta} \ln s \right) \equiv \sigma_{\infty} \quad (4.30)$$

$$f_1^{PPP} \sim c_1 \ln s \left[ \frac{\sigma_\infty - 1}{\sigma_\infty} \right] \quad (4.31)$$

$$f_2^{PPP} \sim \frac{1}{2} c_1^2 (\ln s)^2 \left[ \frac{\sigma_\infty - 2}{\sigma_\infty^2} \right] \quad (4.32)$$

$$f_3^{PPP} \sim \frac{1}{6} c_1^3 (\ln s)^3 \left[ \frac{-2\sigma_\infty^2 + 9\sigma_\infty - 2}{\sigma_\infty^3} \right] \quad (4.33)$$

This asymptotic behaviour, however, might be long delayed as it holds only when  $\alpha'_p \ln(s) \gg \beta$ . When  $s$  is large enough for Regge behaviour but  $\alpha'_p$  is small so that  $\alpha'_p \ln(s) < \beta$  the forms for  $\alpha'_p = 0$  will be more appropriate. Thus we have a new energy scale set by the pomeron slope, and the transverse momentum cut off  $\beta$ . This is

$$s_0 \approx e^{\beta/\alpha'_p} \quad (4.34)$$

The effect of this energy scale is shown for the mean multiplicity of this mechanism in figure 4.4 .



### 4.3 A three component model

The apparent presence of a strong triple pomeron contingent in the triple Regge analysis of inclusive proton spectra, naturally stimulated interest in what sort of multiplicity distribution one should expect. This we outlined in the previous section. Now we ask the question : how does this fit in with the calculations of chapters two and three? Let us examine this mechanism as a third component. We shall take the  $\alpha'_P=0$  case as more representative of energies (even I.S.R.) at which data are available. As remarked in reference 32 this mechanism may well fill in a dip in the multiplicity distribution which might otherwise appear between the low multiplicity diffractive mechanism and the non-diffractive component which has increasing multiplicity. The increasing width ( $f_2$ ) of the triple pomeron mechanism should effectively prevent this dip.

To see how this three component prescription differs from the two component prescription of chapter two, we find it convenient to add first the triple pomeron mechanism to the non-diffractive mechanism, and then to add the low mass diffraction term in as before. Firstly, then, the addition of a small amount of high mass (PPP) diffraction to the non-diffractive term results in a multiplicity distribution with the properties

$$\bar{n} \sim c_1 \cdot \ln s \cdot \left[ 1 - \frac{1}{2} q_2 \right] \quad (4.35)$$

$$f_2 \sim q_1 c_2 \ln s + \frac{q_2 c_1^2}{12} (\ln s)^2 + q_1 q_2 \left( \frac{c_1}{2} \ln s \right)^2 \quad (4.36)$$

with

$$q_1 + q_2 = 1 \quad (4.37)$$

If we replace the non-diffractive component (a) in chapter two with

this combination, we expect roughly the following. As  $f_2^a$  is now not strongly negative as before, the two component effect which we generate by adding the low mass diffraction term (b), (exactly as earlier), may not now need to be so large. Thus the slightly more slowly varying  $\bar{n}_a$ , which we have this time, should not be difficult to accommodate. Another way to see this is to notice that the triple pomeron multiplicity distribution (equations (4.24)-(4.26)) has a very similar form to the one produced after the addition of the two components in chapter two. Thus this third component should not make too much difference when added to the two we have already.

We should also like to note that the calculations of chapter are independent of the energy dependence of the pomeron-particle cross-section. (i.e. of whether we put in a triple pomeron coupling or not). As, for the most part, we factorise out the cross-section, the only place where this may not be immediately obvious is in section 3.1, where the general form for the two particle correlation between two mesons is discussed. For this reason we shall outline the form of the  $pp \rightarrow \pi$  inclusive distribution in this triple pomeron model. We take, then, the relevant term from equation (3.25) and integrate over the momentum of the leading proton. Hence

$$\frac{d\sigma_{ppp}}{dy_\pi} = \int dx dt \frac{|V_R(t)|^2}{16\pi^2} (1-x)^{-1} \frac{d\sigma_{pp}'}{dy_\pi'}(M^2) \quad (4.38)$$

Taking the simple form

$$\frac{d\sigma_{pp}'}{dy_\pi'}(M^2) \approx \theta\left(y_\pi' + \frac{1}{2} \ln \frac{M^2}{s_0}\right) \theta\left(-y_\pi' + \frac{1}{2} \ln \frac{M^2}{s_0}\right) \quad (4.39)$$

for the  $Pp \rightarrow \pi$  inclusive distribution, we have using (3.19)

$$\frac{d\sigma_{ppp}}{dy_\pi} = C \int dx (1-x)^{-1} \theta\left(y_\pi + \frac{1}{2} \ln \frac{s}{s_0}\right) \theta\left(-y_\pi + \ln(1-x) + \frac{1}{2} \ln \frac{s}{s_0}\right) \quad (4.40)$$

Hence

$$\frac{d\sigma_{PPP}}{dy_{\pi}} = C \left[ -y_{\pi} + \frac{Y}{2} \right] \quad (4.41)$$

C here is a constant normalisation factor. Of course there will also be a symmetric term when the proton is observed in the opposite direction and so

$$\frac{d\sigma_{PPP}}{dy_{\pi}} = C \left[ \frac{Y}{2} - y_{\pi} \right] + C \left[ \frac{Y}{2} + y_{\pi} \right] = CY \quad (4.42)$$

Equations (4.23) and (4.24) then imply

$$N_1^{PPP}(y_{\pi}) = \frac{1}{2} c_1 \quad (4.43)$$

This mechanism when added to the non-diffractive mechanism will not disturb the plateau feature of the inclusive distribution, but will break the scaling feature (owing to the form of (4.23) and (4.40)) by logarithmic terms. This result can also be found, for example in reference 40. Thus the long range correlation inherent to the triple pomeron term may change, slightly, the prediction concerning the position of the zeros in  $C_2^{\pi\pi}$  but the long range correlations arising from two component effects should remain substantially unaltered.

#### 4.4 Difficulties with the pomeron

In the previous section we found it appropriate to discuss how a simple triple pomeron mechanism would affect our model of the previous chapters when included in addition to the mechanisms already discussed. In this section we should like to note briefly the difficulties which this simple view of the triple pomeron mechanism runs into. Firstly we have two empirical features of the data. One is that a diffractive peak is observed in the process  $pp \rightarrow pX$  and it is persisting as energy rises. The other is that total cross-sections do rise through I.S.R. energies. One can hardly fail to see the immediate phenomenological attraction of the triple pomeron mechanism discussed. In reference 37, for example, it is pointed out that the rise in the total cross-section is of quite compatible magnitude with the size of the triple pomeron term in the diffractive peak (whether or not  $G_{ppp}(0) = 0$ ). The possible double high mass diffractive term is usually ignored on the basis of an estimate made of it by taking the size of the elastic vertex and the high mass diffractive vertex and assuming factorisation.

If the triple pomeron coupling does not vanish when all three pomerons are massless, then the lack of consistency of a pomeron pole alone is obvious, in that on the one hand the optical theorem gives a constant total cross-section and on the other the integrated triple pomeron contribution rises at least like  $\ln(\ln(s))$ . If it does vanish then even so there are difficulties. In the absence of cuts inequalities have been derived from inclusive sum rules which suggest that  $G_{ppp}(0)=0$  might imply that the pomeron decouples from particle-particle-pomeron vertices at  $t=0$ . Assumptions concerning the analytic continuations involved and the effects of cuts in these derivations have been questioned.

If one is merely discussing  $\ln(\ln(s))$  discrepancies, then one may think that the data do not have any bearing on the discussion.

This, however, is not the case. Perhaps the easiest way of seeing this is in the framework of reference 9 . Here the pomeron pole in the  $n \rightarrow n$  forward elastic amplitude is seen as producing short range correlations, constant total cross-section, and  $\sigma_n$  which fall like a power of  $s$  . This is entirely compatible with a multiperipheral non-diffractive model in which a lower singularity in the multiperipheral chain ( $\sigma_n \rightarrow 0$ ) adds up to a pomeron in the elastic amplitude ( $\sigma_t \rightarrow \text{constant}$ ). The need for any type of mechanism in addition to this must imply a more complicated form for the elastic  $n \rightarrow n$  amplitudes. Viewed this way the need for a two component model implies a priori that the pomeron is a singularity more complicated than a simple pole.

Two contrasting viewpoints emerge from the literature. One is that the triple pomeron term gives the rising total cross-section and that this not asymptotic but is approximate over I.S.R. energies. Before energies become large enough to allow multiple diffractive scattering, then absorption will have to become important. It is not however clear<sup>41</sup> what the effects of  $s$  channel unitarity on current energies might be. The alternate approach<sup>42</sup> is to take a 'bare pomeron' with intercept less than one and allow this to be repeated in amplitudes to obtain an output singularity with unit intercept.

FIGURES FOR CHAPTER FOUR

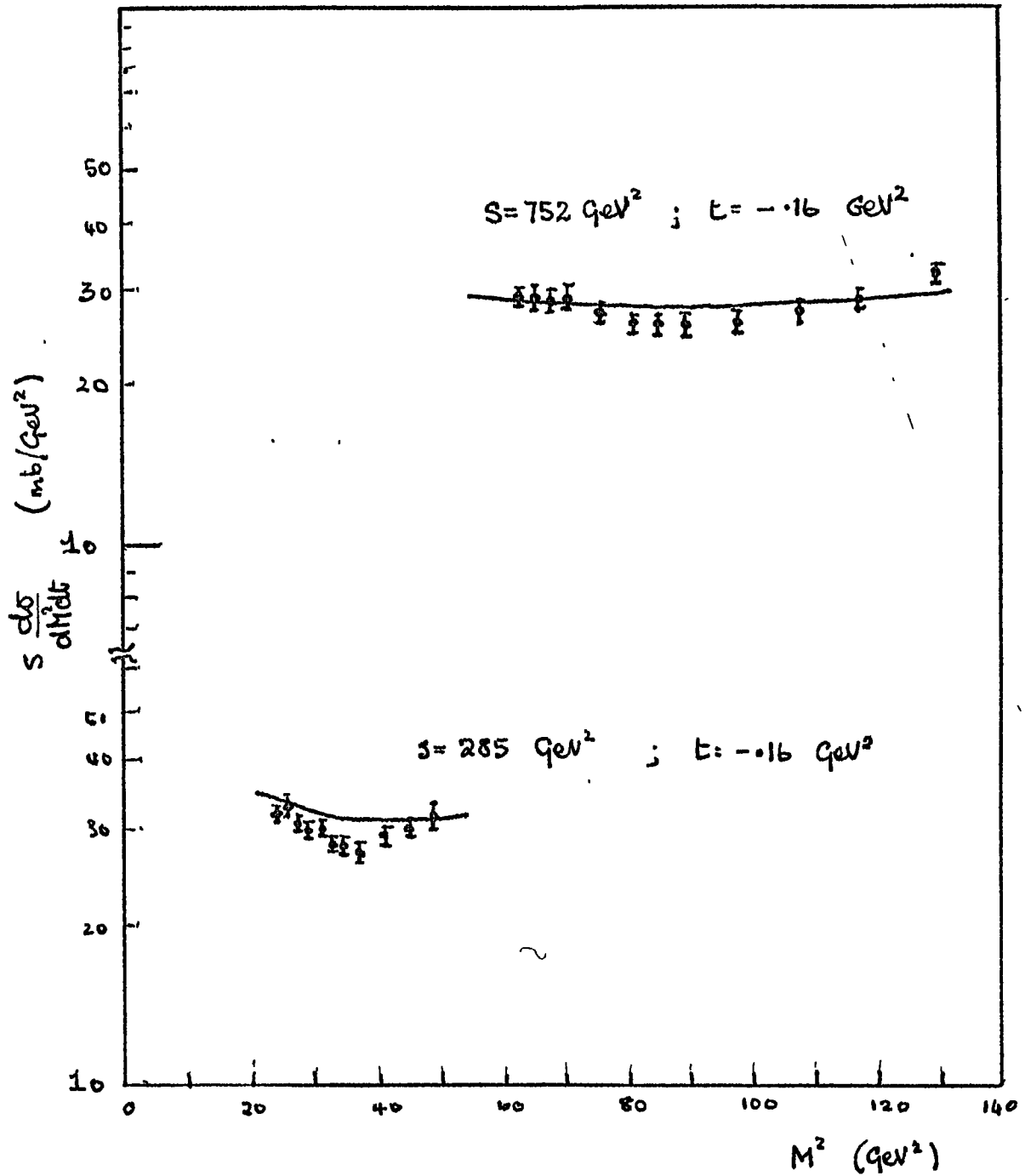


FIGURE 4.1 : The proton inclusive spectrum at small  $|t|$ .

For N.A.L. data see reference 39 .

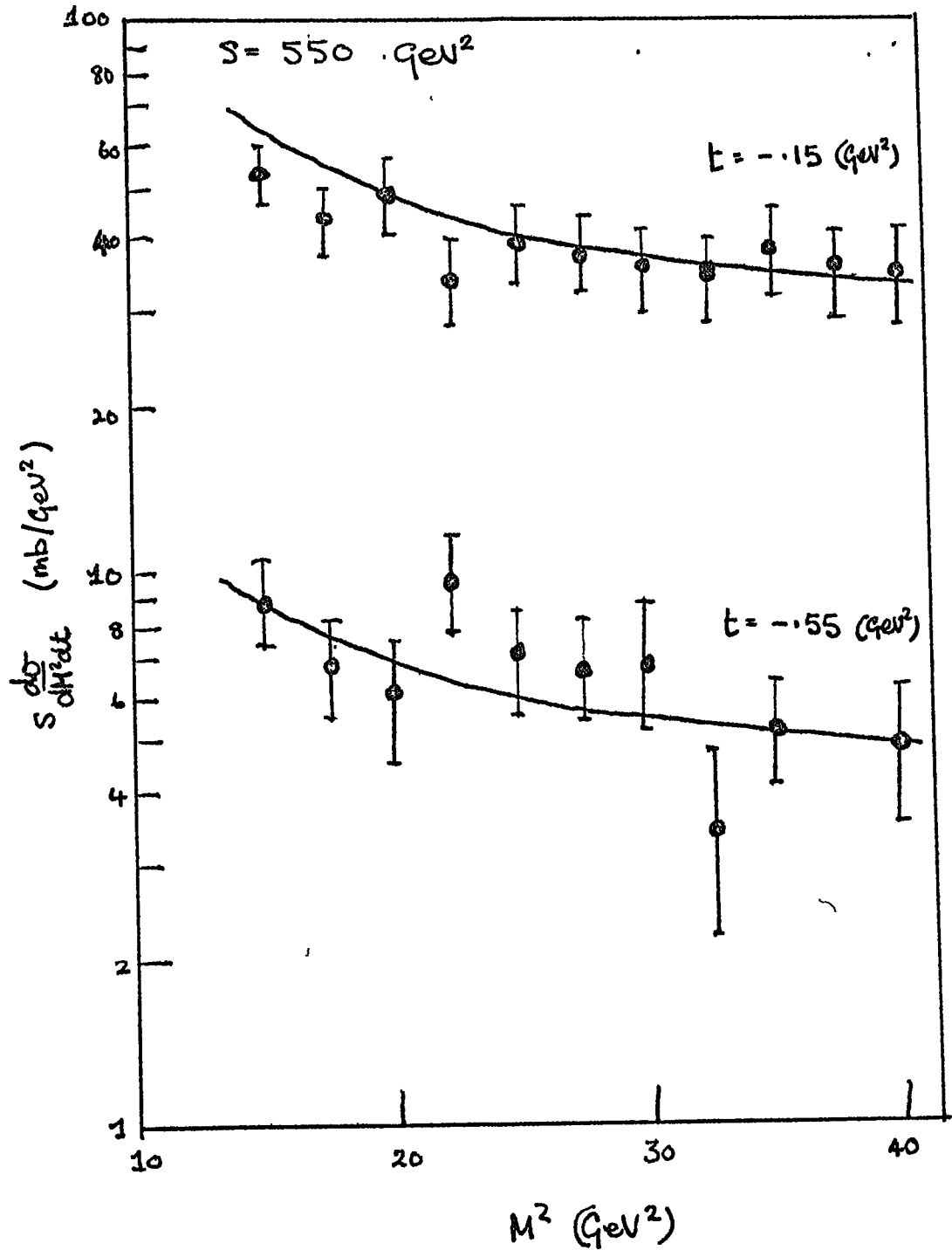
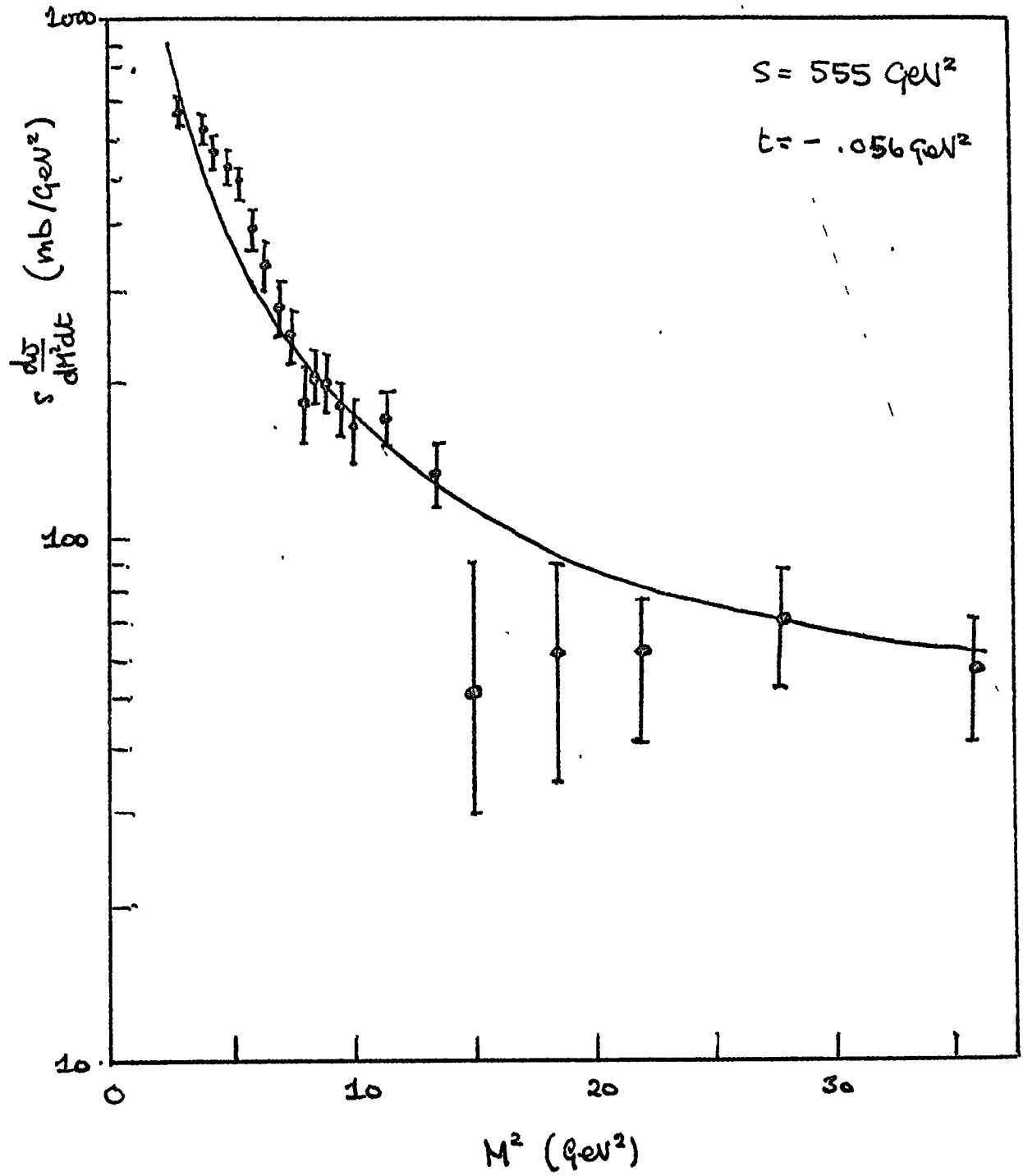
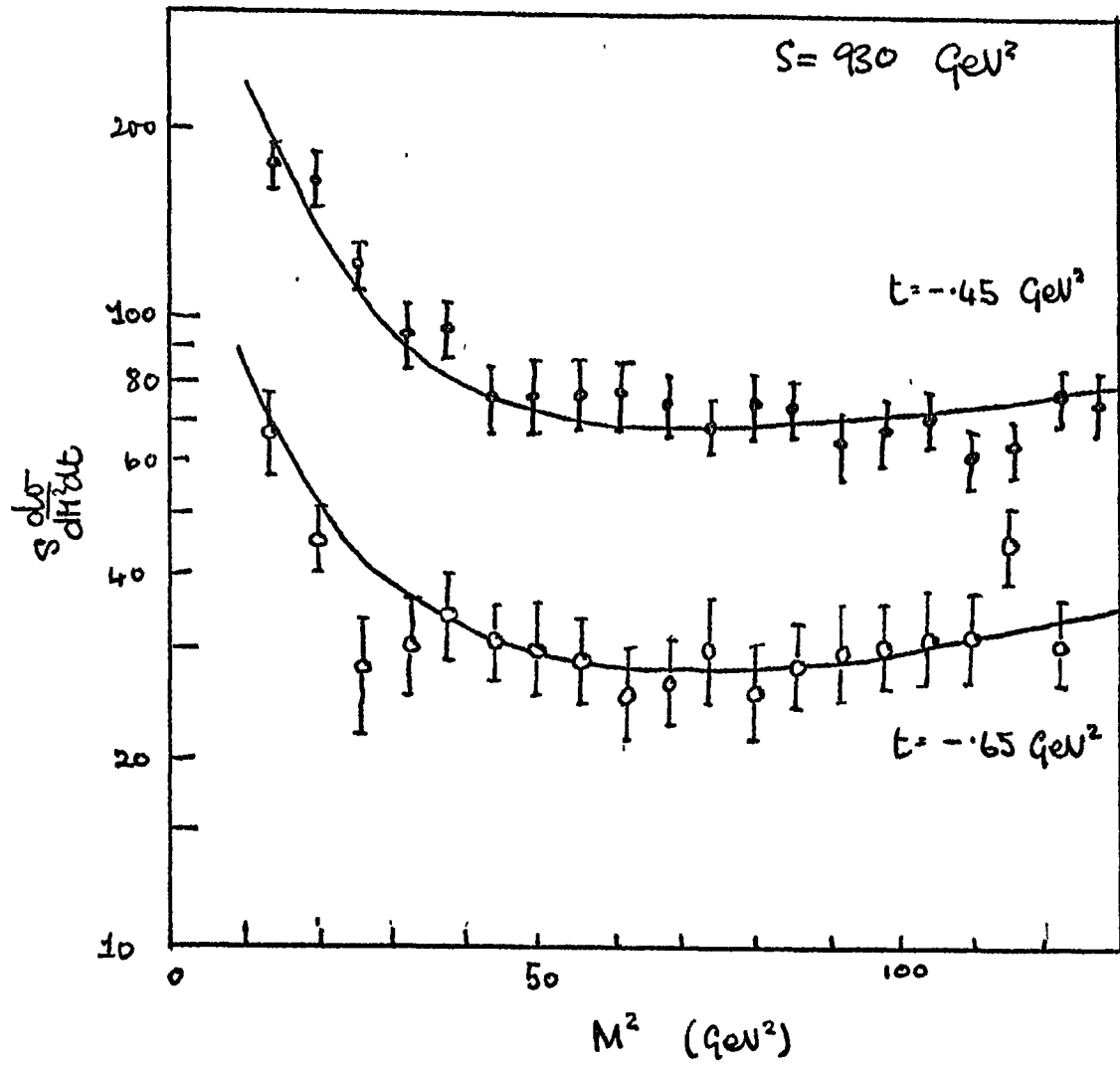


FIGURE 4.2 : Our fit to the proton inclusive distribution at various values of  $s$  and  $t$ . (See also the following two pages.) See also reference 50.







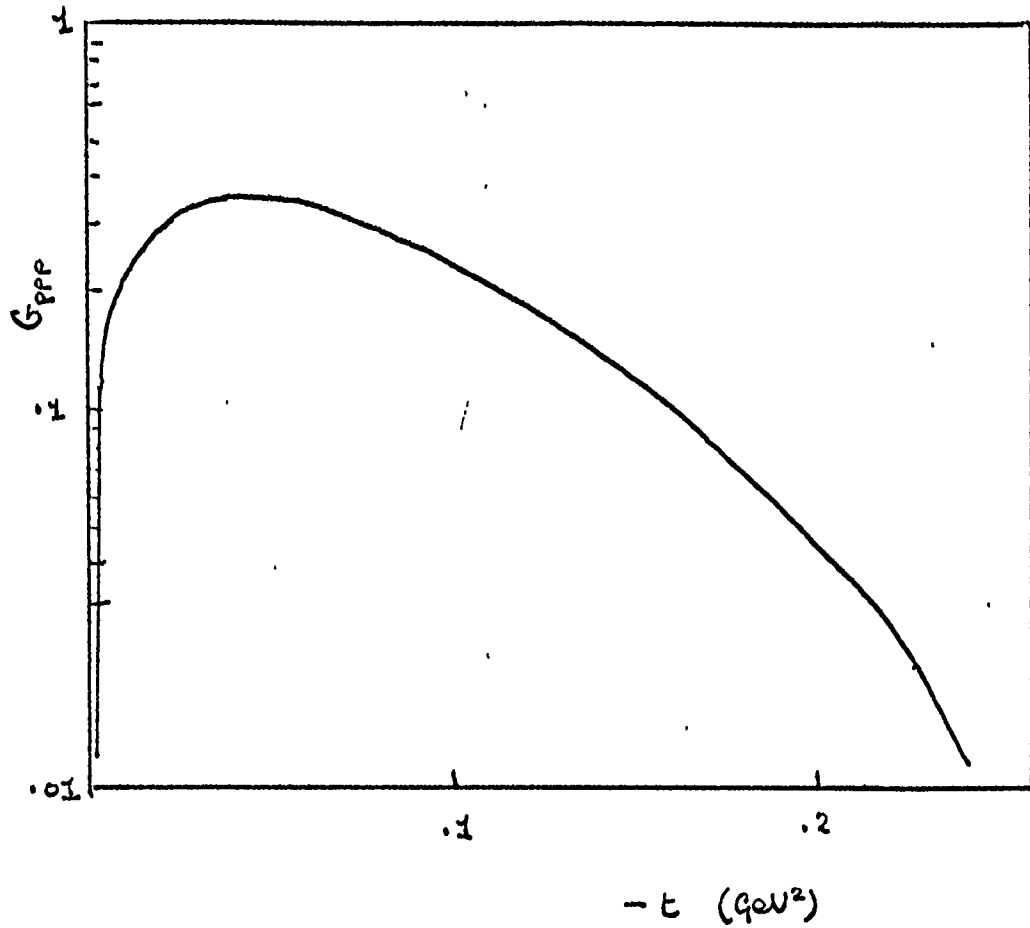


FIGURE 4.3 : The triple pomeron coupling from the fit in the previous figures.

The parameters for the various couplings have the values :

$$A_{PPP} = 23$$

$$b_{PPP} = 23$$

$$A_{PPR} = 9.7$$

$$b_{PPR} = 0.7$$

$$A_{RRP} = 53$$

$$b_{RRP} = 1.1$$

$$A_{RRR} = 38$$

$$b_{RRR} = 11.1$$

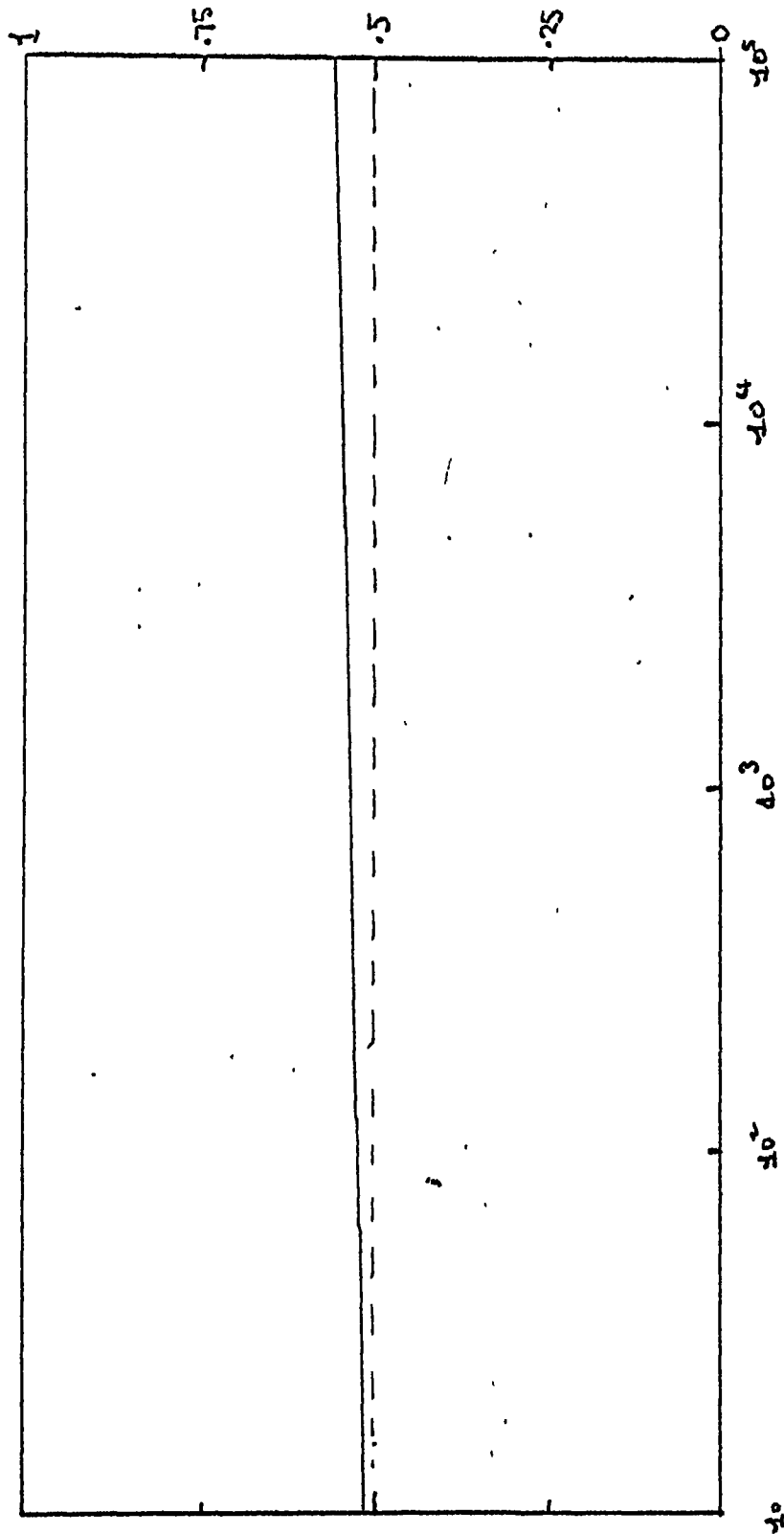


FIGURE 4.4 : The value of the coefficient  $a$  in the equation

$\bar{n}_{ppp} = a \cdot c_1 \cdot \ln(s)$  as a function of  $s$ . The typical values  $\beta = 1$  and  $\alpha'_p = 0.1$  are taken. The asymptotic behaviour is

$$a \xrightarrow{s \rightarrow \infty} 1 .$$

## C O N C L U S I O N S

In the first chapter we gave an introduction to the strong interaction at high energies and some of the quantities which are useful in trying to measure and describe it. We described a basic picture of many-particle phenomena in terms of the Mueller-Regge short range correlation approach and noted where it seems to be inadequate. In particular there was presented an illustration of a case ( antiproton production) where one might expect better results from this approach than one finds. The direct approach indicates that this process should become asymptotic more slowly due to the high threshold and momentum transfers involved.

In the second chapter we derived an integral equation for the generating function of the multiplicity distribution for the scattering of particles involving a Regge exchange having  $\alpha(0) < 1$ . We assumed this to be a meson known from Regge fits to two body scattering. In particular owing to momentum conservation constraints, this multiplicity distribution was not a Poisson distribution. In addition to this the data required a second, diffractive, contribution which we calculated under the assumption that the multiplicity distribution from pomeron-particle collisions is the same as that for a lower reggeon projectile. With this assumption (which is excellently born out by the data as discussed in section 3.2) clustering in the multiperipheral chain was required. (We note that this would have been impossible to tell had we not restricted the freedom of the model by the above assumption.) Our model also required diffraction into low masses, (a PPR term), to fit the multiplicity distribution, in accord with some of the earlier analyses.<sup>20</sup> In section 3.1 the momentum dependence

of the long range correlation was also interpreted as being evidence for diffraction into low masses.

In chapter four a possible mechanism for diffraction into high masses was discussed. From the forms presented there for the multiplicity distribution of the mechanism, we should like to argue that although the fits in chapter two, with the effective trajectory parameter  $\gamma$ , seem to deny the possibility of a triple pomeron mechanism, in fact they do not. Rather that these fits require more strongly the presence of low mass diffraction to fit the lower energy behaviour of the multiplicity distribution.

Chapter three provided support for the hypothesis that in reggeon-particle scattering, multiplicity distributions are independent of the reggeon (including the pomeron), despite the fact that we had to make a much stronger hypothesis to test this. This implies that particle-particle interactions should also provide the same multiplicity distributions. These conclusions also apply to the inclusive quantities normalised by the cross-section, provided that one is careful to avoid processes with a strong leading particle effect. This caveat stems essentially from the fact that the pomeron is not included in a consistent way, but only in a phenomenological approximation. Even so the pomeron does seem to be treatable as a factorising singularity and when considered as a projectile seems to produce, so far as the quantities discussed above are concerned, very similar results to a particle projectile. On the other hand the triple pomeron region seems to be telling us that we need a fully unitary approach to include the pomeron in a properly consistent way. If this is the case it may well be difficult to see why our phenomenological approach seems to indicate that factorisation works so well.

## R E F E R E N C E S

1. Reviews which discuss this data include
  - a) W.R.Frazier, L.Ingber, C.H.Mehta, C.H.Poon, D.Silverman,  
K.Stowe, P.D.Ting, and H.J.Yesian :  
Reviews of Modern Physics 44 284 (1972)
  - b) M.Jacob : Proceedings of the XVI international conference  
on high energy physics - Batavia (1972)
  - c) M.Jacob : CERN publication TH.1683-CERN
2. H.Pilkuhn : The Interactions of Hadrons - North Holland (1967)
3. See for example  
R.J.Eden, P.V.Landshoff, D.I.Olive, and J.C.Polkinghorne :  
The Analytic S-Matrix - Cambridge University Press (1966)
4. A.H.Mueller : Physical Review D2 2963 (1970)
5. For a review of such bounds see for example  
A.D.Martin and T.D.Spearman : Elementary Particle Theory -  
North Holland (1970)
6. Chan Hong-Mo : Lectures given at the 1972 CERN school of physics :  
- publication CERN 72-17
7. B.R.Webber : Nuclear Physics B43 541 (1972)
8. A.H.Mueller : Physical Review D4 150 (1971)
9. M.Le Bellac : Physics Letters 37B 413 (1971)
10. See for example H.M.Chan, C.S.Hsue, C.Quigg, and J.M.Wang :  
Physical Review Letters 26 672 (1971)
11. For a review see
  - a) P.D.B.Collins and E.J.Squires :  
Regge Poles in Particle Physics - Springer (1968)
  - b) P.D.B.Collins : Physics Reports 1c 104 (1971)
12. J.Finkelstein and K.Kajantie : Physics Letters 26B 305 (1968)

13. R.Dolen, D.Horn, and C.Schmid : Physical Review 166 1768 (1968)
14. H.Harari : Physical Review Letters 20 1395 (1968)  
 P.Freund : Physical Review Letters 20 235 (1968)
15. See reference 10 and  
 J.Ellis, J.Finkelstein, P.H.Frampton, and M.Jacob :  
 Physics Letters 35B 227 (1971)  
 M.B.Einhorn, M.G.Green, and M.A.Virasoro :  
 Physics Letters 37B 292 (1971)  
 S.H.H.Tye and G.Veneziano : Physics Letters 38B 30 (1972)  
 M.Kugler, V.Rittenberg, and H.J.Lipkin :  
 Physics Letters 38B 423 (1972)
16. R.Brower and J.Weiss : Physics Letters 41B 613 (1972)
17. H.M.Chan, H.I.Miettinen, D.P.Roy, and P.Hoyer :  
 Physics Letters 40B 406 (1972)
18. S.Humble : Physics Letters 40B 373 (1972)
19. R.Jengo, A.Krzywicki, and B.Petersson :  
 Physics Letters 43B 397 (1973)
20. K.Fialkowski and H.I.Miettinen :  
 Physics Letters 43B 61 (1973)
21. L.Van Hove : Physics Letters 43B 65 (1973)
22. H.Harari and E.Rabinovici : Physics Letters 43B 49 (1973)
23. R.Jengo, A.Krzywicki, and B.Petersson :  
 Nuclear Physics B65 319 (1973)
24. G.F.Chew, M.L.Goldberger, and F.Low :  
 Physical Review Letters 22 208 (1969)
25. As for reference 12
26. H.Harari : Physical Review Letters 29 1708 (1972)
27. G.F.Chew and A.Pignotti : Physical Review 176 2112 (1968)  
 Physical Review Letters 19 614 (1967)



28. C.E.De Tar : Physical Review D3 128 (1971)
29. W.Feller : An Introduction to Probability Theory and its Applications  
- Wiley (1957)
30. W.Frazer and D.R.Snider : Physics Letters 45B 136 (1973)
31. E.Berger and G.Fox : Physics Letters 47B 162 (1973)
32. R.G.Roberts and D.P.Roy : Physics Letters 46B 201 (1973)
33. K.Fialkowski : Physics Letters 41B 379 (1972)
34. P.Firila and S.Pokorski : Physics Letters 43B 502 (1973)
35. J.Whitmore and M.Derrick : N.A.L. preprint - NAL-pub-74/30-EXP (1974)
36. K.Kajantie and P.V.Ruuskanen : Helsinki preprint 5-74 (1974)
37. R.G.Roberts and D.P.Roy : R.H.E.L. preprint RL-74-022 T79 (1974)
38. I.Siotis : Contribution to the IXth Rencontre de Moriond (1974)
39. K.Abe, T De Lillo, B.Robinson, F.Sannes, J.Carr, J.Keyne, and I.Siotis  
Physical Review Letters 31 1530 (1973)
40. H.Harari and E.Rabinovici : Weizmann preprint WIS 73/41 Ph
41. R.Blankenbecler : Physical Review Letters 31 964 (1973)
42. M.Bishari, G.F.Chew, and J.Koplik : Nuclear Physics B72 61 (1974)
43. CERN-Holland-Lancaster-Manchester collaboration :  
Physics Letters 44B 207 (1973)  
Physics Letters 44B 518 (1973)
44. See for example  
Bogert et al. : Preprint NAL-CONF-73/30-EXP (1973) , where total  
cross-section data are summarised.
45. Saclay-Strasbourg collaboration : Physics Letters 41B 547 (1972)
46. CERN-Rome collaboration : Report at the IVth International  
Conference on High Energy Collisions - Oxford (1972)
47. R.D.Field and G.C.Fox : Preprint CALT-68-434 (1974)
48. CERN-Hamburg-Vienna collaboration : Physics Letters 44B 313 (1973)

49. Pisa-Stonybrook collaboration : Physics Letters 48B 359 (1974)
50. CERN-Holland-Lancaster-Manchester collaboration :
- Physics Letters 42B 279 (1972)
- Nuclear Physics B51 388 (1972)
- Nuclear Physics B54 6 (1973)

Some of the work included here has been published as follows :

- I. E.J.Squires and D.M.Webber :
- Lettere al Nuovo Cimento 7 193 (1973)
- II. E.J.Squires and D.M.Webber :
- Il Nuovo Cimento 21A 64 (1974)
- III. E.J.Squires and D.M.Webber :
- Il Nuovo Cimento 21A 413 (1974)

